

Computer Vision Reading on Stickers and Direct Part Marking on Horticultural Products – Challenges and Possible Solutions

Von der Naturwissenschaftlichen Fakultät der
Gottfried Wilhelm Leibniz Universität Hannover

zur Erlangung des Grades

Doktor der Gartenbauwissenschaften (Dr. rer. hort.)

genehmigte Dissertation

von

Felix Amenyo Eyahanyo, M. Sc.

2020

Referent: Prof. Dr. rer. hort. habil. Thomas Rath

Korreferent: Prof. Dr. sc. agr. Hartmut Stützel

Tag der Promotion: 24.09.2020

Dedicated to my lovely wife and children

Rita, Jeanelle and Joella

Computer Vision Reading on Stickers and Direct Part Marking on Horticultural Products – Challenges and Possible Solutions

Abstract

Traceability of products from production to the consumer has led to a technological advancement in product identification. There has been development from the use of traditional one-dimensional barcodes (EAN-13, Code 128, etc.) to 2D (two-dimensional) barcodes such as QR (Quick Response) and Data Matrix codes. Over the last two decades there has been an increased use of Radio Frequency Identification (RFID) and Direct Part Marking (DPM) using lasers for product identification in agriculture. However, in agriculture there are still considerable challenges to adopting barcodes, RFID and DPM technologies, unlike in industry where these technologies have been very successful.

This study was divided into three main objectives. Firstly, determination of the effect of speed, dirt, moisture and bar width on barcode detection was carried out both in the laboratory and a flower producing company, Brandkamp GmbH. This study developed algorithms for automation and detection of Code 128 barcodes under rough production conditions. Secondly, investigations were carried out on the effect of low laser marking energy on barcode size, print growth, colour and contrast on decoding 2D Data Matrix codes printed directly on apples. Three different apple varieties (Golden Delicious, Kanzi and Red Jonaprince) were marked with various levels of energy and different barcode sizes. Image processing using Halcon 11.0.1 (MvTec) was used to evaluate the markings on the apples. Finally, the third objective was to evaluate both algorithms for 1D and 2D barcodes.

According to the results, increasing the speed and angle of inclination of the barcode decreased barcode recognition. Also, increasing the dirt on the surface of the barcode resulted in decreasing the successful detection of those barcodes. However, there was 100% detection of the Code 128 barcode at the company's production speed (0.15 m/s) with the proposed algorithm. Overall, the results from the company showed that the image-based system has a future prospect for automation in horticultural production systems. It overcomes the problem of using laser barcode readers.

The results for apples showed that laser energy, barcode size, print growth, type of product, contrast between the markings and the colour of the products, the inertia of the laser system and the days of storage all singularly or in combination with each other influence the readability of laser Data Matrix codes and implementation on apples. There was poor detection of the Data Matrix code on Kanzi and Red Jonaprince due to the poor contrast between the markings on their skins. The proposed algorithm is currently working successfully on Golden Delicious with 100% detection for 10 days using energy 0.108 J mm^{-2} and a barcode size of $10 \times 10 \text{ mm}^2$. This shows that there is a future prospect of not only marking barcodes on apples but also on other agricultural products for real time production.

Keywords: Apples, Barcode size, Code 128, Data Matrix code, Image processing, Laser, Product identification

Computerbildverarbeitung von Barcodestickern und direkter Produktmarkierung von gartenbaulichen Produkten – Herausforderung und mögliche Lösungen

Zusammenfassung

Die Rückverfolgbarkeit von Produkten von der Produktion bis zum Verbraucher hat zu einem technologischen Fortschritt bei der Produktidentifikation geführt. Es hat eine Entwicklung von der Verwendung traditioneller eindimensionaler Strichcodes (EAN-13, Code 128 usw.) zu 2D (zweidimensionalen) Strichcodes wie QR (Quick Response) und Data Matrix Codes stattgefunden. In den letzten zwei Jahrzehnten haben die Radiofrequenz-Identifikation (RFID) und die direkte Teilemarkierung (DPM) unter Verwendung von Lasern zur Produktidentifikation in der Landwirtschaft zugenommen. In der Landwirtschaft gibt es jedoch immer noch erhebliche Herausforderungen bei der Einführung von Barcodes, RFID- und DPM-Technologien, im Gegensatz zur Industrie, wo diese Technologien sehr erfolgreich waren.

Diese Studie wurde in drei Hauptziele unterteilt. Erstens wurde der Einfluss von Geschwindigkeit, Schmutz, Feuchtigkeit und Strichbreite auf die Barcode-Erkennung sowohl im Labor als auch in einem Blumen produzierenden Unternehmen, der Brandkamp GmbH, bestimmt. In dieser Studie wurden Algorithmen zur Automatisierung und Erkennung von Code 128-Barcodes unter rauen Produktionsbedingungen entwickelt. Zweitens wurden Untersuchungen zum Einfluss einer geringen Lasermarkierungsenergie auf die Barcodegröße, das Druckwachstum, die Farbe und den Kontrast bei der Dekodierung von direkt auf Äpfel gedruckten 2D-Data-Matrix-Codes durchgeführt. Drei verschiedene Apfelsorten (Golden Delicious, Kanzi und Red Jonaprince) wurden mit verschiedenen Energieniveaus und unterschiedlichen Strichcodegrößen markiert. Zur Auswertung der Markierungen auf den Äpfeln wurde Bildverarbeitung mit Halcon 11.0.1 (MvTec) verwendet. Das dritte Ziel schließlich bestand darin, beide Algorithmen für 1D- und 2D-Barcodes auszuwerten.

Den Ergebnissen zufolge führte eine Erhöhung der Geschwindigkeit und des Neigungswinkels des Barcodes zu einer Verringerung der Barcode-Erkennung. Auch die zunehmende Verschmutzung der Barcode-Oberfläche führte zu einer Verringerung der erfolgreichen Erkennung dieser Barcodes. Bei der Produktionsgeschwindigkeit des Unternehmens (0,15 m/s) wurde der Code 128-Barcode mit dem vorgeschlagenen Algorithmus jedoch zu 100% erkannt. Insgesamt zeigten die Ergebnisse des Unternehmens, dass das bildbasierte System eine Zukunftsperspektive für die Automatisierung in gartenbaulichen Produktionssystemen hat. Es überwindet das Problem der Verwendung von Laser-Barcode-Lesegeräten.

Die Ergebnisse für Äpfel zeigten, dass die Laserenergie, die Größe des Barcodes, das Druckwachstum, die Art des Produkts, der Kontrast zwischen den Markierungen und der Farbe der Produkte, die Trägheit des Lasersystems und die Lagertage einzeln oder in Kombination miteinander die Lesbarkeit von Laser Data Matrix Codes und die Implementierung auf Äpfeln beeinflussen. Bei Kanzi und Red Jonaprince war die Erkennung des Data Matrix Codes aufgrund des schlechten Kontrasts zwischen den Markierungen auf ihren Schalen schlecht. Der vorgeschlagene Algorithmus arbeitet derzeit erfolgreich an Golden Delicious mit 100% Erkennung für 10 Tage bei einer Energie von $0,108 \text{ J mm}^{-2}$ und einer Barcode-Größe von $10 \times 10 \text{ mm}^2$. Dies zeigt, dass es eine Zukunftsperspektive gibt, Strichcodes nicht nur auf Äpfeln, sondern auch auf anderen landwirtschaftlichen Produkten für die Echtzeitproduktion zu markieren.

Schlagerworte: Äpfel, Barcode-Größe, Code 128, Data Matrix Codes, Bildverarbeitung, Laser, Produktidentifikation

Table of contents

Dedication.....	i
Abstract	ii
Zusammenfassung	iv
Table of contents	vi
Symbols and abbreviations	ix
Chapter 1	1
1.1 General introduction	1
1.2 Product marking techniques in horticulture and related areas	3
1.3 Research objectives and thesis outline.....	5
Chapter 2.....	8
Theoretical background for image processing and pattern recognition	8
2.1 Image processing techniques for barcode detection.....	8
2.2 Image acquisition	10
2.3 Image preprocessing.....	10
2.3.1 Noise filtering	11
2.3.2 Binary, gray-scale and colour images.....	12
2.4 Image segmentation.....	15
2.4.1 Edge detection	16
2.4.2 Thresholding	20
2.4.3 Region based segmentation methods.....	21
2.4.4 Artificial neural network.....	23
2.4.5 Morphological operation.....	25
2.5 Feature extraction	29
2.5.1 Hough transform.....	30
2.6 Image rectification	32
2.7 Image recognition	33

2.8 Conclusion	33
Chapter 3.....	34
Investigations on the effects of low laser infrared marking energy and barcode size on 2D Data Matrix code detection on apples	34
3.1 Abstract	34
3.2 Introduction.....	35
3.2 Materials and methods	39
3.2.1 Effects of laser energy and print growth on markings and detection on Golden Delicious and Kanzi	39
3.2.2 Effect of barcode size and contrast on laser marking and detection on Golden Delicious and Red Jonaprince	40
3.2.3 Laser setup.....	40
3.2.4 Image acquisition and processing of the Data Matrix code.....	43
3.3 Results and discussion	46
3.3.1 Effects of laser energy and print growth on markings and detection on Golden Delicious and Kanzi	46
3.3.2 Effect of barcode size and contrast on DM readability on Golden Delicious and Red Jonaprince	49
3.4 Conclusion and outlook.....	52
Chapter 4.....	54
Comparison of manual and automatic barcode detection in rough horticultural production systems	54
4.1 Abstract	54
4.2 Introduction.....	55
4.3 Materials and methods	57
4.3.1 Experimental setup for laboratory and company	58
4.3.2 Proposed algorithm.....	62
4.4 Results and discussion	67

4.4.1 Influence of speed and angle placement and other factors on barcode detection	67
4.4.2 Influence of speed on automated image-based barcode detection in the laboratory and the company	69
4.4.3 Robustness of the automated image-based barcode detection system.....	71
4.5 Conclusions.....	73
Chapter 5.....	75
5.1 General discussion	75
5.2 Future research needs.....	77
References.....	78
Appendices.....	96

Symbols and abbreviations

(a) Symbols

<u>Symbols</u>	<u>Description [Units]</u>
B	blue [-]
C_{max}	maximum chroma [-]
C_{min}	minimum chroma [-]
G	green [-]
G _x	gradient in the x-direction [-]
G _y	gradient in the y-direction [-]
H	hue [°]
HomMat2D	homogeneous 2D transformation matrix [-]
HomMat2DIdentity	homogeneous transformation matrix of the identical 2D transformation [-]
HomMat2DRotate	add a rotation to a homogeneous 2D transformation matrix [-]
HomMat2DScale	scaling to a homogeneous 2D transformation matrix [-]
HomMat2DTranslate	add a translation to a homogeneous 2D transformation matrix [-]
n	sample size [-]
ρ	angle of intercept of x and y axis [°]
p	laser power [W]
Phi	rotation angle [°]
P _x	fixed point of the transformation along the x-axis [-]
P _y	fixed point of the transformation along the y-axis [-]
S	saturation [%]
R	red [-]
S _x	scale factor along the x-axis [-]
S _y	scale factor along the y-axis [-]
θ	angle between x and y axis [°]

t	marking time [s per module]
T _x	translation along the x-axis [-]
T _y	translation along the y-axis [-]
V	value [%]
x	distance from the origin in the vertical axis [-]
y	distance from the origin in the horizontal axis [-]

(b) Abbreviations

<u>Abbreviations</u>	<u>Description</u>
1D	one-dimensional
2D	two-dimensional
3D	three-dimensional
AGV	automated guided vehicle
AIDC	automatic identification data capture
ANN	artificial neural network
ASCII	American standard code for information interchange
BPNN	back-propagation neural network
CCD	charge coupled device
CMOS	complementary metal-oxide-semiconductor
CMY	cyan magenta yellow
CMYK	cyan magenta yellow key
COC	coefficient of correlation
DM code	data matrix code
DPM	direct part marking
DW	dirty water
EAN-13	European article number 13
ECC200	error correction code 200
ED	extremely dirty
EU	European Union
FOV	field of view

HAZ	heat affected zone
HHT	hierarchical Hough transform
HIS	hue intensity saturation
HomMat2D	homogeneous 2D transformation matrix
HSV	hue saturation value
HT	Hough transform
ID	interseg delay
JPEG	joint photographic experts group
JSEG	JPEG image segmentation
LASER	light amplification by stimulated emission of radiation
MLP	machine learning process
MSER	maximally stable extremal region
NDVI	normalized difference vegetation index (NDVI)
Nd:YAG	neodymium-doped yttrium aluminium garnet
NGA	national grocers association
NIR	near infra red
NN	neural network
NTSC	national televisions standards committee
OVR	off vector resolution
OVV	off vector velocity
PAL	phase alternating line
PB	plant barcode
PC	personal computer
PDE	partial differential equation
PDF 417	portable data file 417
PED	pline end delay
Phi	rotation angle
PLU	price look-up
PNB	personnel number barcode
POS	points of sale
PSD	parallel segment detection
PSD	pline start delay

PLSD	parallel line segment detector
P _x	fixed point of transformation along the x-axis
P _y	fixed point of transformation along the y-axis
QR	quick response
RAM	random access memory
RFID	radio frequency identification
RGB	red, green, blue
ROI	region of interest
SD	slightly dirty
SE	structure element
SOM	self organizing map
SSIM	structural similarity index
S _x	scale factor along the x-axis
S _y	scale factor along the y-axis
T _x	translation along x-axis
T _y	translation along y-axis
UHF	ultra high frequency
UPC	universal product code
UV	ultraviolet
VIS	visible spectrum
XYZ	lightness, chroma, hue

Chapter 1

1.1 General introduction

Image processing and computer vision is increasingly being used in various fields like medicine, logistics, industry, archaeology, geophysics, oceanography and agriculture for object recognition and classification, real time image detection, medical imaging, automation, etc. (Babu and Sulthana, 2017). In recent years where technology and innovations keep on changing and advancing, acquisition and distribution of information is vital if companies and firms want to keep up with development and increase production. Increasing productivity and profitability is always the aim of companies and firms, and as such, automation of production activities has always been sought for and encouraged. Automatic Identification Data Capture (AIDC) and image processing have been used to help solve the problems associated with manual data entry and collection and to aid in automation of production activities by providing a quick, accurate and efficient means of capturing, analysing and storing data (Singh et al., 2014; Borgohain et al., 2015; Babu and Sulthana, 2017; Trappey et al., 2017).

There are several types of AIDCs, and these include barcodes, Radio Frequency Identification (RFID), magnetic stripes, smart cards, biometrics and optical character recognition (Furness, 2000; Li et al., 2006; Hodgson et al., 2010; Musa et al., 2014; Singh et al., 2014; Borgohain et al., 2015; Mishra et al., 2015; Vieira et al., 2016; Liukkonen and Tsai, 2016; Ahson and Ilyas, 2017; Trappey et al., 2017). AIDCs work by reading data and transmitting the decoded data directly to a computer for immediate use or storing it for future use (Trappey et al., 2017). The most common of these technologies used extensively in horticultural production systems is barcodes (Hansen, 2012; Qian et al., 2012; Várallyai, 2012).

Over the last 40 years barcode recognition methods have been developed and applied in various fields to help in the processes of automation and detection. However, automation with barcodes in horticultural production systems is still a problem for these reasons: as line of sight is required for identification, multiple barcodes cannot be read at one time with laser scanners and there is the risk of losing some barcodes in the production process (Liao, 1995; Huang and Zhao, 2011; Pihir et al., 2011; Fang et al., 2012; Creusot and Munawar, 2015; Meththa, 2015; Şimşekli and Birdal, 2015; Dutt et

al., 2016). Also, attempts to use barcodes to track trays in large nursery production systems have failed as soil and water often covered the barcodes making them dirty, hence preventing successful scanning. Furthermore, growth of the plants leads to increased crop canopy, covering the barcodes, leading to reduction in successful barcode scans, thereby making identification difficult (Swedberg, 2010; Curry, 2010; Pihir et al., 2011; Prasad et al., 2014; Badia-Melis et al., 2015; Kumari et al., 2015).

Due to these aforementioned problems with barcodes in automation, RFIDs have been introduced to help solve the problems. Also compared to barcode, using RFID reduces labour hours spent in searching for and deploying trays. These hours can be re-allocated to other greenhouse tasks, thereby increasing profitability and productivity (Swedberg, 2009; 2010). However, this technology also has its limitations with automation in horticultural production systems as crop canopy, metal, water and greenhouse structures all affect the RFID signals and performance (Andrade-Sanchez, 2007; Tate et al., 2008). The radio signal strength of RFID tags is significantly reduced or attenuated as it passes through various objects and equipment in the greenhouse, including metals and water (Tate et al., 2008).

Finally, using laser (light amplification by stimulated emission of radiation) marking technology to permanently tag agricultural products has increased tremendously in the last ten years (Etxeberria et al., 2009; Marx et al., 2013; Nasution and Rath, 2017; Pullman, 2017; Eppenberger, 2018), but the challenge still exists in how to improve the technology to identify etched Data Matrix (DM) codes or QR (Quick Response) codes for real time production. Presently logos, numbers, symbols, country of origin and words are permanently being marked on products (EU, 2013; Pullman, 2017; Eppenberger, 2018). Currently, only fruits with non-edible outer skins, e.g. pomegranates, avocados, coconuts and melons, are being marked. There is an increasing interest in marking edible fruit skins, e.g. apples, tomatoes, bell peppers and nectarines (Pullman, 2017; Eppenberger, 2018). Furthermore, successful recognition of directly marked barcodes on agricultural products is still a challenge. The water content of the product, the surface (skin/peel) of the product, colour, variance within the products, laser energy, barcode size, type of labels, etc. are challenges facing successful decoding of markings on horticultural products (Wang and Madej, 2014; Li et al., 2016; Denkena et al., 2016; Ventura et al., 2016; He and Joseph, 2017; Bassoli, 2018).

There is therefore a need to find solutions to all these problems associated with the automation of barcodes in horticultural production systems, and with successful recognition of Data Matrix code on agricultural products.

1.2 Product marking techniques in horticulture and related areas

There are different ways of marking products in horticulture. Barcodes in the form of stickers/labels, RFID tags and direct part marking (DPM) where lasers are used are some of the methods of marking horticultural products. When using stickers and RFID tags on products, it is vital that they are placed on the right product and the information provided must be accurate. Since they are not permanently etched on the product they can easily be detached or switched (Ventura et al., 2016). There are different types of barcode stickers that are used in horticulture which are designed to be durable and weather resistant. These include pot labels, loop lock labels, stick in labels and bed cards (Schlösser et al., 2002). Barcodes are simply the machine-readable vertical black stripes with white spaces which are printed and found on most products (Raj, 2001; Katona and Nyúl, 2012; Bodnár and Nyúl, 2012a; Dinesh et al., 2013; Kaur and Maini, 2014; Creusot and Munawar, 2015; Chen et al., 2017). There are over 200 barcode symbologies based on the design, method of encoding, check sum specifications, etc. The barcode symbology is basically the language of the barcode containing the information to be decoded (Raj, 2001; Katona and Nyúl, 2012; Dinesh et al., 2013; David et al., 2015). There are different types of barcodes which include: Numeric-only barcodes such as Codabar, EAN-13 (European Article Number) and UPC-A (Universal Product Code); Alpha-numeric barcodes such as Code 128 and Code 39; 2D (two-dimensional) barcodes such as Data Matrix code, PDF417 (Portable Data File) and QR code (Katona and Nyúl, 2012; Gayathri and Vinoth, 2012; Powers and Reddy, 2014; David et al., 2015; Dutta et al., 2016).

Advancement in using the barcode technology has led to 2D barcodes being developed which do not come in the form of bars but in various shapes and designs (Raj, 2001; Kato and Tan, 2007; Gao et al., 2007; Woollaston, 2013; Mehta, 2015; Dutta et al., 2016). This technology is being applied in many fields due to ease of implementation; cost effectiveness (printing of labels is not too expensive compared to other technologies such as RFID and laser); and the speed, efficiency and high accuracy of gathering and storing information (Youssef and Salem, 2007; Creusot and Munawar, 2015).

Barcodes have been employed in horticultural production systems to track planting trays containing flowers and seedlings, gather information on the availability and re-ordering of planting stock or cuttings that are finished, and to store information on the planting stock for planting and distribution, and at the points of sale (POS) to check and prevent theft and to speed up sales. Barcodes have also been used in orchards for tree identification (Kondo, 2010; David et al., 2015; Zhou and Gou, 2016).

Direct Part Marking (DPM), unlike stickers, is a permanent way of imprinting usually a 2D barcode directly on the surface of a product (Royce, 2004; Datalogic, 2013; Wang and Madej, 2014; Li et al., 2016; Denkena et al., 2016; Ventura et al., 2016; He and Joseph, 2017; Bassoli, 2018). The need to track products throughout the whole supply chain from beginning to end has made DPM a fast and increasingly popular technology in various commercial applications (Denkena et al., 2016; Ventura et al., 2016; He and Joseph, 2017; Bassoli, 2018). DPM was first used in the automotive industry, however, it is now being used in electronics and computers, aerospace, health care, defense, agriculture and many more fields (Royce, 2004; Wang and Madej, 2014; Li et al., 2016; Denkena et al., 2016; Ventura et al., 2016; He and Joseph, 2017; Bassoli, 2018). The main advantage of adopting DPM instead of stickers as labels is its durability. Due to the permanent marking of DPM technology the item can be identified when exposed to harsh weather conditions throughout its supply chain and full life cycle. Another very important use of DPM is marking of very small codes in limited spaces where the traditional 1D (one-dimensional) barcodes cannot be used (Li et al., 2016). In order to successfully implement DPM technology several factors (type of surface material, cost, damage on the surface, etc.) have to be considered for full life cycle tracking of the product. There are different methods of DPM (chemical etching, inkjet printing, dot peening and laser marking), with laser marking being the most popular and rapid method used for product identification. Laser marking provides high contrast and a permanent mark on the surfaces of the products such as metal, wood, ceramics and glass (Li et al., 2016; Bassoli, 2018).

Laser marking or etching on fruits and vegetables is one of the technologies that has been encouraged and used in the last 10 years to help solve the problems associated with sticky labels. PLU (Price Look-up) numbers are required by The National Grocers Association (NGA), USA, to be placed on all types of fruits and certain vegetables. These numbers help to quickly access the information on the product and prevent theft at the POS (Drouillard and Kanner, 1997). In the poultry industry, eggs are being marked with lasers to show the production date and the best-use-by date. Also, in horticulture, especially with fruits and vegetables, laser marking is being used extensively, for product identification.

As an alternative to sticky adhesive labels, laser etching on products limits the risks of mixing and loss of products, increases traceability, and makes storage easier. Also, PLU number, QR codes and barcodes can be added to the products with additional information (EU, 2013; Pullman, 2017; Eppenberger, 2018). Although laser marking has a lot of potential in permanently marking products, only logos, numbers, symbols and words were previously etched, but with the current approval by the European Union, matrix codes, barcodes, QR codes and additional information can now be etched for identification and tracking (EU, 2013; Pullman, 2017; Eppenberger, 2018).

1.3 Research objectives and thesis outline

The main objective of this study is to propose algorithms for detection of stickers (1D barcodes) and directly marked 2D barcodes on complex backgrounds and to provide appropriate solutions to the problems affecting successful marking and detection of 2D barcodes on horticultural products.

To achieve this goal, the specific objectives of this study are as follows:

1. Determine the effect of speed, dirt, moisture and bar width on barcode detection in horticulture production systems.
2. Investigate the effect of low laser marking energy on barcode size, print growth, colour and contrast on decoding 2D Data Matrix code on horticultural products.
3. Propose appropriate algorithms for decoding stickers and directly marked 2D Data Matrix codes.

The research objectives of this thesis are formulated to provide information on the factors affecting automation with barcodes in horticulture production systems and provide information on how print growth, colour backgrounds of horticultural products, energy and barcode size affect barcode detection. Full automation and recognition of barcodes is vital in horticultural production systems. For this purpose, an alternative to hand laser readers and robust image processing algorithms to read the barcodes is necessary. According to literature, recognition of directly marked 2D barcodes on horticultural products is still a challenge. Much work has been done on marking fruits, vegetables and other products by lasers. However, most of these experiments have been centered on the effects of laser on these products, the longevity of the products after the laser has been applied, the health implications and the edibility of the products. There was no literature on how algorithms have been

designed and evaluated to detect barcodes on laser marked products in horticulture until recently on Cavendish banana. Unlike in industry where products tend to have a uniform colour, for horticultural products there are variations in colour on even the same product. Therefore, each product requires a different algorithm for detection due to the water content, skin and colour of the product. Also, the effect of factors such as laser energy, barcode size, contrast, print growth, water content, color, skins of fruits and vegetables etc. on laser marking and recognition has not been considered in detail.

This thesis is structured in 5 chapters, an introductory chapter (chapter 1), 3 main chapters (chapters 2, 3 and 4) addressing the three research questions, and a summary and conclusion chapter (chapter 5). Chapters 3 and 4 form the core of corresponding articles that were prepared for peer-reviewed journals and may be read independently from the others. Each of these main chapters has an introduction, detailed description of material and methods, results, discussion and conclusions. The last chapter (chapter 5) of the thesis gives an overall summary of the thesis results and recommendations for future work.

Chapter 2 provides information on the theoretical background of image processing and pattern recognition. This chapter shows the general image processing techniques that are used for barcode recognition from image acquisition, processing, and finally decoding.

Chapter 3 attempts to provide solutions to objective 1 and the first part of objective 3 dealing with stickers, regarding: determine the effect of speed, dirt, moisture and bar width on barcode detection in horticulture production systems. This chapter tries to solve these problems by comparing a hand-based laser detection system to an image-based barcode detection system to determine which provides more reliable, stable and faster results, by proposing a new image processing algorithm for robust barcode (stickers) detection and evaluation. Finally, the proposed system was analysed and evaluated in real horticultural production systems. To achieve this, objective, image processing and statistical analysis was carried out using R-Statistical Package 3.4.4 (<http://cran.r-project.org/>) to create ggplot (<http://ggplot2.org/>). 95% confidence intervals for the difference of proportions were estimated to determine the proportion of successful readings. A Mosaic plot (<http://ggplot2.org/>) was created using a colour chart to show the percentages of success and failure. Pairwise comparison tests using the equality differences of proportions were conducted between pairs of treatments using Pearson Chi

Square test after adding 0.5 to each count as a continuity correction. The raw p-value as well as the adjusted p-values for multiple testing using the Holm method was also performed.

Chapter 4 attempts to provide solutions to the research question in objective 2. The quality and readability of Data Matrix code depends on factors such as the energy, print growth and the colour background of the horticultural product. Therefore, this chapter attempts to provide a solution by testing different laser marking energies and barcode sizes on some horticultural products. This chapter also addresses the problems associated with reading 2D barcodes directly marked on a horticultural product (objective 3). An algorithm using Halcon was also proposed for decoding and grading the quality of the marked Data Matrix code. The optimal laser energy, barcode size and storage time were evaluated. These objectives are achieved by using image processing and a generalized linear model with the logit link function and the Quasibinomial assumption. Statistical analysis was carried out using R-Statistical Package 3.4.4 (<http://cran.r-project.org/>) to create ggplot (<http://ggplot2.org/>). Based on the fitted models, analysis of deviance followed by F-Tests and Pearson Chi²-Tests was performed. Also, the mean success rates for the factor levels were computed using multiple comparison tests and the Tukey method for the P value adjustment at a Confidence level of 0.95.

Chapter 2

Theoretical background for image processing and pattern recognition

2.1 Image processing techniques for barcode detection

There are various digital image processing techniques for recognizing or decoding a captured image. The use of the various techniques depends on the quality of the image captured. Clearly captured images with little or no noise are easily processed, while images with noise require a longer time to process. Also, noise in the image may prevent successful processing. Various procedures can be used in the processing and analysis of captured images, including preprocessing to enhance the image, segmentation, and image pattern recognition. Digital image processing aims to process data images for transmission, representation and storage for machine viewing. It also can be used to improve pictorial information for the purposes of human interpretation (Alkoffash et al., 2014). Digital image processing changes reflected light from three-dimensional (3D) images into two-dimensional (2D) image values that are useable for representation and quantitative morphology description (Samantaray et al., 2011; Alkofash et al., 2014). Image acquisition, image preprocessing (noise filtering, colour mode conversion), image segmentation (edge, region, morphology), feature extraction (Hough Transform) and image recognition are some of the fundamental steps used in digital image processing for detecting barcodes in horticulture production systems (Khirade and Patil, 2015; Varshney and Dalal, 2016; Babu and Sulthana, 2017; Prakash et al., 2017; Singh and Misra, 2017; Darwish, 2018).

There are several image processing technologies to localize barcodes with accuracy and speed. However, there are problems associated with each different type of barcode and as such there is the need for a continuous and effective solution for improved barcode localization. Due to the different types of barcodes, scenarios and cameras, localization is a difficult step in decoding the barcode. Localization of barcodes is based on two main properties, i.e., a barcode has several parallel edges and a stronger directional continuity in one particular orientation than the other (Juett and Qi, 2005; Bodnár and Nyúl, 2013; Chen et al., 2017). High speed processing activities such as automated

production and conveyor belts where a missed detection results in loss of profit requires automatic barcode detection with great accuracy (Katona and Nyúl, 2012, 2013; Bodnár and Nyúl, 2013).

Over the last 4 decades different mathematical image processing algorithms such as Hough transform (Youssef and Salem, 2007; Dwinell et al., 2012), morphological methods (Chai, 2005; Tunistra, 2006; Tekin and Coughlan, 2009; Bodnár and Nyúl, 2012a, 2012b; Daw-Tung et al., 2010; Lin et al., 2011; Gayathri and Vinoth, 2012; Katona and Nyúl, 2012; Dinesh et al., 2013), blob analysis (Huang and Zhao, 2011) and bottom hat filtering (Juett and Qi, 2005; Katona and Nyúl, 2012, 2013; Kaur and Maini, 2014; Zhou and Guo, 2016) have been used to decode the information contained on the barcode. However, these methods have been used mostly in combination with each other to help localize barcodes. In recent years deep learning and artificial intelligence are being used to detect barcodes (Wang et al., 2016; Li et al., 2017; Zhang et al., 2018; Bodnár et al., 2018). Also, Parallel Line Segment Detector (PLSD) has been used with Hough transform and morphological operations to detect barcodes in real time (Creusot and Munawar, 2016; Chen et al., 2017). Furthermore, barcodes have been detected by the Zamberletti algorithm in recent years (Chowdury et al., 2019). Figure 2-1 is a proposed block diagram/flow chart for 2D barcode detection.

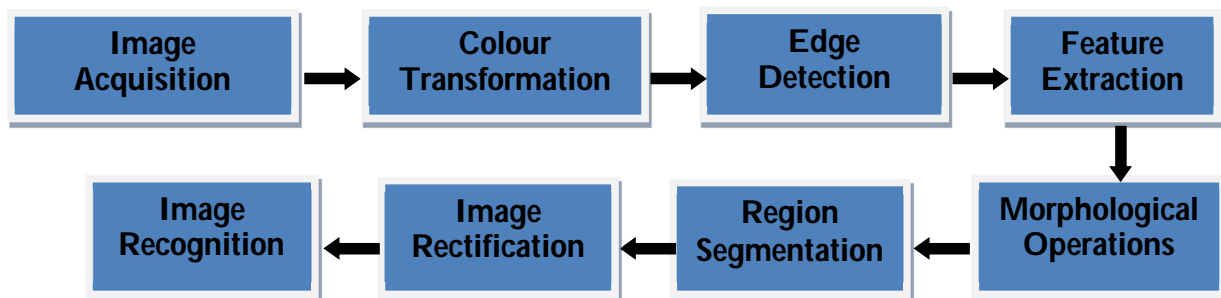


Figure 2-1: Block diagram of proposed 2D barcode recognition method

2.2 Image acquisition

Image acquisition is the first process in digital image processing (Khirade and Patil, 2015; Babu and Sulthana, 2017; Singh and Misra, 2017; Prakash et al., 2017). It is the most important step in image processing as a bad image will result in more work in processing whereas a good image will result in less work in processing (Darwish, 2018). Basically, image acquisition involves three steps: energy reflected from the object, an optical system that focuses the energy, and a sensor that measures the amount of energy (Moeslund, 2012). The image is acquired by a camera which needs measurable energy in the form of light or electromagnetic waves (Khirade and Patil, 2015; Babu and Sulthana, 2017; Singh and Misra, 2017). An adequate source of energy to illuminate the scene is needed to capture the energy reflected from the object. In daylight the sun acts as the source of energy while at night or in dark rooms, artificial light acts as the source of energy. In order to capture useful barcode images marked on products, a controlled source of light distribution and shading is required (Darwish, 2018). Images of barcodes are acquired and read by laser readers and CCD (charged coupled device) cameras in horticulture production systems. To process the acquired image, digitization is used to convert the acquired image to a numerical form (Prakash et al., 2017). The representation of a 2D image as a limited set of digital values called picture elements or pixels is known as a digital image.

2.3 Image preprocessing

Image preprocessing is the next step after acquiring the image, where different steps or processes are used to increase the chances of successfully recognizing, improving or decoding the image. Preprocessing is required to remove noise from the image and enhance the quality of the image (Khirade and Patil, 2015; Babu and Sulthana, 2017; Prakash et al., 2017). In the process of acquiring images with a digital camera, the illumination conditions may affect the brightness and contrast of the image, thereby affecting the amount of image enhancement and noise reduction required before further analysis is possible (Dinesh et al., 2013; Chitradevi and Srimathi, 2014; Monga and Ghogare, 2015; Jeyavathana et al., 2016; Babu and Sulthana, 2017; Prakash et al., 2017). Some of the steps involved in preprocessing and enhancing the image are scaling, magnification, noise filtering, binarization and conversion of a coloured image to gray image, histogram modification, contrast and

edge enhancement and sharpening (Chitradevi and Srimathi, 2014; Monga and Ghogare, 2015; Jeyavathana et al., 2016; Babu and Sulthana 2017).

2.3.1 Noise filtering

The degradation of the visual quality of digital images by unwanted random digital interference of the original signal is called noise. During the process of image acquisition and transmission, digital images can be corrupted by noise. There are different types of noise such as Gaussian, Salt and Pepper, Speckle, Poisson and Shot noise (Farooque and Rohankar, 2013; Patil and Jadhav, 2013; Kaur et al., 2014; Kumari and Chadha 2014; Jain and Tyagi, 2016). Removal of noise or image denoising is very important for further processing of the image. A major problem facing image denoising is to remove the noise as much as possible while preserving the most representative features of the image, like corners, other sharp structures and edges (Jain and Tyagi, 2016).

Filtering is the most basic computer vision and image processing operation that is used for noise removal, resolution enhancement and reduction, image smoothing and sharpening, edge detection and feature extraction (Jain and Tyagi, 2013; 2016). Filters are used to remove unwanted and unnecessary information from acquired digital images. Also, with the help of filters, different types of noise can be removed or reduced from the image for further processing. Filters are also used to blur the image by removing small details from the image initially before extracting the object and closing of small gaps in curves or lines (Chitradevi and Srimathi, 2014; Monga and Ghogare, 2015). Noise filtering is mostly interactive and is usually achieved by using either non-linear or linear filters (Chitradevi and Srimathi, 2014; Boyat and Joshi, 2015). Linear filters, also called low pass or averaging filters, work by averaging the gray levels in the neighborhood defined by the filter mask through replacing the value of each pixel. This leads to images with smoother transition in gray levels. Gaussian filter and Gabor filter are examples of low pass filters (Boyat and Joshi, 2015). Linear filters are rarely used for noise reduction because of the problem of blurring the image when used for filtering. However, as the basis for non-linear noise reduction filters, linear filters are often used (Farooque and Rohankar, 2013). Non-linear filters such as Max filter, Median filter and Min filter work by finding the brightest and darkest points in the image by ordering the pixels found in the image and changing the center pixel with the value determined by the ranking result (Boyat and Joshi, 2015; Jeyavathana et al., 2016). The median filter is used to remove noise from the captured 2D Data Matrix code on the products.

2.3.2 Binary, gray-scale and colour images

Preprocessing the image into appropriate channels is another means of enhancing the detection of the image elements. There are three types of images: binary, grayscale and colour images. Binarization converts an image into black (0) and white (1) pixels (Puneet and Naresh, 2013; Saxena and Kourav, 2014; Jyotsna et al., 2016). Where the general outline or shape information of the image is required, a binary image is used in computer vision. Generally, a binary created from a gray-scale image is called 1 bit/pixel image (Saxena and Kourav, 2014). Binarization reduces noise in the original image leading to better processing and recognition of the image. Selection of the appropriate binarization algorithm is challenging as each algorithm gives a different outcome (Puneet and Naresh, 2013; Jyotsna et al., 2016). Based on the variation in contrast and illumination, binarization is classified as Global (Otsu, Kittler and Fixed Thresholding Methods) or Local (Niblack, Sauvola, Bernsen and Adaptive Methods). Local binarization uses different values of the threshold for every pixel in the whole image. This method gives poor results with images having a lot of noise in the background. Global binarization on the other hand uses a single threshold value on the whole image. Although this process is fast, it gives poor results on images with complex backgrounds (Puneet and Naresh, 2013; Jyotsna et al., 2016). Thresholding is the simplest way to binarize an image where an optimal threshold value is first selected and the pixels in the image are categorized as background pixels or foreground pixels by comparing them to the selected threshold value (Jyotsna et al., 2016).

Grayscale images, also known as intensity, one-colour or monochrome images, include a number of different arrays of single or double [0, 1], 8-bit storage [0, 255] etc. whose pixel values specify intensity values. The most commonly used is the 8-bit storage where there are 256 gray levels with the intensity of each pixel ranging from 0 (black) to 255 (white). The different gray levels are represented by values between 1 to 254 (Kumar and Verma, 2010; Saxena and Kourav, 2014).

Colour images also known as RGB (Red, Green and Blue) images quantify the amount of light in each of the red, green, and blue spectrums recorded in each pixel. The three dimensions, XYZ, which are the lightness, chroma and hue, represent the RGB colour values (Figure 2-2). The RGB colour space is an additive system, based on the three primary colours, red, green and blue (Georgieva et al., 2005; Ibraheem et al., 2012; Loesdau et al., 2014). One needs to know about the colour image before converting it to a grayscale image. The number of bits the camera can support determines the quality of the colour. 8-bit represents basic colour image, 16-bit high colour image, 24-bit true colour image and 32-bit deep colour image, with the number of bits determining the maximum number of different

colours supported by the camera (Kumar and Verma, 2010; Saravanan, 2010; Saxena and Kourav, 2014; Azad et al., 2017). The RGB colour space can be shown as a cube with the colour values in the range of 0-1 (Figure 2-2) (Georgieva et al., 2005; Ibraheem et al., 2012). Although, the RGB colour space helps in the processing of colours, it is poor in helping the eye to differentiate between colours (Cheng et al., 2001; Loesdau et al., 2014). Therefore, this colour space is not good for colour image processing of 1D and 2D barcode images, and as such, a different colour space is used.

Three other colour models are CMY and CMYK (cyan, magenta, yellow and key (black)), HSV and HIS (hue, saturation, value and intensity), and YUV and YIQ which are based on luminance and chrominance in the PAL (Phase Alternating Line) and NTSC (Nationalized Televisions Standards Committee) broadcasting system respectively (Kumar and Verma, 2010; Saravanan, 2010; Saravanan et al., 2016; Azad et al., 2017). The HSV colour space is consistent with human perception of colour and is often used in computer vision and image processing (Figure 2-3) (Loesdau et al., 2014; Chernov et al., 2015). Equations 2-1, 2-2 and 2-3 show the transformation from RGB to HSV colour space (Georgieva et al., 2005; Saravanan et al., 2016).

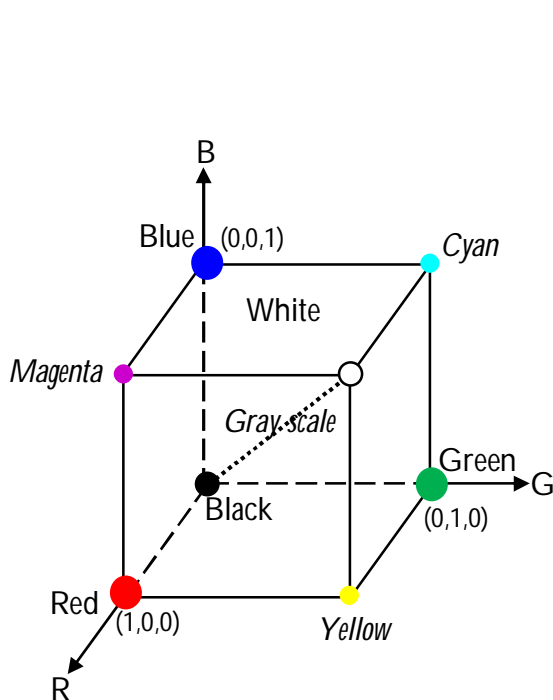


Figure 2-2: RGB colour model

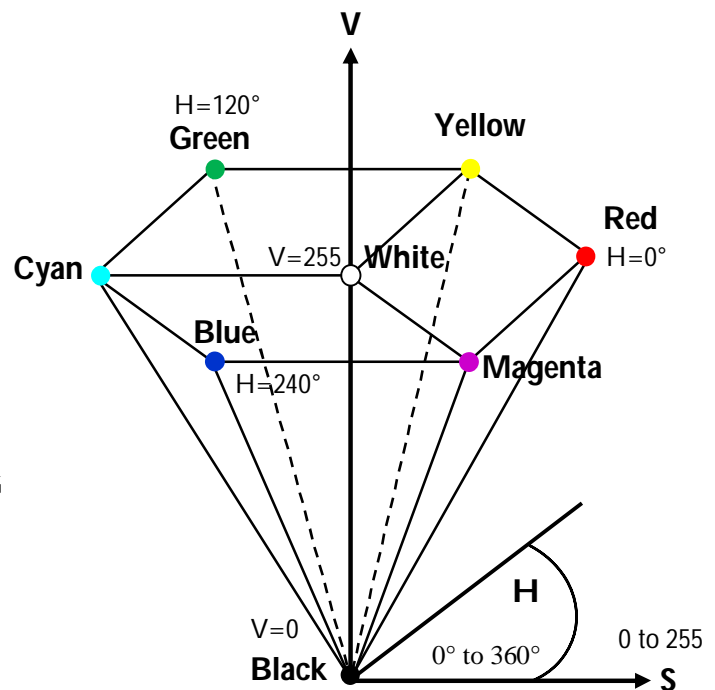


Figure 2-3: HSV colour model

Transformation formula from RGB to HSV:

The R, G, B values are divided by 255 to change the range from [0-255] to [0-1]:

Range of values: $RGB = [0-255]$, $H = [0-360^\circ]$, $S = [0-100\%]$, $V = [0-100\%]$

R =Red, G =Green, B =Blue, H =Hue, S =Saturation, V =Value

$$\begin{aligned} R' &= R/255; G' = G/255; B' = B/255 \\ C_{max} &= \max(R', G', B') \\ C_{min} &= \min(R', G', B') \\ \Delta &= C_{max} - C_{min} \end{aligned}$$

Hue calculation:

$$H = \begin{cases} 60^\circ \times \left(\frac{G' - B'}{\Delta} \text{ mod } 6 \right), & C_{max} = R' \\ 60^\circ \times \left(\frac{B' - R'}{\Delta} + 2 \right), & C_{max} = G' \\ 60^\circ \times \left(\frac{R' - G'}{\Delta} + 4 \right), & C_{max} = B' \end{cases} \quad (2.1)$$

Saturation calculation:

$$S = \begin{cases} 0, & C_{max} = 0 \\ \frac{\Delta}{C_{max}}, & C_{max} \neq 0 \end{cases} \quad (2.2)$$

Value calculation:

$$V = C_{max} \quad (2.3)$$

2.4 Image segmentation

The process of differentiating or partitioning images from their background into constituent objects or parts is segmentation (Dass et al., 2012; Babu and Sulthana, 2017; Prakash et al., 2017; Singh and Misra, 2017; Darwish, 2018). Images are separated into meaningful regions and basic properties of features are identified, like edge, intensity and texture (Kaur et al., 2012; Khan, 2013; Dhankhar and Sahu, 2013; Chitradevi and Srimathi, 2014; Jeyavathana et al., 2016; Prakash et al., 2017; Darwish, 2018). Selecting a suitable technique is still a challenging task when one desires a good segmentation of the image (Dass et al., 2012; Khan, 2013). Segmentation and analyzing of an image depends on each person's own perception in studying the image, the problem being solved and the particular type of image (Dass et al., 2012; Kaur et al., 2012; Dhankhar and Sahu, 2013; Khan, 2014; Kumar et al., 2014; Velsusamy et al., 2014). The problem to be solved determines the level to which the image will be partitioned, i.e., once the objects of interest have been isolated, segmentation should stop (Chitradevi and Srimathi, 2014).

Image segmentation algorithms are based on the principle of similarity or discontinuity (Dass et al., 2012; Kumar et al., 2014; Savant, 2014). The principle of similarity is to group pixels based on common properties, while the principle of discontinuity is to extract regions that differ in colour, texture, intensity or any other image values (Kumar et al. 2014; Savant, 2014). Some of the most popular image segmentation methods are the following: Edge based segmentation, Threshold based segmentation, Region based segmentation, Clustering based segmentation, Artificial Neural Network (ANN) based segmentation, Watershed based segmentation and Partial Differential Equation (PDE) based segmentation (Figure 2-4) (Dhankhar and Sahu, 2013; Khan, 2013; Kaur and Kaur, 2014; Jeyavathana et al., 2016).

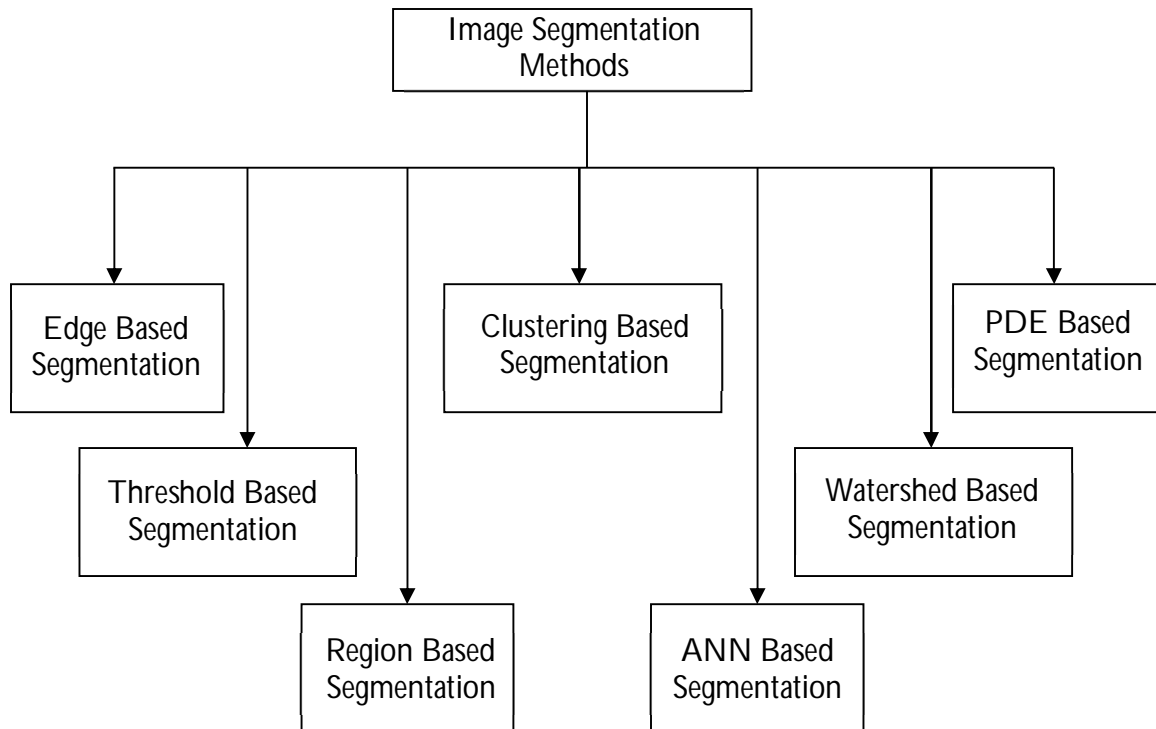


Figure 2-4: Various image segmentation methods

2.4.1 Edge detection

The most common approach to identifying and locating sharp discontinuities in an image is known as edge detection (Dass et al., 2012; Bansal et al., 2012; Kaur et al., 2012; Ojha and Sakhare, 2015). The boundary between two regions with relatively different gray level properties or where the intensity and brightness change sharply is called edge. Some vital features such as lines, curves and corners can be extracted from the edge of the image. Edge detection partitions the image into multiple regions of pixels (Dass et al., 2012; Kaur et al., 2012; Dhankhar and Sahu, 2013; Kumar et al., 2014). The discontinuities in the image, which are detected by using first and second order derivatives, are sudden changes in pixel intensity, which distinguish boundaries of objects in a scene (Bansal et al., 2012; Kaur et al., 2012). There are extremely large numbers of available edge detection operators which are sensitive to certain types of edges. Edge orientation and noise environment are variables involved in the selection of an edge detection operator (Bansal et al., 2012).

In edge orientation, the geometry of the operator shows a characteristic direction in which it is most sensitive to edges by optimizing the operators to search for diagonal, vertical or horizontal edges. Noise and edges have high frequency content. Hence, edge detection is difficult in noisy images (Bansal et al., 2012; Dhankhar and Sahu, 2013; Ojha and Sakhare, 2015). Image smoothing, enhancement, detection of edge points and edge localization are the four fundamental steps in edge detection (Shah et al., 2013; Singh and Datar, 2013; Savant, 2014). Image smoothing helps to preserve the true edges of the image by suppressing as much noise as possible in the image. Image enhancement improves the quality (sharpness) of the edges of the image by applying a filter. Detection of the edge points helps to determine which edge pixels should be preserved and which should be discarded as noise. Finally, edge localization helps to find the exact location of the edge by using edge thinning (Shah et al., 2013; Singh and Datar, 2013; Savant, 2014).

There are different methods or techniques of edge detection but these can be grouped into two main categories: Gradient (Sobel, Prewitt and Robert's operators) and Gaussian-based (Laplacian of Gaussian and Canny edge detection) (Bansal et al., 2012; Kaur et al., 2012; Dhankhar and Sahu, 2013; Kobylin and Lyashenko, 2014). The gradient technique uses the maximum and minimum in the first derivative of the image to detect the edges while the Gaussian-based technique uses zero crossing in the second derivative of the image to find the edges (Bansal et al., 2012; Shah et al., 2013; Savant, 2014; Fatima et al., 2017).

2.4.1.1 Sobel edge detection

The Sobel operators proposed by Erwin Sobel uses 3×3 convolution kernels where one kernel is simply the other rotated at 90 degrees to detect the edge of the image. The Sobel operator uses central difference by giving greater weight to the pixels in the centre of the image when averaging. The first order derivative of the image G_x and G_y are the common masks used in Sobel operator (Figure 2-5) (Kaur et al., 2012; Dhankhar and Sahu, 2013; Shah et al., 2013; Singh and Datar, 2013; Savant, 2014; Das, 2016; Fatima et al., 2017).

$$G_x = \begin{bmatrix} -1 & -2 & -1 \\ 0 & 0 & 0 \\ 1 & 2 & 1 \end{bmatrix} \quad \text{and} \quad G_y = \begin{bmatrix} -1 & 0 & 1 \\ -2 & 0 & 2 \\ -1 & 0 & 1 \end{bmatrix}$$

Figure 2-5: The masks used by Sobel operator

2.4.1.2 Prewitt edge detection

The Prewitt edge detector, named after Judy Prewitt, is similar to the Sobel Operator. Computationally, it is slightly simpler to implement than the Sobel operator but produces a rather noisier result (Singh and Datar, 2013; Das, 2016). It also relies on the idea of central difference. The horizontal edge of the image is calculated by the G_y mask and the vertical edge by the G_x mask (Figure 2-6). The intensity of the gradient in the selected pixel is shown by $|G_x| + |G_y|$ (Singh and Datar, 2013).

$$G_x = \begin{bmatrix} -1 & -1 & -1 \\ 0 & 0 & 0 \\ 1 & 1 & 1 \end{bmatrix} \quad \text{and} \quad G_y = \begin{bmatrix} -1 & 0 & 1 \\ -1 & 0 & 1 \\ -1 & 0 & 1 \end{bmatrix}$$

Figure 2-6: The masks used by Prewitt operator

2.4.1.3 Roberts edge detection

This is one of the first edge detectors, proposed in 1963 by Lawrence Roberts. The Roberts edge operator is used on an image to compute a simple quick 2D gradient measurement (Singh and Datar, 2013; Das, 2016; Fatima et al., 2017). Regions of high spatial frequency which often correspond to the edges are highlighted by this operator (Singh and Datar, 2013). This operator is not often used as its two convolution masks G_x and G_y (Figure 2-7) are limited to edges that are multiples of 45° (Das, 2016; Fatima et al., 2017).

$$G_x = \begin{bmatrix} -1 & 0 \\ 0 & 1 \end{bmatrix} \quad \text{and} \quad G_y = \begin{bmatrix} 0 & -1 \\ 1 & 0 \end{bmatrix}$$

Figure 2-7: The masks used by Robert operator

2.4.1.4 Laplacian of Gaussian edge detection

The Laplacian of Gaussian, sometimes called Marr-Hildreth edge detector or Mexican hat operator, combines Gaussian filtering with the Laplacian for detecting edges (Singh and Datar, 2013; Mahbubun and Sujun, 2014; Das, 2016). It makes the image smooth by first convolution with Gaussian-shaped

kernel, followed by the Laplacian operator (Das, 2016). The Laplacian of Gaussian edge detection shown by the G_x and G_y is shown in Figure 2-8. The Laplacian of an image $f(x, y)$ is a second order derivative shown as:

$$\Delta^2 f = \frac{\partial^2 f}{\partial x^2} + \frac{\partial^2 f}{\partial y^2}$$

The 3 x 3 Laplacian operator mask is:

$$\begin{bmatrix} 0 & -1 & 0 \\ -1 & 4 & -1 \\ 0 & -1 & 0 \end{bmatrix}$$

$$G_x = \begin{bmatrix} 0 & -1 & 0 \\ -1 & 4 & -1 \\ 0 & -1 & 0 \end{bmatrix} \quad \text{and} \quad G_y = \begin{bmatrix} -1 & -1 & -1 \\ -1 & 8 & -1 \\ -1 & -1 & -1 \end{bmatrix}$$

Figure 2-8: The Laplacian of Gaussian mask

2.4.1.5 Canny edge detection

The Canny edge detector, proposed by John F. Canny in 1986, is a robust edge detector that detects a wide range of edges in images by using a multi-stage algorithm (Singh and Datar, 2013; Das 2016; Fatima et al., 2017). It finds edges without affecting the features in the image, by isolating noise from the image and then applying the tendency, to find the critical value for threshold and edges (Minaksi and Sourabh, 2013, Fatima et al., 2017). Firstly, the Canny edge detector smoothes the image to eliminate noise using the Gaussian filter with a specified standard deviation. Then it highlights regions with high spatial derivatives by finding the image gradient at each point. After that it performs edge tracking along these regions and pixels that are not at the maximum are suppressed (Singh and Datar, 2013; Das 2016; Fatima et al., 2017). The Canny operator is shown by the second order derivative of the G_x and G_y masks (Figure 2-9).

$$G_x = \begin{bmatrix} -1 & 0 & 1 \\ -2 & 0 & 2 \\ -1 & 0 & 1 \end{bmatrix} \quad \text{and} \quad G_y = \begin{bmatrix} 1 & 2 & 1 \\ 0 & 0 & 0 \\ -1 & -2 & -1 \end{bmatrix}$$

Figure 2-9: The Canny operator mask

Monteiro and Campilho (2008) proposed a new image segmentation method with the help of spectral method and Morphological Watershed algorithms that combine edge and region-based information. They used the Berkley segmentation dataset. Firstly, as a preprocessing step, bilateral filter was used to filter noise from the image. Secondly, preliminary segmentation was done using region merging and finally Multi-class Normalized Cut method (Hameed et al., 2013) was used for the graph-based region grouping. Their technique outperformed the Mean Shift, Multi Scale Graph Based Segmentation and JSEG (JPEG Image Segmentation). Also, Cui and Zhang (2010) proposed an edge-based auto threshold select method by using band weight and Normalized Difference Vegetation Index (NDVI) to calculate edge weight to generate multi-scale image segmentation. Their technique kept the object boundaries and maintained the object information while segmenting the image. Moreover, Fabijańska (2011) used a new method for edge detection using Variance Filter. Her proposed technique did better than edge detecting with the Sobel Edge Detector. Furthermore, Islam et al. (2011) developed a quality inspection system using edge-based segmentation (Sharif et al., 2011). They used the Sobel Edge Detector for edge detection and the Otsu thresholding technique to localize the foreground and background pixels. Their method outperformed the edge detection based on artificial neural network both in accuracy and time of processing.

2.4.2 Thresholding

Thresholding is one of the simplest, intrinsic and fastest pixel-based techniques of segmenting an image where a histogram divides the image into different parts with different peaks and valleys (Dass et al, 2012; Mitsuru et al., 2012; Kaur and Kaur, 2014; Bali and Singh, 2015; Jeyavathana et al., 2016). The value in the histogram that divides intensities into two parts (foreground and background) is called the threshold. The foreground is the first part that has pixel intensities greater than or equal to the threshold while the background has pixel intensities lesser than the threshold. The right choice of the threshold value is very important for segmentation (Darwish, 2018). A high threshold value may lead to some important pixels merging with background pixels which results in under-segmentation. Furthermore, if a low threshold value is set it may result in over-segmentation (Darwish, 2018).

In thresholding, to divide the image pixels into several regions and separate objects from the background, a multilevel image is converted into a binary image by choosing a proper threshold T . If the intensity of any pixel (x, y) is greater than or equal to the threshold value i.e., $f(x, y) \geq T$, it is considered as part of the foreground otherwise the pixel belongs to the background (Dass et al., 2012;

Kaur and Kaur, 2014; Kumar et al. 2014). Global and local thresholding are basically the two types of thresholding methods differentiated by the number of threshold values used. Only one threshold value is selected for the whole image when using global thresholding while different threshold values for different regions are selected when using local thresholding (Dass et al., 2012; Kaur and Kaur, 2014; Bali and Singh, 2015). Multiple thresholding is separating more than one object with different gray levels using more than one threshold value (Kaur and Kaur, 2014; Jeyavathana et al., 2016). When the background illumination is uneven Global thresholding can fail. However, to compensate for uneven illumination local thresholding is used (Dass et al., 2012). Thresholding cannot be used for multichannel images due to the generation of only two classes. Also, thresholding is sensitive to noise which corrupts the histogram of the image making separation more difficult because it does not take into consideration the spatial characteristics of the image (Dass et al., 2012).

Zhu et al. (2007) proposed a new threshold-based edge detection algorithm for image segmentation. Their result, when compared to the Canny Edge Detector, did better as it simultaneously performed edge detection and segmentation. Xu et al. (2010) used threshold-based segmentation with Fast Marching Method for medical segmentation (Yasmin et al., 2012). Their method produced accurate, clearer and more perfect segmentation of the images. Also, Kaihua and Tao (2011) used a new optimal threshold segmentation method based on Genetic algorithm and entropy criteria to improve image acquisition. Their proposed method was more efficient in searching and finding threshold-based segmentation of an image than using the Otsu algorithm. Furthermore, Jiang et al. (2012) proposed a new multilevel threshold-based segmentation method that is best for real time applications in hostile environments.

2.4.3 Region based segmentation methods

Region based segmentation is very simple and immune to noise, compared to edge detection. It divides an image into different regions based on similarity or pre-defined criteria, like the intensity, object or colour (Dass et al., 2012; Khan, 2013; Kumar et al., 2014; Bali and Singh, 2015). A connected homogenous subset of an image with respect to some condition like gray level or texture is called a region. A group of connected pixels in an image with similar properties is a region. In region-based segmentation each pixel is allotted to a particular region or object (Kumar et al., 2014). The most important principles in region-based segmentation are spatial proximity (which includes compactness

of a region and Euclidean distance) and value similarity (which consists of gray value variance and gray value differences) (Kumar et al., 2014). The two main methods of region segmentation are: (1) Region Growing (2) Region Splitting and Merging (Dass et al., 2012; Khan, 2013; Kumar et al., 2014; Bali and Singh, 2015).

Region Growing is a method or technique for extracting a region of the image that is connected based on some predefined criteria like intensity. In region growing, pixels in the whole image are grouped into larger regions or sub regions. Four steps are used for this method (Dass et al., 2012; Kumar et al., 2014; Bali and Singh, 2015). Firstly, a group of seeds (initial pixels) in the original image are selected. Secondly, seeds with similar intensity or gray value are identified and combined. Thirdly, the regions are grown by adding the seeds with the same intensity, gray value or same value. Finally, when there is no seed which has the same value or intensity, the process is stopped (Dass et al., 2012; Kumar et al., 2014; Bali and Singh, 2015). The drawback of using this method is that a seed point is needed for each region to be segmented, which generally means manual interaction (Kumar et al., 2014).

Region splitting and merging segmentation uses splitting and merging techniques to segment an image into various regions. Images are divided into regions having similar characteristics using splitting, while merging combines the adjacent similar regions (Kaur and Kaur, 2014). Region splitting uses a top-down approach by starting with a whole image and dividing it up such that the separated parts are more homogeneous than the whole image (Kumar et al., 2014). Splitting and merging is opposite of region growing, therefore, instead of choosing seed points, an image can be divided into a set of random separated regions and then merge the regions together (Kumar et al., 2014). This technique is normally applied with theory based on the quad tree data (Figure 2-10) (Dass et al., 2012; Kaur and Kaur, 2014; Kumar et al., 2014; Bali and Singh, 2015).

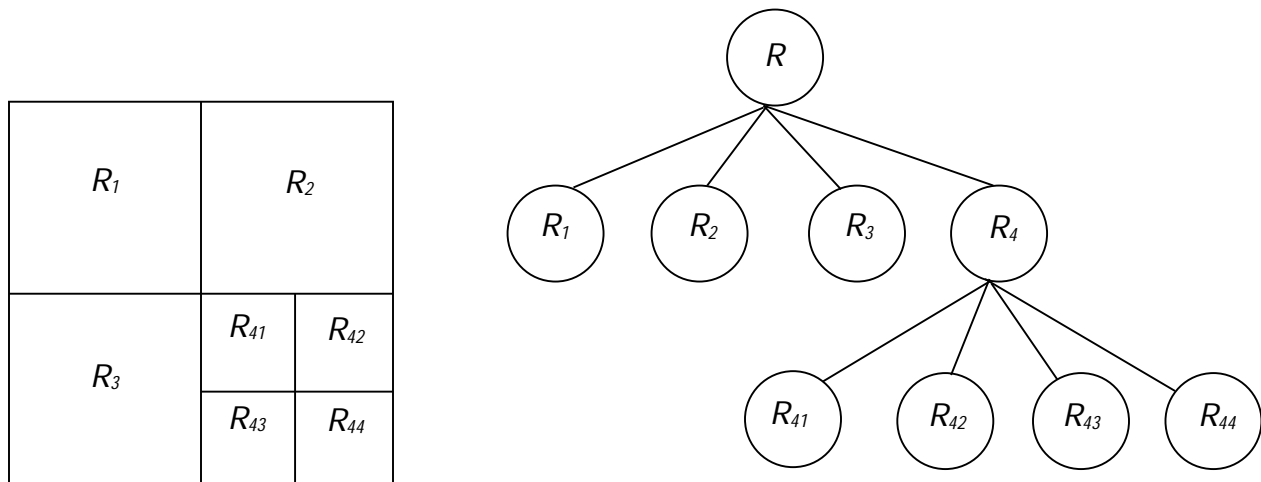


Figure 2-10: Divisions of regions based on quad tree

Barbosa et al. (2012) proposed a new image segmentation method with the help of spectral method and Morphological Watershed algorithms that join edge and region-based information. Firstly, as a preprocessing step, Magnitude Gradient was used to filter noise from the image. Secondly, preliminary segmentation was done using region merging and finally Multi Class Normalized Cut method was used for the graph-based region grouping. Their technique overcomes spectral clustering when compared to the Mean Shift, MNCUT and JSEG. Also, Chen et al. (2009) proposed a new region-based method that is fast and extracts features more accurately than the Otsu and Chan-Vese methods. Their method was based on the Least Square method. Hua et al. (2010) proposed a new segmentation method based on region growing by using Gabor filter (Sharif et al., 2011) and Gauss-Laplace filters (Sharif et al., 2012) to extract gray values and edges of the input image. They then used ANN methods to extract the region of interest. Their algorithm segmented the image perfectly and found the most important edges which other methods cannot.

2.4.4 Artificial neural network

Artificial Neural Network (ANN) based segmentation is an artificial representation of the human brain that tries to simulate its learning process and strategies (Yasmin et al., 2013; Kaur and Kaur, 2014; Kumar et al., 2014). Recently, it is being used extensively in barcode detection. In this method the image is mapped into a neural network where each neuron is the pixel in which the new image is to

be segmented (Bali and Singh, 2015). A neural network is made of large number of connected nodes with a particular weight to each connection (Kaur and Kaur, 2014). Image training samples are used in the form of neural networks to determine the connection between the neurons, i.e., pixels (Khan, 2013). Neural networks are used to extract patterns and detect trends that are complicated, to be detected by either humans or conventional technologies (Stergiou, 1996; Kaur and Kaur, 2014). This method has the advantage of not being dependent on the probability density distribution function, thus, can operate with noisy or missing data and can learn to perform tasks based on data given for training or initial experience (Stergiou, 1996; McGarry et al., 1999; Kaur and Kaur, 2014). It also decreases human involvement during image segmentation due to the training of the neural network for automation (Kaur and Kaur, 2014). Feature extraction and image segmentation are the two steps involved in artificial neural network segmentation (Senthilkumaran and Rajesh, 2009; Kaur and Kaur, 2014; Bali and Singh, 2015). Back Propagation Neural Network (BPNN) and Machine Learning Process (MLP) are some of the most used neural networks for barcode segmentation.

Due to the above advantages of neural networks, Liao et al. (1995) proposed a Back-Propagation Neural Network (BPNN) to help detect barcodes. Their proposed system performs some preprocessing procedures such as edge detection to remove noise, boundary classification using the least-squared error method to determine the best fitting line segment, and to reduce the size of barcode image for detection. A heuristic segmentation procedure is then carried out to determine the orientation and position of the barcode, by traversing along the perpendicular direction of the barcode stripes. Active pixels greater than the threshold along the direction of the barcode stripes are reported as 1 for detection or 0 for non detection. This sequence of binary numbers is then fed into the BPNN for training and decoding of the barcode. Finally, if the output is less than the preset threshold of the BPNN the barcode is undetected or output values more than the preset threshold are detected.

Furthermore, Howlett et al. (1997) also propose another method of detecting industrial barcodes using neural networks. Due to the difficulty in segmenting barcodes from backgrounds they proposed a method where the monochrome image of the EAN-13 barcode was captured in the manufacturing cell using a camera with spatial resolution of 512 by 512 pixels. The captured image was then trained from the input-vector and output-vector pair and the barcode was located within the image using NNs. The pan, zoom and tilt mechanisms of the camera were used to focus on the barcode image in order to get a very clear image. Finally, the barcode was detected using conventional algorithmic techniques.

Also, Youssef and Salem (2007) proposed an automated smart barcode detection method using a trained BPNN and hierarchical Hough Transform (HHT) for detecting the barcode. Moreover, Zhao et al. (2010) proposed a new image segmentation algorithm based on textural features (Sharif et al., 2012) and back propagation neural network to separate image from background. The proposed technique outperformed threshold based and region-based segmentation methods on the basis of accuracy of segmentation and speed. Furthermore, Zhang and Deng (2010) proposed a new image segmentation method for colour images based on neural network. They combine Self Organizing Map (SOM) and Wavelet Decomposition for the new method SOM-NN for segmentation. Their technique is effective in producing accurate segmentation and reducing noise. Finally, Ahmed et al. (2011) also used ANN successfully for texture classification and segmentation of images.

2.4.5 Morphological operation

Morphology describes the structure and shape of the object in an image. The removal of imperfections in the shape and texture of the image is the principal aim of morphological operations. In image segmentation, it plays a very important role as it deals directly with extraction of the shape of the image (Ravi and Khan, 2013; Gaur and Tiwari, 2014; Kim and Lee, 2016; Li et al., 2016). Instead of using the numerical value of the pixel, morphological operations use set theory and relative ordering of the pixel. The raw and primitive images are the input data used for morphological operations. This operation uses structuring elements, which are small matrix structures, to interact with the image. The final image processing result depends on the shape and size of the structuring element that is used (Ravi and Khan, 2013; Gaur and Tiwari, 2014; Kim and Lee, 2016; Li et al., 2016). Dilation, erosion, opening and closing are some fundamental morphological operations used in processing the image.

Dilation makes the boundaries of the images smooth, enlarges the area of the region of the image and closes or bridges the gap between the smaller and bigger spaces in boundaries of the image. Erosion on the other hand makes the boundaries of the image smooth while the area of the region of the image reduces. The connected regions of the images may be split but they remain as one region (Ravi and Khan, 2013; Gaur and Tiwari, 2014; Kim and Lee, 2016; Li et al., 2016). Opening the contours of the image eliminates thin protrusions, lines or points, and breaks narrow isthmuses in the image. Closing on the other hand makes the region boundaries of the image smooth and closes the small

gaps between adjacent regions and holes smaller than the structure element (Ravi and Khan, 2013; Li et al., 2016). All these methods have been used in various combinations to enhance barcode detection.

Daw-Tung et al. (2010), proposed a system of using various cluster and morphological methods for automatic detection of omnidirectional multiple barcodes with complex backgrounds. To remove background clutter and noise they used the max-min differencing approach on the grayscale image of the barcode. The Gaussian smoothing filter was further used to remove noise and fill in the gaps in the image as the max-min differencing did not completely remove the noise. The boundary regions of the barcodes were then successfully extracted by dilating the smoothed image by a square structure element and further dilating the resulting image by a circular image. Having completed these processes, the decoding of the image was successful (Daw-Tung et al., 2010).

Also, Bodnár and Nyúl (2012) also proposed an automatic barcode detection method using various morphological methods. They used the Canny edge detector for edge detection and median filters to reduce salt-and-pepper noise in the image as a preprocessing tool. The max-min difference operation was then used to reduce noise and manage distorted and blurred images. Dilation and erosion were then applied to close and fill up small gaps in the image. Local clustering was then used to detect the image region with similar cluster pixels for decoding. The images were then decoded by rotation in every 15° from 0° to 180° using the Gaussian blur filter with a kernel size of 5×5 and a 5% step additive noise from 0% to 50%. The decoding proved to be highly accurate and efficient for the barcodes (Bodnár and Nyúl, 2012).

Furthermore, Gayathri and Vinoth (2012) also proposed a real time barcode detection method by using Xilinx block filters to reduce noise in the image before decoding. Their proposed system first converted the RGB values of the image to intensity values, then used a feature calculation on the black and white pixels as well as the width of the bar for recognition. Having done all these calculations and comparing it with a barcode comparison block, the intensity values are converted back to the RGB scale before decoding the image.

Tuinstra (2006) and Dinesh et al. (2013) also proposed a method for decoding barcodes using basic morphological operations. The idea was to first use preprocessing operations such as quantization to convert the input images into other range of intensity values (e.g. binary images). By using the barcode region where the intensity differences between the black and white stripes are high, the bars are highlighted using a gradient calculation. Sobel kernels are then used to calculate the gradient in the x

and y directions. A hit-or-miss transformation with a line structure element is then used on the binary image to remove objects that do not contain the barcode. Dilation is then used to compose a region by merging nearby but not necessarily connected objects (Tuinstra, 2006; Dinesh et al., 2013). Using a structure element size greater than that used for the dilation, erosion is done to remove thin objects from the image. Finally, a solidity test to remove false positive objects so as to keep only the barcode regions was completed by comparing the number of pixels in a region to the convex hull of the region (Tuinstra, 2006).

Mathematical methods such as Blob analysis have also been employed in detecting barcodes. Blob analysis involves using mathematical methods to compute the effective regions of the image by comparing the contrast of the image to its surrounding background (Huang and Zhao, 2011). To localize the barcode for recognition, Huang and Zhao (2011) proposed an algorithm for multiple barcode recognition in complex backgrounds. The barcode was first divided into a number of tiles which were then scanned to determine a pattern of strips associated with the barcode in at least one of the tiles (Figure 2-11a). The candidate region was then determined by analyzing the pattern of strips (Figure 2-11b). Finally, Blob analysis was used to calculate the effective affine region of the barcode.

The affine rectangular region was calculated by first dividing the image and computing the threshold value. The barcode region of the image was then extracted and grouped according to angle of inclination. The basic information of the barcode such as the average angle, average height, the mean breadth etc., was then calculated. Barcodes with the same direction and width were then grouped and the affine rectangular region was then determined. Finally, redundant affine rectangular regions were deleted before the barcode was decoded. The entire Blob analysis step led to a certain level of robustness, efficiency, and accuracy of detecting the barcode (Huang and Zhao, 2011).

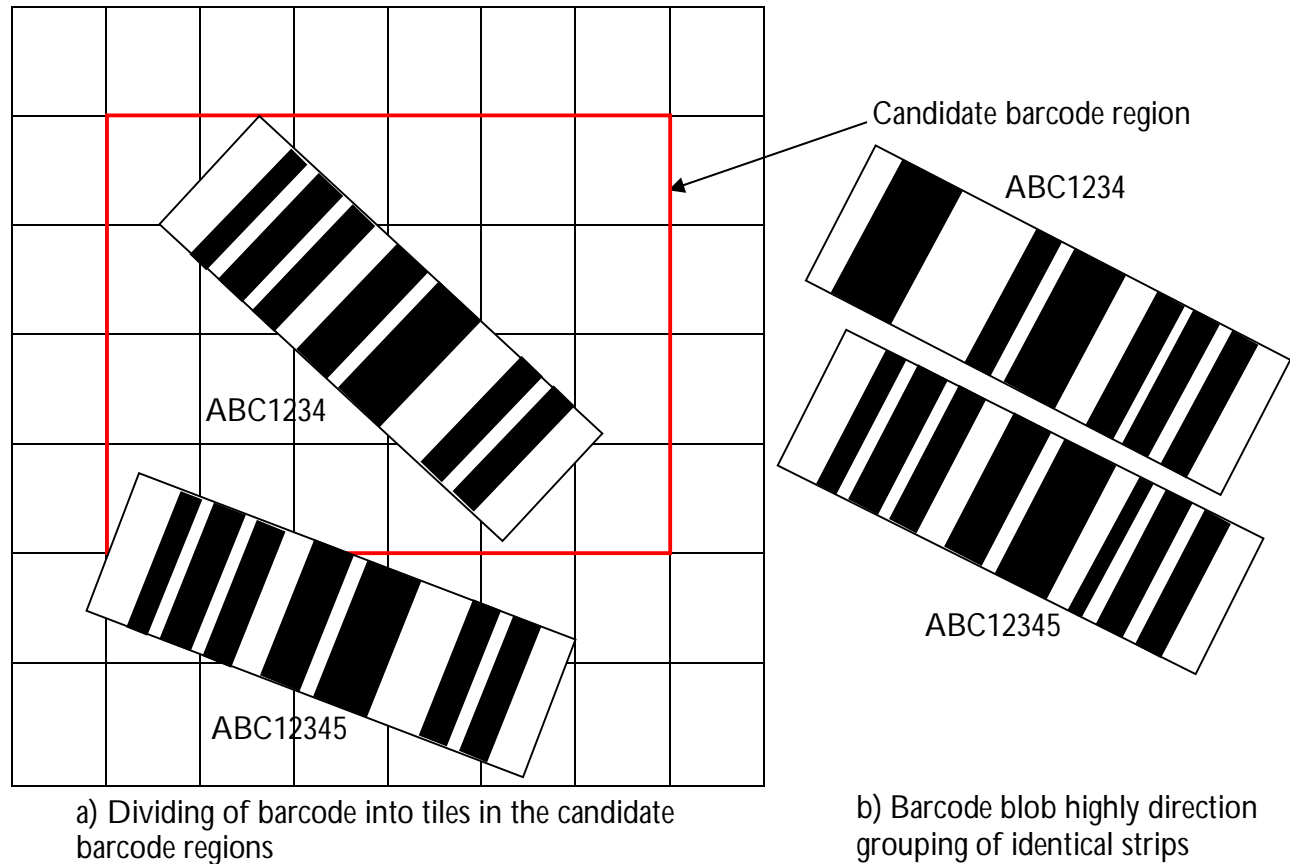


Figure 2-11: Detecting of barcode using blob analysis

Furthermore, Juett and Qi (2005), Katona and Nyúl (2012, 2013), Kaur and Maini (2014) and Zhou and Guo (2016) also proposed a method of decoding barcodes using the bottom hat filtering method. This method works by subtracting the original image from the closing of the image. Since the white areas in an image are expanded when the image is closed only the black areas are left when the original image is subtracted. A square structure element (SE) of 25×25 on images with 720×480 pixels was used to detect the bars in the barcodes. However, in less complex images after the gradient has been calculated the false areas are fewer when the bottom hat filtering is applied (Juett and Qi, 2005; Katona and Nyúl, 2012, 2013; Kaur and Maini, 2014). The algorithm works for both coloured and grayscale images but if the image is coloured the algorithm first converts it to a grayscale by quantization. Non-ideal images are corrected using simple contrast stretching during preprocessing of the image to highlight differences between and dark and light areas.

A contour is defined after converting the images into binary images. Erosion of the binary image using a 5×5 SE is carried out and subtracted from the original binary image. 16 different orientations of the barcode using a step of 11.25° are then performed using a relatively large linear SE by directional image openings. This is done so that the barcode can be detected irrespective of its orientation. A summary of low resolution density images is then calculated after the directional image openings and the images are converted back into binary images. Potentially each region detected is a barcode region. Finally, objects which have smaller areas as compared to the threshold are removed, centroids of the remaining object lines and corner points of the barcode are calculated and the barcode is detected (Juett and Qi, 2005; Katona and Nyúl, 2012, 2013; Kaur and Maini, 2014).

2.5 Feature extraction

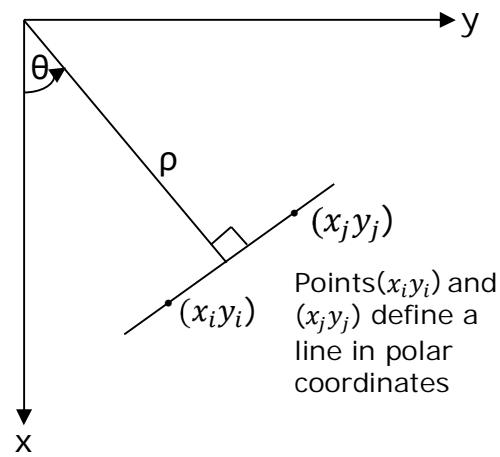
Feature extraction is vital in classifying and identifying the image. Feature extraction aims at selecting the most important feature contained in a pattern so that classification of the pattern and recognition of the image is made easier (Kumar and Bhatia, 2014; Khirade and Patil, 2015; Darwish, 2018). The main objective of extracting the feature is to get the most relevant information from the input data and reduce the dimension of the data to be processed (Kumar and Bhatia, 2014; Babu and Sulthana, 2017; Darwish, 2018). The selection of the extracted features should be carefully done so that, instead of the full input data, the relevant information from the reduced data can be used to carry out the required task of classification and identification of the image (Darwish, 2018). The morphology, colour, texture, edge, brightness etc., are some of the features that are considered for recognition of the image (Kumar and Bhatia, 2014; Khirade and Patil, 2015; Darwish, 2018). The morphology of the image has been known to give better result than the other features (Jhuria et al., 2013; Khirade and Patil, 2015). Selection of the features is very important in a high detection rate. A good feature set has discriminating information and must be as robust as possible, which enables it to differentiate one object from another (Darwish, 2018). Feature extraction methods can be classified into three main groups: Statistical Features (e.g. Crossing and Distances, Zoning, Characteristic Loci), Global Transformation and Series Expansion Features (e.g. Fourier Transforms, Walsh Hadamard Transform, Hough Transform, Gabor Transform, Wavelets etc.) and Geometrical and Topological Features (e.g. Stroke Directions and Bays; Strokes, Chain Codes etc.) (Darwish, 2018).

2.5.1 Hough transform

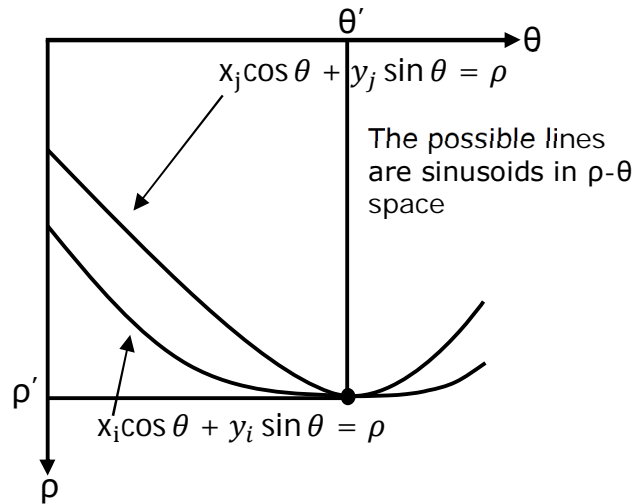
The Hough transform (HT) (Duda and Hart, 1972; Illingworth and Kittle, 1988) is very popular feature extraction technique for detecting lines, ellipses, circles and curves in an image (Mukhopadhyay and Chaudhuri, 2015; Singh and Datar, 2013; Kim and Lee, 2016). HT can accurately detect the skew angle of an image. The HT has a finite number of lines as all pairs of values of θ and ρ must fulfill the Equation 2.4 passing through the Cartesian space (x - y). Using the equation shows that Figure 12a, $\theta = \pm 90$ with respect to the x -axis for a horizontal line $\theta = 0^\circ$ and $\rho = x$ intercept while for a vertical line $\theta = 90$ and $\rho = y$ intercept or $\theta = -90$ and $\rho = -y$ intercept. All points in the Cartesian space (x - y) must satisfy this equation. Thus, each line is transformed into a single point using the Hough space (θ, ρ) for detecting the barcode image (Zamberletti et al., 2013; 2015; Kim and Lee, 2016; Gonzalez and Woods, 2018).

The Hough Transform chooses a voting procedure to detect the set of linear shapes L in a given image I for line detection. If (x_i, y_i) is any point in the plane (Figure 2-12a), any line passing through the point will have Equation 2.4. This corresponds to sinusoids in the Hough Transform space (θ, ρ) (Figure 2-12b). Two points $(x_i, y_i), (x_j, y_j)$ possess the same discrete parameter values if they are on the same line. The corresponding sinusoids intersect at a point (ρ', θ') (Figure 12b) (Zamberletti et al., 2013; 2015; Kim and Lee, 2016; Gonzalez and Woods, 2018).

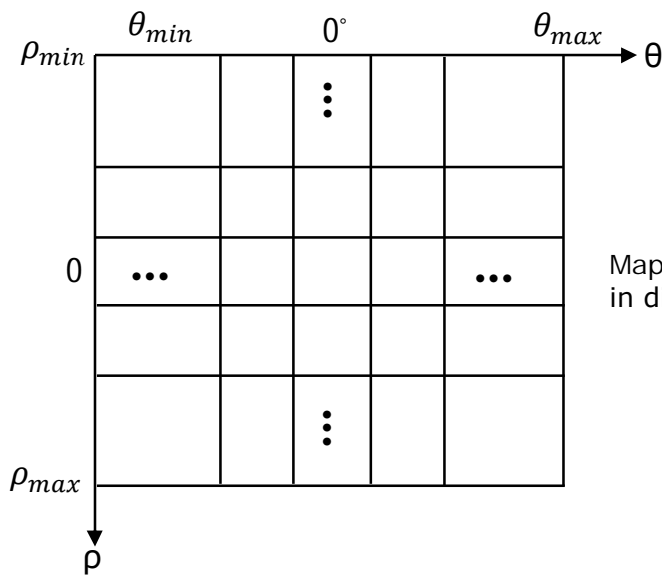
However, HT has a limiting factor for computation complexity when wide detection range and high detection accuracy are desired (Youssef and Salem, 2007). Most skew detection algorithms based on Hough Transform limit their computation to only a subset of $0, 180$ (Hinds, Fisher, and D'Amato, 1990; O'Gormann and Kasturi, 1995). To avoid its huge computational and storage requirements HT detects skew angles in a limited regular range. Therefore, Youssef and Salem (2007) proposed an improvement of the HT by using hierarchical Hough Transform (HHT) for skew detection. They used the integral of the sinusoidal curve in the Hough space to increase the detection of the skew angle. The formal error method (Shapiro, 1978a; Shapiro, 1978b) was used to make up for the quantization error during the increment step.



(a) (ρ, θ) parameterization of line in the xy -plane



(b) Sinusoidal curves in the ρ, θ - plane; the point of intersection (ρ', θ') corresponds to the line passing through points (x_i, y_i) and (x_j, y_j) in the xy -plane.



Map possible sinusoids into cells in discrete ρ - θ space

(c) Subdivision of the $\rho\theta$ -plane into cells

$$\rho = x_i \cos(\theta) + y_i \sin(\theta) \tag{2.4}$$

Figure 2-12: Representation of the Hough transform

The average of the neighborhood values in the Hough space was used to replace the accumulator values. Due to their improvement in the HT, lines with similar angles but different polar distances had the same effect in the skew detection resulting in faster detection of the barcode during automation (Youssef and Salem, 2007). Also due to the intensive computational problem with HT, Dwinell et al. (2012) proposed another improved method of HT for detecting 1D barcodes. The initial orientation of the barcode was determined by using the low-level grayscale domain. Instead of calculating the entire Hough space, only the initial angle was computed. The optimized HT served as a very efficient and powerful algorithm for detecting noisy and badly damaged barcodes. Singh and Datar (2013), also used the Hough transform to find missing edges in objects.

2.6 Image rectification

Affine and bilinear transformations are used after morphological operations to help preserve the straight line in the images, but do not necessarily preserve the angles between the lines and points (Kim and Lee, 2016). Affine transformation allows the image to be rotated, scaled, translated and skewed (Liu, 2010; Liu et al., 2010; Kim and Lee, 2016). Rotation allows the image to be rotated to x- and y-axes from the origin. Scaling changes the scale of the image by reducing or expanding in the x and/or y direction. Translation shifts the image from the origin to a new location. Finally, skewing changes the shape to a parallelogram with a slanted direction and allows for affinity (non-perpendicularity) between the axes (Kim and Lee, 2016).

Lines that are vertical or horizontal in the image are preserved by bilinear transformation. Points along the vertical and horizontal lines including borders in the image remain equally spaced. However, diagonal lines are not preserved because they are not oriented along the vertical and horizontal directions. Rather, the output image of diagonal lines is mapped onto quadratic curves (Kim and Lee, 2016).

2.7 Image recognition

This is the final step in image processing, where meaning is assigned to the recognized image. Having applied the techniques used by the operational system to process the image, it can either be accepted as good or bad. A score of one is give when the image is detected and zero if it is not detected.

2.8 Conclusion

It is clear that there is no perfect method or technique for image preprocessing, edge detection, image segmentation and feature extraction. All these methods depend on many factors such as the texture, colour, intensity, morphology, problem to be solved and image information. Therefore, it is not possible to use a single method for all types of images, nor can all methods work effectively for a particular type of image. For this reason, it is advisable to use multiple methods for image processing and pattern recognition.

Chapter 3

Investigations on the effects of low laser infrared marking energy and barcode size on 2D Data Matrix code detection on apples

Felix Eyahanyo^{a,*}, Thomas Rath^b.

^aLeibniz Universität Hannover, Institute of Horticultural Production Systems, Biosystems Engineering Section, Herrenhäuser Straße 2, 30419 Hannover, Germany; ^b University of Applied Sciences Osnabrück, Biosystems Engineering Laboratory (BLab), Oldenburger Landstraße 24, 49090 Osnabrück, Germany

* *Corresponding author.* Leibniz Universität Hannover, Institute of Horticultural Production Systems, Biosystems Engineering Section, Herrenhäuser Straße 2, 30419 Hannover, Germany. Tel.: +49 511 762 5344; Email: eyahanyo@bgt.uni-hannover.de (F. Eyahanyo)

Accepted: Journal of Applied Engineering in Agriculture (ASABE)

3.1 Abstract

Product marking in horticulture aims at providing robust and permanent means of marking products and preventing theft, tampering and cheating by customers. Direct part marking has sought to provide solutions to these problems. However, unlike in industry where it has been successful, in horticulture there are still a lot of challenges that prevent successful marking and reading of directly marked barcodes on horticultural products. The laser energy, barcode size, product colour and days of storage are very important factors that affect the marking, quality and readability of directly marked Data Matrix (DM) code on apples. Therefore, the objective of this study was to solve the aforementioned problems with these factors by using Synrad 48-5 CO₂ laser (10600 nm), to mark some apples using very low energy levels. Laser energy, the skin of the product and the inertia of the laser beam affected the printing of the DM on the apples. Incomplete marking of the DM at some of the energies used resulted in the DM not being decoded. Generally, there was successful decoding on Golden Delicious compared to Kanzi and Red Jonaprince for 10 days of storage. On the average, the smaller barcode size (8 × 8 mm²) produced a better detection of the code than the bigger size (10 × 10 mm²). The

better detection on Golden Delicious can be attributed to the better contrast between the DM and its colour. As the days of storage increased, detection decreased for Kanzi and Red Jonaprince. There is a future prospect of directly reading marked apples in the real production systems.

Keywords: *Product marking, Apple, Data Matrix code, Laser, Barcode size, Apple Skin*

3.2 Introduction

The need to monitor and trace products through the production, supply and marketing channels from the manufacturer to the consumer in various commercial applications has increased tremendously in the last decade (Kang and Lee, 2013; Kemény et al., 2014; Tekin, 2014; Ventura et al., 2016). Product marking is valuable for: providing information; improving security by preventing theft, tampering with the product and cheating; enhancing the traceability of the product; and acquiring real time information about how the product is faring on the market (Bassoli, 2018). There are various techniques of marking and storing information on products such as adhesive stickers (barcodes, icons etc.) and RFID tags. The former can easily be detached from the product while the later suffers from interference of signals, metal and water (Bassoli, 2018). There is therefore the need to provide permanent, robust and durable alternative methods of marking and identifying products even when exposed to harsh weather conditions throughout its supply chain and full life cycle. Direct part marking (DPM) has sought to solve these aforementioned problems. DPM is a permanent way of imprinting information in the form of barcodes, numbers, dates and logos directly on the surface of a product (Wang and Madej, 2014; Denkena et al., 2016; Li et al., 2016; Ventura et al., 2016; He and Joseph, 2017; Bassoli, 2018). Laser marking or etching or branding is the most popular of DPM. Laser marking provides a high contrast and a permanent mark on the surfaces of the products such as metal, wood, ceramics and glass (Li et al., 2016; Bassoli, 2018). Laser marking to provide a permanent tag on agricultural products has increased tremendously in recent years due to its long term environmental efficiency in energy, plastic, carbon dioxide emissions and profitability (Pullman, 2017). Products such as vegetables (e.g. onion, tomato or pepper), fruits (e.g. citrus, avocado or apple), eggs, flowers and beaks of chickens have been marked by researchers (Table 3-1). Also marketing strategies focus since several years on laser marking on apples using UV laser systems (Becker, 2015). DPM together with 2D barcodes such as Quick Response (QR) and Data Matrix (DM) codes are usually used for marking

products (Li et al., 2016). Data Matrix codes are used extensively in DPM because of its property of storing data in two directions unlike 1D barcodes. Also, DM codes are robust and not susceptible to printing defects on the products like 1D barcodes (GS1, 2018; MVTec, 2018).

Unlike in other industries where products tend to be uniform in colour, size and shape, in the agricultural and horticultural industry this is a big challenge. Agricultural products of the same variety or species come with different sizes, shapes and colours (Kondo, 2010). These problems along with other factors such as the type of skin, water content in the product and variance within the products make it difficult in directly marking barcodes on agricultural products. The main factors influencing decoding of 2D barcodes on directly marked products in horticulture are laser energy, laser power, contrast, print growth, barcode size and edge length of the barcode. Print growth is simply the growth or shrinkage of the barcode size during marking from its intended target size (Figure 3-1). Although it is not normally considered in horticultural production, it is very important when considering using low and high laser energy. As the size of DM code shrinks or grows, its readability and quality becomes sensitive to print growth (Li et al., 2016). Print growth is divided into three stages: shrinkage (< 100% where the pattern marked is incomplete), perfect (equal to 100%) and growth (> 100% where there is increase in the barcode size and burning of the edges of the barcode) (Jangsombatsiri and Porter, 2006, 2007; GS1, 2015; Li et al., 2016). The heat affected zone (HAZ) affects the print growth of small size modules and bigger ones (Li et al., 2016). Also, a small HAZ will lead to shrinkage at the edges of big DM codes as enough heat is required to complete the marking. According to literature some work has been done on the effect of laser energy and power on readability of DM codes (Table 3-1) but at high marking energies. Laser markings of apples with lasers powers of 5-10 W ($0.19-0.38 \text{ J mm}^{-2}$) by Marx et al. (2013) resulted in decreased detection and reduction in the quality of the laser markings due to increase carbonization, browning and ablation in the heat affected zone. Therefore, they proposed that for future work markings should be carried out with energies less than 0.19 J mm^{-2} as low laser energies reduce the risk of tissue shrinkage, water loss and risk of infection.

Barcode size is another very important factor in successful decoding of marked DM code on horticultural and biological products. Fröschle et al. (2009) applied 10×10 and 12×12 DM codes on frozen matured chicken beaks and proposed that readability of 10×10 DM codes produced the best result. Also, Marx et al. (2013) showed that the edge length and spaces between the barcodes are very critical for readability of 2D barcodes. The wider the spaces between the barcode patterns the

better the detection. However, in their study with a small code length, $3 \times 3 \text{ mm}^2$, no information was provided during storage regarding the stability of the code's readability. Also, Nasution and Rath (2015) showed the effect of various DM code size and different modules (6 mm (10×10 modules), 8 mm (12×12 modules), 10 mm (14×14 modules) and 12 mm (16×16 modules)) on readability on Cavendish banana. They showed that as the amount of module in the code increases the readability decreases. Furthermore, the smaller the barcode size, the readability of the code decreases.

Also, a good contrast between the marking and background of the product is required for successful decoding of the barcode (Ventura et al., 2016; Li et al., 2016; He and Joseph, 2017). According to literature, little information is available in detecting laser marked 2D barcodes on horticultural products. Although laser marking and detection of 2D barcodes have been successful on some biological/horticultural products, there has been little information on the algorithms used for the detection of these products. Only Marx et al. (2013) and Nasution and Rath (2017) reported the image processing steps for detecting the Data Matrix codes by using the Halcon software (Halcon 11.0.1, MVTec Software GmbH, Munich, Germany). Marx et al. (2013) detected a simple 2D pattern on rhododendron cuttings and apples. Nasution and Rath (2017) evaluated the readability of DM code on Cavendish banana. Therefore, the objectives of this study were to determine the effect of low laser marking energy on marking by considering its effect on print growth and the effect of barcode size and contrast on the quality and readability of Data Matrix codes on an important horticultural product like apples. To determine the effect of the stability of the barcode size on detection during storage the same module size (10×10 modules) but with different DM codes with edge lengths (8 mm and 10 mm) (Figure 3-1) were used.

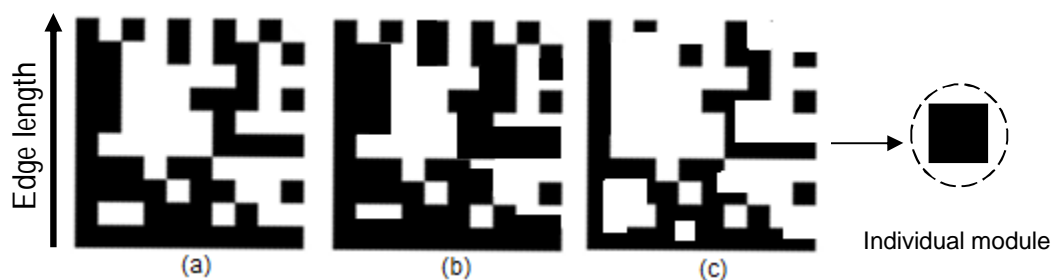


Figure 3-1: ECC200 Data Matrix code encoded with 123456 showing: (a) perfect marking (b) growth of the barcode (c) shrinkage of the barcode and the individual module

Table 3-1: State of the art of laser parameter investigations and applications on horticultural/biological products

Parameters			Products	Literature
Laser energy	Laser power	Barcode Size		
●			Fruits, Vegetables, Eggs, Wood etc.	
●			Lemon, orange	Drouillard and Kanner (1997)
●			Citrus fruits, green pepper, apple, peach, tomato, onion, plum, kiwi, pears	Drouillard and Kanner (1999)
●			Scots pine	Barcikowski et al. (2006)
●			Tomato, avocado, oranges, potatoes, pepper, cucumber	Etxeberria et al. (2006)
●			Lemon, orange	Heck et al. (2007)
●			Apple, watermelon	Longobardi (2007)
●			Tomato	Yuk et al. (2007)
●			Grapefruit, tangerines	Sood et al. (2008)
●			Avocado, pumpkin, tomato	White (2008)
●			Lemon	Etxeberria et al. (2009)
		●	Chicken beaks	Fröschle (2009)
●			Grapefruit	Sood et al. (2009a)
●			Grapefruit, tangerine, tomato and pepper	Sood et al. (2009b)
●			Tomato	Danyluk et al. (2010)
●			Eggs	Griffiths et al. (2011)
●			Chicken beaks	Mc Inerney et al. (2011a)
●			Chicken beaks	Mc Inerney et al. (2011b)
●			Eggs	Parker (2011)
●			Citrus fruits	Danyluk et al. (2013)
●		●	Apple, rhododendron cuttings	Marx et al. (2013)
●			Citrus leaves	Etxeberria and Gonzalez (2014)
	●	●	Cavendish banana	Nasution and Rath (2015)
●			Coconut	Zighelboim (2015)
●			Citrus leaves	Etxeberria et al. (2016)
●			Apple and banana	Hoult, (2017)
	●	●	Cavendish banana	Nasution and Rath (2017)
●			Citrus fruits	Chih-Hsing et al. (2019)

3.2 Materials and methods

3.2.1 Effects of laser energy and print growth on markings and detection on Golden Delicious and Kanzi

In the first experiment to determine the effect of laser energy and print growth on laser marking and detection, two varieties of apples (*Malus domestica*) 'Golden Delicious' and 'Kanzi' purchased from a local grocery supermarket were used. The products were stored at a room temperature of 16-17 °C and relative humidity of 62% to see the rate of deterioration during storage. Seven laser powers were used for marking a Data Matrix code size (8 × 8 mm², (64 mm²)). Therefore, seven laser energies were used for marking the apples (Table 3-2). On an average it took 0.110 s per module to mark the barcode size of 8 × 8mm². The apples were stored for 10 days. Twenty replications were done for each laser marking energy. Two fruits were chosen for each energy level and 10 replicates per fruit were marked.

Table 3-2: Laser energy (Joules per module) applied on Golden Delicious and Kanzi based on laser power (W) and marking time (s per module)

Laser power (W)	Energy (J)
	Code size 8 × 8 mm ² t ₁ = 0.110 s
p ₁ = 0.50	p ₁ t ₁ = 0.055
p ₂ = 0.57	p ₂ t ₁ = 0.063
p ₃ = 0.64	p ₃ t ₁ = 0.070
p ₄ = 0.70	p ₄ t ₁ = 0.077
p ₅ = 0.77	p ₅ t ₁ = 0.085
p ₆ = 0.84	p ₆ t ₁ = 0.092
p ₇ = 0.91	p ₇ t ₁ = 0.100

3.2.2 Effect of barcode size and contrast on laser marking and detection on Golden Delicious and Red Jonaprince

Two varieties of apples ‘Golden Delicious’ and ‘Red Jonaprince’ from the storage room of the Department of Fruit Science, University of Applied Sciences, Osnabrück, Germany were used for the second experiment involving the effects of barcode size and contrast on laser marking and detection. The products were stored at a cold temperature of 20 °C and relative humidity of 78%. These apples were chosen due to the difference in their background colours. On an average it took 0.154 s per module to mark Data Matrix code (10 × 10 mm², (100 mm²)). The products were stored for 10 days. Two fruits were chosen for each energy level and 10 replicates per fruit were marked. Therefore, twenty replications were performed for each laser marking energy. Table 3-3 below shows the laser energy (J per module) used for the experiment for both barcode sizes.

Table 3-3: Laser energy (Joule per module) applied on Golden Delicious and Red Jonaprince based on the laser power (W) and marking time (s per module)

Laser power (W)	Energy (J)	
	Code size (8 × 8 mm ²) t ₁ = 0.110 s	Code size (10 × 10 mm ²) t ₂ = 0.154 s
p ₁ = 0.50	p ₁ t ₁ = 0.055	p ₁ t ₂ = 0.077
p ₂ = 0.57	p ₂ t ₁ = 0.063	p ₂ t ₂ = 0.088
p ₃ = 0.64	p ₃ t ₁ = 0.070	p ₃ t ₂ = 0.099
p ₄ = 0.70	p ₄ t ₁ = 0.077	p ₄ t ₂ = 0.108

3.2.3 Laser setup

The laser tests were carried out in the Laboratory of the Department of Biosystems Engineering, University of Applied Sciences Osnabrück, Germany. The experimental setup similar to Marx et al. (2013) was used for all the experiments (Figure 3-2). The laser (Synrad 48-5 carbon dioxide, Synrad Inc., Mukiltoe, USA) with wavelength 10600 nm, output power 50 W, speed 380 mm/s and SH3-200C marking head controlled by a PC (personal computer) and the laser marking software (WinMarkPro®, Synrad Inc., Mukiltoe, USA) with the following laser marking parameters (Table 3-4 see Appendix V) was used for shooting the ECC200 Data Matrix codes onto the apples. Based on the

GS1 Data Matrix code symbol attributes (square form), 10×10 modules were used for marking the apples. The Data Matrix code was shot onto the products 246 mm away from the laser marking head. The number 123456 was encoded on the DM code for marking based on the maximum data capacity of both the numeric and alpha-numeric data of the module that was selected. The DM code was designed and saved in a bit map format at 45° angle to ensure better marking on the product.

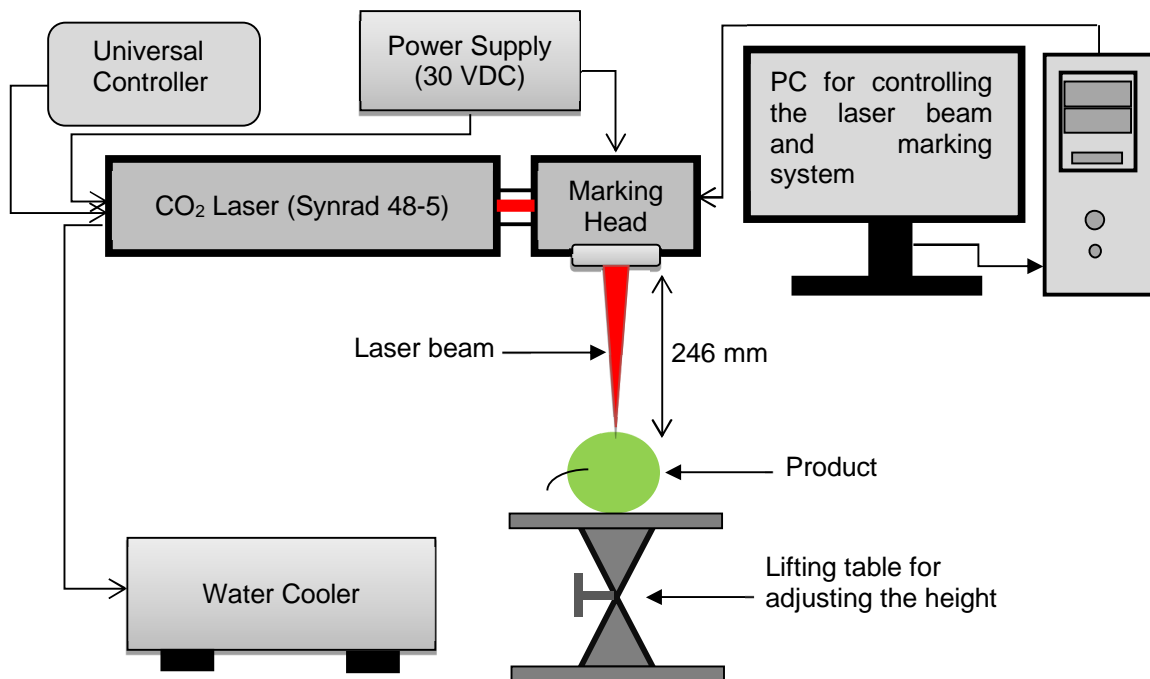


Figure 3-2: Laser marking experiment setup showing the CO₂ laser, marking head, product positioning and computer-based control

Table 3-4: Laser marking parameters for marking the ECC200 Data Matrix code on the apples

Marking Parameters	Value
Velocity ¹ (mm/sec)	381
Resolution ² (dots per inches)	1000
Pline Start Delay ³ (µsec)	100
Pline End Delay ⁴ (µsec)	450
Interseg Delay ⁵ (µsec)	350
Off Vector Delay ⁶ (µsec)	300
Bi-Directional Raster ⁷ (Yes/No)	Yes
Interseg Break Angle ⁸ (°)	30
Off Vector Velocity ⁹ (mm/sec)	1905
Off Vector Resolution ¹⁰ (dots per inches)	300
Raster Scan Direction ¹¹ (horizontal/vertical)	Horizontal

¹ **Velocity:** The marking speed (X-Y optical scanner speed) of the object. It determines how fast the galvanometer moves and how fast each microvector is marked.

² **Resolution:** The minimum galvanometer step distance or microvector. This affects how the markings appear. A small resolution increases the marking time but results in poor marking of the object while a bigger resolution delays the marking time but results in better marking of the object.

³ **Pline Start Delay:** The delay at the beginning of a polyline (or series of polylines) that compensates for the time difference between the laser firing and the actual movement of the mirror. It reduces hotspots (dwells) at the beginning of a polyline or a series of polyline.

⁴ **Pline End Delay:** The time delay between the target and the actual mirror position at the end of a polyline (or series of polylines). It ensures that a polyline is completed before moving unto the next one by maintaining the right beam at the end of a polyline or series of polylines.

⁵ **Interseg Delay:** The time delay between the target and the actual mirror position of two connecting on-vectors. It connects polylines when the end point of one polyline is the start of the next polyline in the object by setting a delay between them. The sharpness of the points where the polylines are connected is increased by Interseg Delay.

⁶ **Off Vector Delay:** The time delay between the target and the actual mirror position of an off-vector connecting to an on-vector. It is used to set a proportional delay to remove "tails" i.e., extension of polylines when moving between non-connected polylines during all laser off-vector moves.

⁷ **Bi-Directional Raster:** Shows if the scanlines will be marked in both directions (top/bottom, left/right) when marking a raster fill or bitmap. It can increase the marking speed when enabled.

⁸ **Interseg Break Angle:** The break angle between two connected polylines. If the angle between the polylines is greater than break angle, Interseg Delay is used. However, when the angle between two marked polylines is less than the specified angle Interseg Break Angle is not used.

⁹ **Off Vector Velocity:** The velocity at which the galvanometer moves between line segments.

¹⁰ **Off Vector Resolution:** The resolution used when making laser-off moves in dots per inch.

¹¹ **Raster Scan Direction:** Shows the direction in which the markings should be done whether horizontally or vertically.

3.2.4 Image acquisition and processing of the Data Matrix code

The proposed algorithm (Figure 3-3) for decoding the laser markings was divided into two phases (preprocessing and detection phases). For the ECC200 Data Matrix codes the main aim was to find the 'L' shape pattern which runs down from the left hand side and across the bottom perimeter cells of the code on the fruit (Figure 3-1a). At the beginning, images of the Data Matrix code marked on the products were acquired using a camera (Canon EOS Digital Rebel XSI/450D with a zoom lens of EF-S 18-55mm, f3.5-5.6 IS). The images were acquired under lighting conditions using 3 Osram L 18 W 840 Lumilux 59cm – Cool White fluorescent tubes (Osram GmbH, Munich, Germany). The image processing software (Halcon 11.0.1, MVTec Software GmbH, Munich, Germany) was used in analyzing the images. Having acquired the images, the marked areas were filtered to reduce noise in the background of the image. A gray value opening of the image with a 7×7 rectangular mask was performed on the images. Smoothing of the image to reduce noise and suppress unwanted objects was then done using the 3×3 Median filter. The image was then transformed from the three channel RGB colour space to the HSV colour space (see Halcon 11.0.1, MVTec Software GmbH, Munich, Germany). The most useable channels S and V were then selected and combined by pixelwise averaging. The S and V image channels were selected. The edges of the image were then detected using the 3×3 Sobel operator (Equation 3.1) (Jähne et al., 1999; Marx et al., 2013). Hough transformation was then performed to connect the lines at the edge of the image by using local gradient direction and returning them in the normal form. Hough transform allowed the mapping of all the possible straight lines through a minimum number of 10 points at an angle resolution of 1° (an allowed direction of uncertainty of 2°) using a Gaussian filter of size 5×5 to smooth the image to detect all possible edge points of the laser markings that lie along the straight line of the image (Duda and Hart, 1972; Marx et al., 2013).

The images were further processed using mathematical morphological operators (region growing, closing, connection, select shape, union, and opening). The next step was to ensure that rotation of the image was performed in the right direction by ensuring that a right handed coordinate system for the image was obtained. Therefore, affine transformation was performed to preserve the points and straight lines of the image. Dilation was also performed on the transformed region of the image to close the gaps between the smaller and the bigger spaces in the boundaries of the image. The shape

and size of the region of interest was maintained by performing a rigid affine transformation using a rotation and a translation vector, from a point and two corresponding angles.

Finally, the images were detected using the shape-based matching algorithm by performing scaling, rotation, translation and affine transformation on the image (Figure 3-3). A score of one was given when the algorithm detected the Data Matrix code and zero if it was not detected. The success of matrix detection was based on the formula below (Equation 3.2).

$$Gx = \begin{bmatrix} 1 & 2 & 1 \\ 0 & 0 & 0 \\ -1 & -2 & -1 \end{bmatrix} \quad \text{and} \quad Gy = \begin{bmatrix} 1 & 0 & -1 \\ 2 & 0 & -2 \\ 1 & 0 & -1 \end{bmatrix} \quad (3.1)$$

Where,

Gx = the mask in the x direction

Gy = the mask in the y direction

$$S = \frac{D}{n} \times 100 \text{ (\%)} \quad (3.2)$$

where,

S = Success

D = Detection

n = Replication (20)

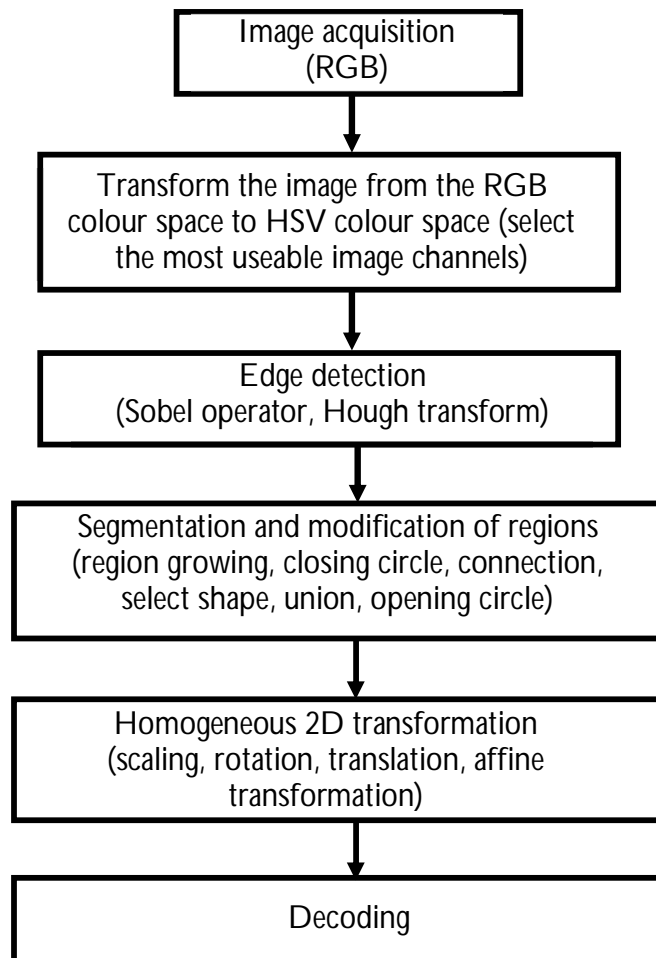


Figure 3-3: Flow chart showing the proposed image processing algorithm and for the shaped based matching algorithm for decoding the laser images on the apples. (see also Halcon 11.0.1 Documentation)

3.3 Results and discussion

3.3.1 Effects of laser energy and print growth on markings and detection on Golden Delicious and Kanzi

Figure 3-4 shows the effect of increasing laser energy and days of storage on successful decoding of Data Matrix code on Golden Delicious and Kanzi. There was a 100% decoding for Golden Delicious at 0.070 J mm^{-2} for all the 10 days of storage. Generally, there was rather low success with Kanzi. The laser energy either resulted in low print growth/shrinkage i.e. incomplete marking of the DM or no printing of the DM on the apples (Figure 3-6). There was no marking of the DM at the lowest marking energy because the heat affected zone temperature was insufficient for oxidation reactions to occur and for a high contrast module of the DM code to appear on the apples (Ventura et al., 2016; Li et al., 2016). At the last two energies ablation, carbonation and browning in the heat affected zone resulted in shrinkage and poor quality of the marking (Marx et al., 2013; Li et al., 2016) (Figure 3-5). Shrinkage occurred for all the products that were marked with the highest energy level (Figure 3-4 & 3-5). Due to various factors such as barcode size, laser energy, variety and skin surface properties of the product, it is unavoidable that there will be some shrinkage or growth of the DM code during the marking process (GS1, 2015). Shrinkage leads to failure in readability of the barcodes as the "L" finder pattern of the Data Matrix code could not be decoded.

In both apples, the energy and the skin affected the print growth, with the highest energy resulting in an increased shrinkage. The shrinkage of the markings can be attributed to insufficient power at the end of the marking (Marx et al., 2013; GS1, 2015; Li et al., 2016). Furthermore, the effect of print growth on DM code can be attributed to the inertia of the laser beam. The speed of the initial and final stages of travel of the laser beam is slower than what was set for marking. Therefore, the laser beam works at a speed lower than what was set when the travel of the beam is short (Synrad 2012; Li et al., 2016). When Nd:YAG Q-switched lasers are used in marking of DM the first pulses are always more powerful than the later ones resulting in a deeper and wider marking in the initial stages (Li et al., 2016). Our experiments using CO₂ laser also reported the same phenomenon during the marking process where the inertia of the energy from the laser beam at the initial stage of travel was higher than at the final stage of travel (Synrad, 2012). This is the cause of the shrinkage of the DM codes on the products. Also, according to Jangsombatsiri and Porter (2007), the direction of the print growth

(X or Y-axis) has a significant effect on the quality of the DM code. They reported that the print growth in the X-axis had more effect on the quality and final grade of the DM code than the print growth in the Y-axis. In contrast, our experiments showed that the marking of the DM code in the Y-axis had a critical effect on the final marking and quality of the DM code than the marking of the DM code in the X-axis.

Furthermore, during storage of the apples, ripening occurs resulting in increased ethylene production and rise in cellular respiration as the days of storage increased. Increased oxidation occurs around the marked area of the apples with the DM code resulting in a browning and better contrast of the marking as the days of storage increases. According to Nasution and Rath (2017), laser power and time is responsible for producing high contrasts in the DM codes on Cavendish banana. They showed that the contrast values increase as the days of storage increased. In our experiment, as the days of storage increased decoding of the barcodes for Golden Delicious (Figure 3-4) increased due to a better contrast between the marking on the yellowish green skin whereas that of Kanzi decreased due to a decrease in contrast of the markings on the deep reddish yellow skin (Figure 3-5).

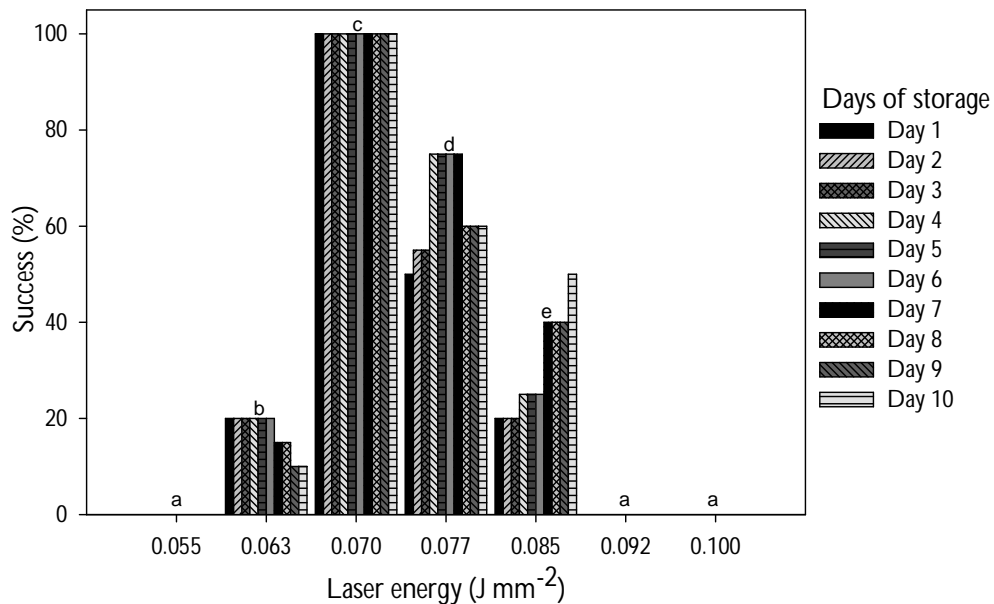


Figure 3-4: Effect of energy and days of storage on successful decoding of Data Matrix code on Golden Delicious, n = 20, (using Tukey Multiple Comparison test, $\alpha = 0.05$)

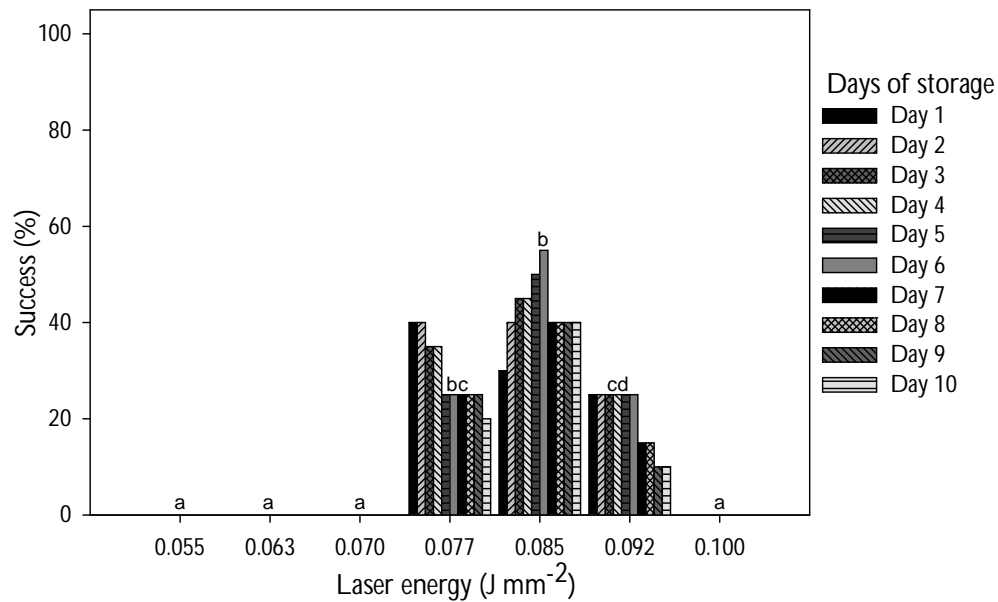


Figure 3-5: Effect of energy and days of storage on successful decoding of Data Matrix code on Golden Kanzi, n = 20 (using Tukey Multiple Comparison test, $\alpha = 0.05$)

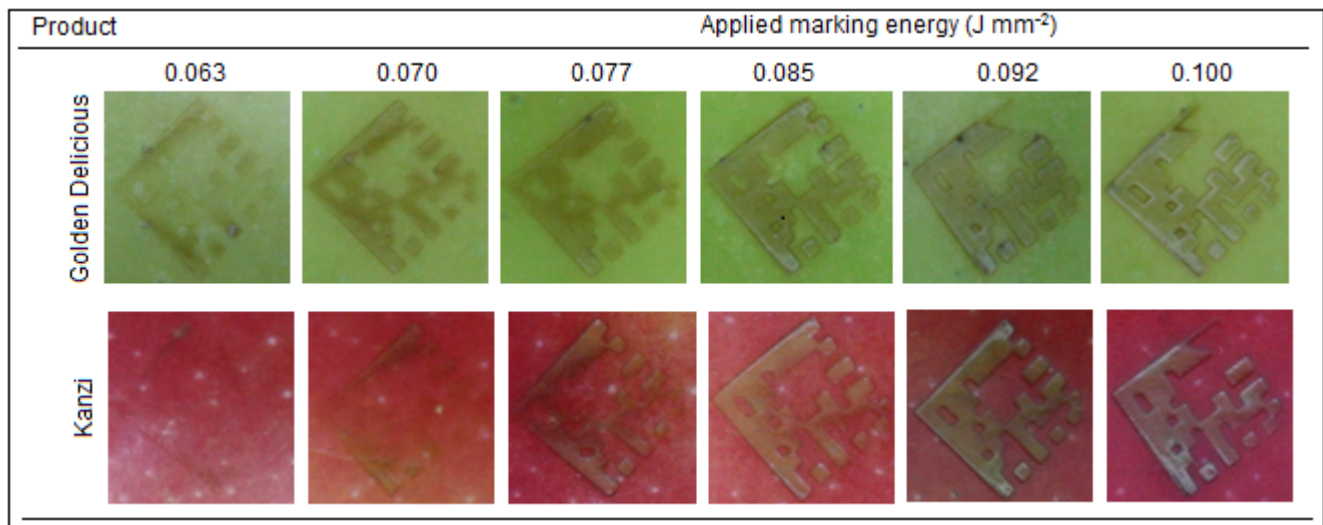


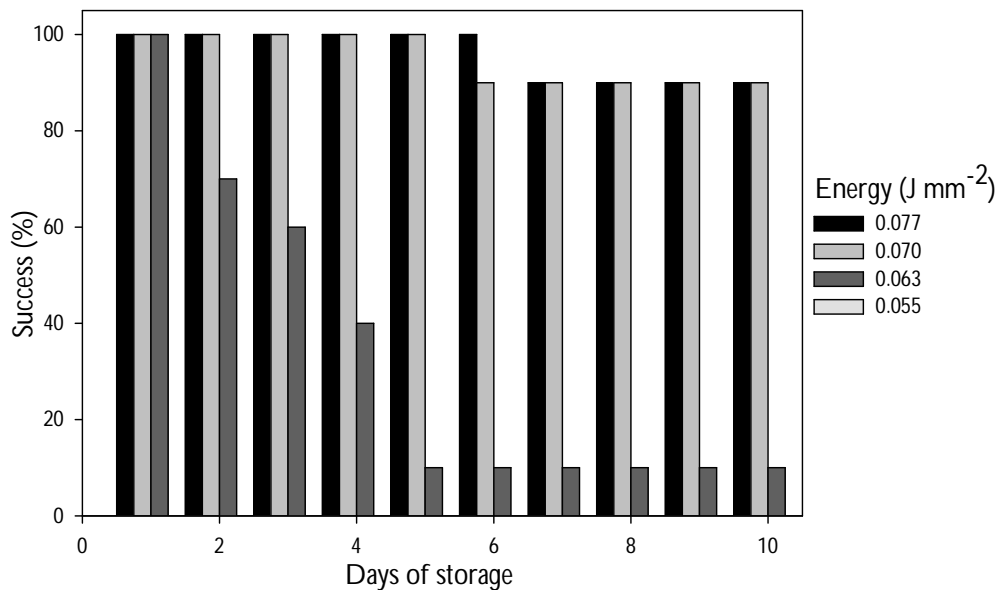
Figure 3-6: Effect of increasing marking energy on printing of Data Matrix code on the skin of Golden Delicious and Kanzi

3.3.2 Effect of barcode size and contrast on DM readability on Golden Delicious and Red Jonaprince

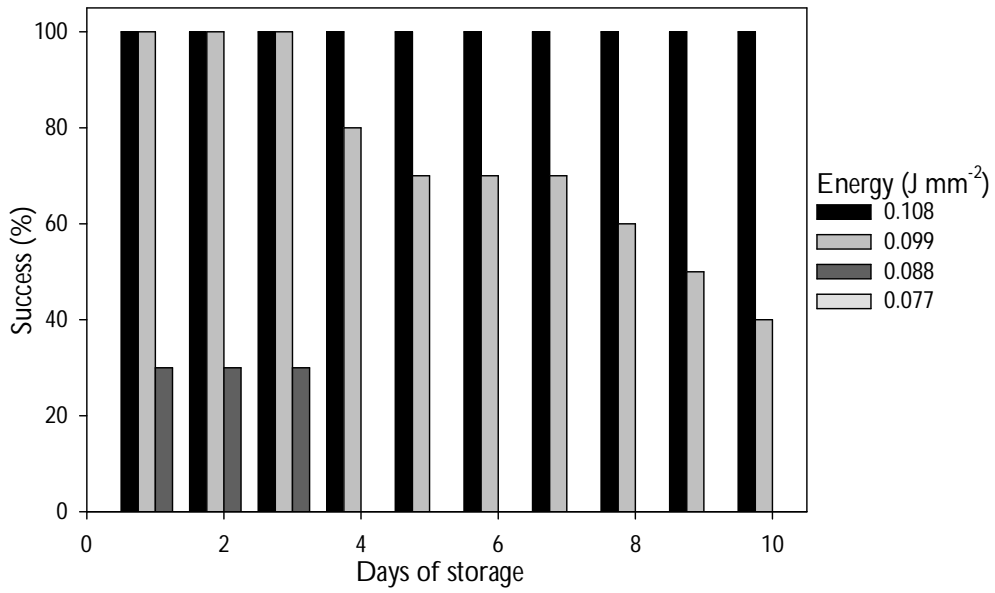
The comparison between the effect of energy and barcode size on detection after ten days of storage showed that there was very good detection for both barcode sizes of Golden Delicious. There was rather a poor detection for Red Jonaprince with detection only at the highest marking energy for both barcode sizes (Figure 3-7). This can be attributed to the contrast between the markings on both apples. A significant contrast between the colour of the apple and the laser markings is necessary for successful decoding of the barcode (Wang and Madej, 2014; Ventura et al., 2016; Li et al., 2016; He and Joseph, 2017; Bassoli, 2018). In order to reduce interference of noise and distinguish between the dark and light elements of the markings, strong contrast is needed to create a strong signal. This also results in an increased chance of decoding the barcode at even longer distances (Bassoli, 2018; GS1, 2018). Therefore, the better detection of the markings on Golden Delicious can be attributed to the better contrast between the Data Matrix code and the yellowish green colour of the Golden Delicious as the days of storage increased. Moreover, the poor detection of the Red Jonaprince is due to the weak contrast between the Data Matrix code and the dark reddish colour of the Red Jonaprince as the days of storage increased (Figure 3-7).

Also, the choice of marking energy to successfully decode the DM code depends on the product. An increase in marking energy leads to carbonisation, ablation and browning in the heat-affected zone as a result of increased rate of water loss from the apples, which negatively affects the decoding of the barcode (Marx et al., 2013). Therefore, the low energy levels used resulted in the markings being visible on the next day. However, there was no marking at the lowest energies for both barcode sizes due to insufficient energy for oxidation reaction to occur on the surface of the apples (Li et al., 2016). However, as the laser marking energy increased, oxidation reactions on the skin of the apples was caused by the heat from the laser leading to carbonisation, ablation and browning (Marx et al., 2013; Li et al., 2016). According to Marx et al. (2013), increase in the laser marking energy affected the decoding of the correctly shaped patterns one day after marking. In our experiments there was a better detection at the highest marking energy and bigger barcode size for ten days (Figure 3-7b).

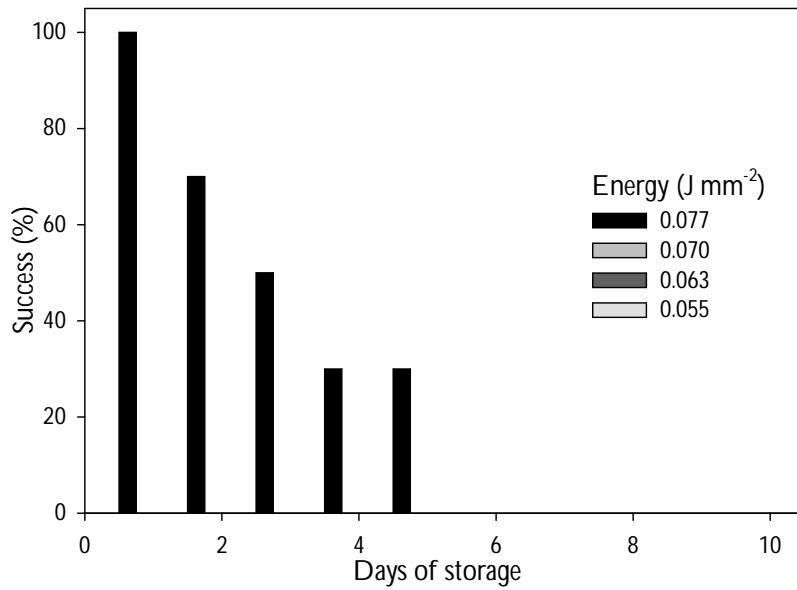
Furthermore, the barcode size played a very significant role in successful detection of the barcode (Marx et al., 2013; Nasution and Rath, 2015; Li et al., 2016). Marx et al. (2013) suggested that an increase in the minimum pattern size for marking apples was 3 mm. An increase in the pattern size of apples led to a better marking and decoding as the minimum distance between the modules increased. Based on the detection at the various sizes of our experiment, marking at a barcode size $10 \times 10 \text{ mm}^2$ more energy was used compared to $8 \times 8 \text{ mm}^2$. This resulted in a better detection of the DM code at $10 \times 10 \text{ mm}^2$ for Golden Delicious at the highest marking energy for 10 days (Figure 3-7b). However, this resulted in increased ablation, carbonisation and browning in the heat affected zone. Furthermore, with the subsequent lower energies, there was a better detection with barcode size $8 \times 8 \text{ mm}^2$ compared to $10 \times 10 \text{ mm}^2$ (Figure 3-7a). Since the aim is to minimize the effect of heat damage on the skin of the apples, barcode size $8 \times 8 \text{ mm}^2$ is recommended for marking as it also resulted in 100% detection for 6 days at 0.077 J mm^{-2} for Golden Delicious (Figure 3-7a).



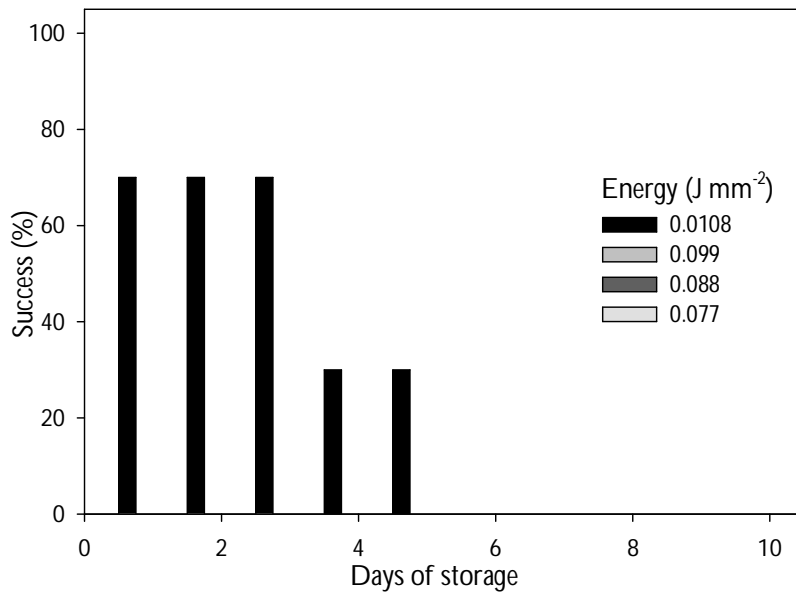
a) Code size $8 \times 8 \text{ mm}^2$ (64 mm^2), Golden Delicious



b) Code size 10 × 10 mm² (100 mm²), Golden Delicious



c) Code size 8 × 8 mm² (64 mm²), Red Jonaprince



d) Code size $10 \times 10 \text{ mm}^2$ (100 mm^2), Red Jonaprince

Figure 3-7: The effects of energy and barcode size on Data Matrix code detection on Golden Delicious and Red Jonaprince ($n = 20$ for both apples)

3.4 Conclusion and outlook

The findings of this research are that laser energy, barcode size, print growth, type of product, contrast between the markings and the colour of the products, the inertia of the laser system and the days of storage all singularly or in combination with each other influence the readability of laser DM codes and implementation on apples.

- The proposed algorithm is currently only working successfully on Golden Delicious with 100% detection for 10 days at energy 0.108 J mm^{-2} using a barcode size of $10 \times 10 \text{ mm}^2$. The contrast between the markings and skin resulted in a better detection for Golden Delicious than Red Jonaprince and Kanzi.
- High laser marking energy resulted in ablation, browning and carbonisation which decreased detection of the Data Matrix code.

- The bigger barcode size $10 \times 10 \text{ mm}^2$ had better detection as a result of higher energy being used in marking. However, since this resulted in ablation, carbonisation, and browning of the heat affected zone on the skin, the smaller barcode size $8 \times 8 \text{ mm}^2$ is recommended as it gave a better marking at the lower marking energies.
- The working direction of the laser beam affected the print growth of the DM code as the energy of the laser beam at the initial marking stage was higher than at the final stage.
- Finally, oxidation around the marked DM code resulted in better contrast of the markings as the days of storage increased resulting in better detection of the DM code for Golden Delicious.

It has to be stated that the experiments were done with a CO_2 laser because of the high absorption of laser energy within the infrared waveband. Therefore, one should be careful to transfer the results to other laser wavelengths and configurations especially usage of classical marking lasers in the UV or blue waveband. Nevertheless, successful detection of Data Matrix code on horticultural products is still a challenge because in our experiments only Golden Delicious had successful detection. More marking systems with different wavelengths, laser beam parameters and energy settings, more varieties of apples and other horticultural products have to be analysed with the proposed algorithm to see its performance in the near future.

Chapter 4

Comparison of manual and automatic barcode detection in rough horticultural production systems

Felix Eyahanyo¹, Thomas Rath²

¹*Leibniz University of Hannover, Institute of Horticultural Production Systems, Biosystems Engineering Section, Herrenhäuser Straße 2, 30419 Hannover, Germany;* ²*University of Applied Sciences Osnabrück, Biosystems Engineering Laboratory (BLab), Oldenburger Landstraße 24, 49090 Osnabrück, Germany)*

¹*Corresponding author.* Leibniz Universität Hannover, Institute of Horticultural Production Systems, Biosystems Engineering Section, Herrenhäuser Straße 2, 30419 Hannover, Germany. Tel.: +49 511 762 5344; Email: eyahanyo@bgt.uni-hannover.de (F. Eyahanyo)

Published in: International Journal of Agricultural and Biological Engineering (2019), DOI: 10.25165/j.ijabe.20191206.4762

4.1 Abstract

Automation of production in the nurseries of flower producing companies using barcode scanners have been attempted but with little success. Stationary laser barcode scanners which have been used for automation have failed due to the close proximity between the barcode and the scanner, and factors such as speed, angle of inclination of the barcode, damage to the barcode and dirt on the barcode. Furthermore, laser barcode scanners are still being used manually in the nurseries making work laborious and time consuming, thereby leading to reduced productivity. Therefore, an automated image-based barcode detection system to help solve the aforementioned problems was proposed. Experiments were conducted under different situations with clean and artificially soiled Code 128 barcodes in both the laboratory and under real production conditions in a flower producing company. The images were analyzed with a specific algorithm developed with the software tool Halcon. Overall, the results from the company showed that the image-based system has a future prospect for automation in the nursery.

Keywords: *automation, barcode detection, horticultural production systems, image processing, barcode scanners*

4.2 Introduction

Automation of production systems has always been sought and encouraged in horticulture, logistics and many other fields to increase production, productivity and profitability. Automatic Identification Data Capture (AIDC) are technologies that have been developed to replace manual data collection and to provide an accurate, quick, and efficient means of capturing and storing data (Singh et al., 2014; Borgohain et al., 2015; Trappey et al., 2017). There are several types of AIDCs and these include barcodes, Radio Frequency Identification (RFID), magnetic stripes, smart cards, biometrics and optical character recognition. Barcodes are the most common of the AIDCs that have been used over the last 5 decades (Kurtz et al., 2007, Bodnár et al., 2018). Barcodes are simply the machine-readable vertical black strips with white spaces which are printed and found on most products (Creusot and Munawar, 2015; Chen et al., 2017; Chowdhury et al., 2019). Advancement in barcode technology has led to two-dimensional (2D) barcodes being developed (Mehta, 2015, Dutta et al., 2016; Bodnár et al., 2018). Barcodes have been used extensively in horticultural production systems to help solve the problem of laborious and time consuming process of manual data entry and capturing information on plants and products to which they are attached (Youssef and Salem, 2007; Creusot and Munawar, 2015). Flower producing companies mainly use barcodes in their production to track planting trays containing flowers and cuttings, gather information on the availability and re-ordering of planting stock, store information on the planting stock for planting and distribution. Furthermore, at the points of sale (POS) barcodes are used to check theft and speed up sales (Kondo, 2010; David et al., 2015; Zhou and Guo, 2016). All these practices with barcodes are done manually using a laser barcode scanner. For the flower producing companies it is important to have the barcode data so as to know how they are faring in their production process and where to make changes and improvements.

However, full automation in the area of planting flower cuttings in greenhouses is still a big challenge as the conventional systems of using laser barcode scanners are still being employed. These barcode scanners require a line of sight for identification. Therefore, one has to get close to the barcodes with the scanner before the sensor can generate a reading. Also dirty, damaged, faded and multiple barcodes cannot be read or are difficult to read and there is also the risk of losing some barcodes in the production process (Hong-Yuan et al., 1995; Pihir et al., 2011; Hansen, 2012; Fang et al., 2012; Mehta, 2015; Şimşekli and Birdal, 2015; Dutta et al., 2016). Furthermore, attempts to use barcodes to track trays in large nursery production systems have failed as soil and water often covered the barcodes

making it dirty and hence preventing successful scanning. Also, the growth of the plants leads to an increase in the crop canopy which sometimes covers the barcodes, resulting in reduction in successful barcode scans and thereby making identification difficult (Curry, 2010; Swedberg, 2010).

Over the years several barcode recognition methods have been developed to help in the processes of automation and detection. There are different localization and re-identification methods based on accuracy and speed. However, there are problems associated with each different type of barcode and as such there is the need for continuous and effective solutions for improved barcode localization. High speed processing activities such as automated production and conveyor belts where a missed detection results in loss of profit requires automatic barcode detection with great accuracy (Katona and Nyúl, 2013; Chowdury et al., 2019). Different image processing methods and techniques have been used to decode barcodes in the last four decades. Hough transform (Youssef and Salem, 2007; Dwinell et al., 2012; Zamberletti et al., 2015) or Mathematical methods like morphological operations involving extraction of various texture-like properties of the image for detection such as erosion, dilation, opening, closing, etc. (Juett and Qi, 2005; Tuinstra, 2006; Bodnár and Nyúl, 2012; Dinesh et al., 2013) have all been used successfully in decoding barcodes. However, these methods have been used mostly in combination with each other. In recent years deep learning and artificial intelligence is increasingly being used to localize and decode barcodes. A machine learning algorithm to create a classifier by using the support vector machine with Hough transform has been used to for barcode detection (Wang et al., 2016). Creusot and Munawar (2016) have employed a method called Parallel Segment Detector which uses Maximal Stable Extremal to find the black stripes in the barcode and Hough transform to detect the vertical line of the barcode. Also, Chen et al. (2017) used Parallel Line Segment Detector with basic morphological operations to decode barcodes in real-time. Li et al. (2017) proposed the detection of one-dimensional (1D) barcodes using deep convolutional neural networks. Furthermore, Zhang et al. (2018) used SSD network which is based on forward-propagating convolutional neural network with Hough transform to detect 1D and Data Matrix code in real time. Moreover, Bodnár et al. (2018) also used conventional and deep rectifier neural networks for 1D and 2D barcode localization. Chowdury et al. (2019) used Zamberletti algorithm to detect multiple 1D and 2D barcodes from a snap. Most of these methods have tried to localize barcodes in real-time when the images are stable and not in motion. In summary, according to literature and practice: speed, dirt, moisture, uneven illumination and complex background hinder successful barcode detection. Therefore, there is a need to find appropriate solutions to overcome these problems.

The objective of this research was to provide a robust system for successful automatic detection of barcodes in horticultural production. This was achieved by comparing a hand-based barcode laser detection system to an image-based barcode detection system to know which provides more reliable, stable and fast results under various conditions. We proposed a new image processing algorithm for robust barcode detection and evaluation using Halcon. Also, shading and lighting system was constructed on the conveyor system to prevent interference of outside light on detection of the barcodes. For evaluation of the proposed system, experiments were conducted under real horticultural production conditions in a flower producing company (Brandkamp GmbH, Isselburg-Anholt, Germany).

4.3 Materials and methods

In the experiments conducted, two types of barcodes were chosen (technical definition: Code 128). One shows the variety, factory week and tray type of the cutting to be planted "Plant Barcode (PB)" (Figure 4-1a) and the other the personal number showing who did the planting, used to trace back to the person in case of any problem during production "Personal Number Barcode (PNB)" (Figure 4-1b). A monochrome USB industrial camera (DMK 41BU02.H, The Imaging Source Europe GmbH, Bremen, Germany) with a CS-IR lens (H3Z 4512, The Imaging Source Europe GmbH, Bremen, Germany) were used for all the experiments. The MVTec Halcon 11.0.1 (CGI Systems GmbH, Seeshaupt, Germany) image processing software was used to decode the barcodes. Statistical analyses for the experiments were done using R-Statistical Package 3.4.4 (<http://cran.r-project.org/>). Confidence intervals of 95% for the difference of proportions were estimated to determine the proportion of successful readings. A Mosaic plot to create a colour chart using ggplot2 (<http://ggplot2.org/>) was done to show the percentage of success and failure in barcode detection. Pairwise comparison tests using the equality differences of proportions were carried out to compare pairs of treatments using Pearson Chi Square test. The raw p-value as well as the adjusted p-values for multiple testing using the Holm method was also performed. Graphs were created using SigmaPlot 12 (Systat Software Inc, USA).

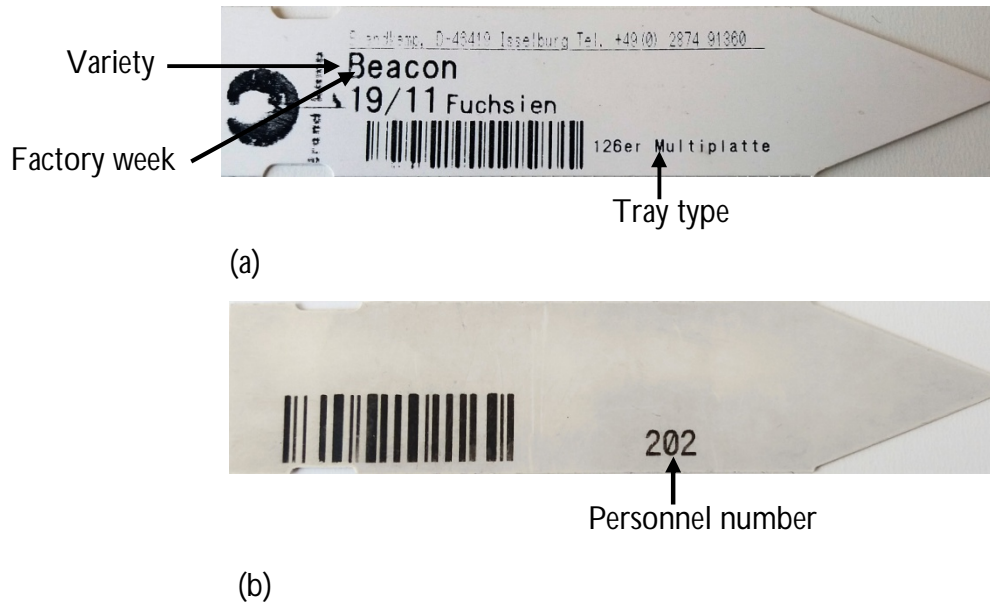


Figure 4-1: (a) Barcode showing tray type, variety and factory week and (b) Barcode showing personnel number

4.3.1 Experimental setup for laboratory and company

For all the experiments at the laboratory of the Department of Biosystems Engineering, Leibniz University of Hannover and the company Brandkamp GmbH, 400 replications were carried out. Experiments were conducted in the laboratory to determine the effects of angle placement and speed on barcode detection. Seven different conveyor belt speeds (0.03, 0.07, 0.11, 0.17, 0.21, 0.26, 0.30 m/s) were used for the clean barcodes experiments in both the laboratory and company. However, for the treatments with dirt and water that was carried out in the company only two speeds (0.11 and 0.15 m/s) were used.

The laboratory experiment setup consists of two parallel conveyor belts on top of which are movable plates. At the ends of the conveyor belts are two opposite rotating plates, which act as a switching function between the two belts (Figure 4-2). The system forms a closed loop with an adjustable front conveyor belt on which a shading system was constructed. The maximum test speed of the system is 0.30 m/s. This was used to determine whether it was possible to automate barcode detection at this speed. The test system was controlled by (SPS Control System, Automation and Construction GmbH, Lübeck, Germany) located in front of the conveyor belt (Figure 4-2). Shading of the image-based

barcode recognition system to reduce the effect of reflection on the barcode detection was done using a black fine-twill viscose material after performing a reflectance experiment on 8 different black materials. Also, 3 Osram L 18 W/840 Lumilux 59cm – Cool White fluorescent tubes (Osram GmbH, Munich, Germany) were used for lighting the system (Figure 2). Only clean PB labels were used in the laboratory experiments.

The second part of the experiments were conducted in the flower producing company (Brandkamp GmbH, Isselburg-Anholt, Germany) to see the effect of speed, dirt and moisture on automation of barcodes in real production conditions. The setup of the company is as shown below (Figure 4-2). Both PB and PNB labels were used for these experiments (Figure 4-1). Fresh cuttings of various flowers such as *Chrysanthemum*, *Impatiens*, *Fuchsia*, etc. are produced in the company. These cuttings are brought in the morning in plastic bags, moistened to keep them fresh and then planted manually in the trays already filled with soil. In practice the barcodes are then scanned while stationary with a Datalogic Memor Mobile barcode scanner (Opal Associates GmbH, Munich, Germany) before they are moved on a conveyor belt. For our experiments an additionally image processing system with camera was installed on the conveyor belt system to read the labels (Figure 4-2). A summary of the test materials and general parameters used for all the experiments are shown below (Table 4-1).

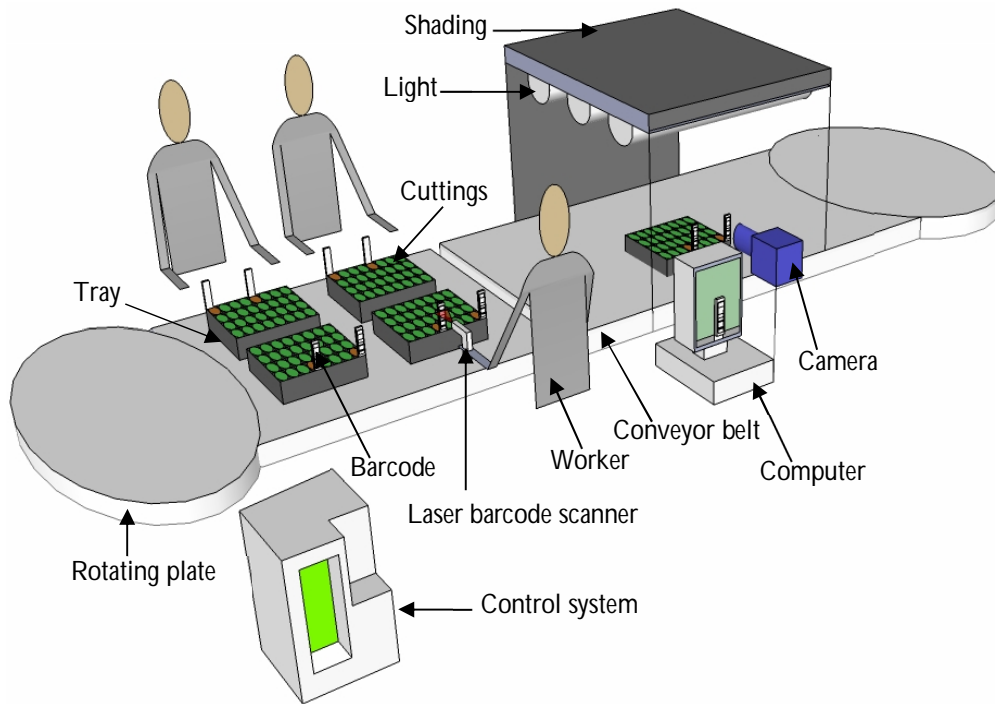


Figure 4-2: Laboratory and company image-based and hand held barcode recognition system

Table 4-1: General parameters and test materials for the experiments

Parameters/test materials	Laboratory Experiment	Company Experiment 1 using Image-based recognition system (speed, bar width and dirt treatments)	Company Experiment 2 using Datalogic Memor X3 mobile computer (speed and dirt treatments)
Speed (m/s)	0.03, 0.07, 0.11, 0.17, 0.21, 0.26, 0.30	0.03, 0.07, 0.11, 0.17, 0.21, 0.26, 0.30	Speed of barcode scanner
Angle of orientation around the <i>x</i> -axis	60°, 75° and 90° *	90°	-
Barcode (Code 128)	PB	PB and PNB	PB and PNB
Shading material	dark fine twill viscose and dark cotton	dark fine twill viscose and dark cotton	dark fine twill viscose and dark cotton
Camera and Lens	DMK 41BU02.H camera and lens H3Z 4512 CS-IR	DMK 41BU02.H camera and lens H3Z 4512 CS-IR	DMK 41BU02.H camera and lens H3Z 4512 CS-IR
Datalogic Memor Mobile barcode scanner	-	-	Used
Lighting	Three cool white 18 W fluorescent tubes	Three cool white 18 W fluorescent tubes	Three cool white 18 W fluorescent tubes
Replication	400	400	400
1 L Spray bottle	-	For dirt treatments	For dirt treatments
Potgrond soil	-	20g for dirt treatments	20g for dirt treatments

*The x and y direction is in the view plane of the camera

4.3.1.1 Robustness of the automated image-based barcode detection system

To determine the robustness of the image-based system, various dirt (artificially soiled) treatments were applied to the surface of both types of barcodes. 20g of Potgrond P (Klasmann-Deilmann GmbH, Geeste, Deutschland) soil was put in a 28 cm plant pot saucer and mixed with 20 ml of water. This was then rubbed randomly on all the barcodes as shown (Figure 4-3a and b) to get a slightly dirty surface; i.e., 10-20% of the surface was dirty. The mixed soil medium was also vigorously applied to the surface of the slightly dirtied barcodes to make the barcodes extremely dirty; i.e., 50-60% of the surface was dirty (Figure 4-3c and d). Finally, 20g of planting soil medium was put in a 1L spray bottle

and 750 ml water was added, stirred to mix well and sprayed on the dirtied barcodes to see the effect of moisture on barcode detection.

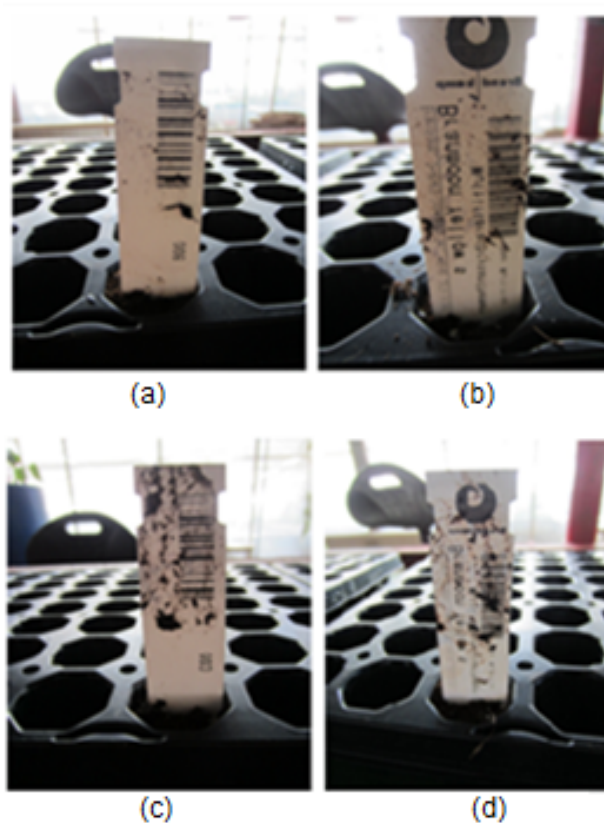


Figure 4-3: Dirt treatment of barcodes a) Slightly dirty PNB; b) Slightly dirty PB; c) Extremely dirty PNB; and d) Extremely dirty PB

4.3.2 Proposed algorithm

The proposed algorithm (Figure 4-4) which was based on mathematical morphological methods was used for all the experiments. The system was divided into two main parts: preprocessing and detection. Images were initially captured using the DMK 41BU02.H CCD USB 2.0 Monochrome Industrial Camera, the CS mount lens (H3Z 4512 CS-IR) and the image acquisition software IC Capture 2.2 (The Imaging Source Europe GmbH, Bremen, Germany). IC Capture allows the images to be captured from the camera and saved in three different ways. The images can be saved manually as single images, manually as image sequences and finally image sequences can be saved via a timer. The images were grabbed asynchronously so that while an old image is being processed a new one can also

be grabbed in the process. Also, the images were grabbed asynchronously so that images can be grabbed and stored intermittently when they become available. The RGB image was then converted into three one-channel images with the same definition domain using the function `decompose3` in Halcon. The three channels of the image were passed as three separate images on input and output so that only the channel of interest was chosen for further processing. The best image access channel was then selected. The third image channel was chosen for all the experiments. The selected images were then smoothed to reduce noise using the Gaussian filter of size 11×11 where $\sigma = 2.550$.

The second step used morphological operators to find the region containing the code. The smooth (Gauss) image was segmented into regions of the same intensity using the morphological operator `region growing`. The region boundaries were then smoothed and the small gaps between adjacent regions and holes smaller than the structure element were closed using the morphological operator `closing circle`. The regions of interest were then selected according to shape and merged together using the operators `select shape` and `union` respectively. Further smoothing of the region boundaries and removing of regions smaller than the structure element were opened using the morphological operator `opening circle`. The shape and size of the region of interest was maintained by performing a rigid affine transformation using a rotation matrix and a translation vector from a point and two corresponding angles, and a scaling by scale factors along the x-axis and y-axis based on the following equation:

$$HomMat2D = \begin{bmatrix} \cos(\Phi) & -\sin(\Phi) & 0 \\ \sin(\Phi) & \cos(\Phi) & 0 \\ 0 & 0 & 1 \end{bmatrix} * \begin{bmatrix} 1 & 0 & Tx \\ 0 & 1 & Ty \\ 0 & 0 & 1 \end{bmatrix} * \begin{bmatrix} Sx & 0 & 0 \\ 0 & Sy & 0 \\ 0 & 0 & 1 \end{bmatrix} \quad (4.1)$$

where,

HomMat2D = homogeneous 2D transformation matrix [-]

Phi = rotation angle [°]

Tx = translation along x-axis [-]

Ty = translation along y-axis [-]

Sx = scale factor along x-axis [-]

Sy = scale factor along y-axis [-]

The final part of the system was to decode the image data by performing a 2D Homogeneous and Affine Transformation on the image to enable detection from various angles. The image was first scaled, then rotated and finally translated before the code was detected. This was done by using the shape-based matching algorithm to find the region of interest (scan lines) on the barcode (Table 4-2). If the image was decoded a green rectangle and the number on the barcode was displayed. The result was then stored in a data sheet in the form of the company's name, type of production, production speed, date and time when it was captured. However, if the image was not decoded, no rectangle was displayed and the result was stored as zero.

Table 4-2: Shape-based matching algorithm

```
NumMatches: = |Row|
if (NumMatches>0)
  if (|ScaleR|=1)
  endif
  if (|ScaleC|=1)
  endif
  if (|Model|=0)
  elseif (|Model|=1)
  endif
  for Index: = 0 to |ModelID|-1 by 1
    get_shape_model_contours (ModelContours, ModelID[Index], 1)
    dev_set_color (Color[Index%|Color|])
    for Match: = 0 to NumMatches-1 by 1
      if (Index=Model[Match])
        hom_mat2d_identity (HomMat2DIdentity)
        hom_mat2d_scale (HomMat2DIdentity, ScaleR[Match], ScaleC[Match], Px, Py,
          HomMat2DScale)
        hom_mat2d_rotate (HomMat2DScale, Angle[Match], Px, Py, HomMat2DRotate)
        hom_mat2d_translate (HomMat2DRotate, Row[Match], Column[Match],
          HomMat2DTranslate)
        affine_trans_contour_xld (ModelContours, ContoursAffinTrans, HomMat2DTranslate)
        dev_display (ContoursAffinTrans)
      endif
    endfor
  endfor
  return ()
```

$$HomMat2DIdentity = \begin{bmatrix} 1 & 0 & 0 \\ 0 & 1 & 0 \\ 0 & 0 & 1 \end{bmatrix} \quad (4.2)$$

$$HomMat2DScale = \begin{bmatrix} Sx & 0 & 0 \\ 0 & Sy & 0 \\ 0 & 0 & 1 \end{bmatrix} * HomMat2D \quad (4.3)$$

$$S = \begin{bmatrix} Sx & 0 \\ 0 & Sy \end{bmatrix} \quad (4.4)$$

$$P = (Px, Py) \quad (4.5)$$

where,

HomMat2DIdentity = homogeneous transformation of the identical 2D transformation

S = scalar factor

Px = fixed point of the transformation along the x-axis

Py = fixed point of the transformation along the y-axis

ScaleR = Sx (scale factor along x-axis)

ScaleC = Sy (scale factor along y-axis)

Row = translation vector Tx (translation along x-axis)

Column = translation vector Ty (translation along y-axis)

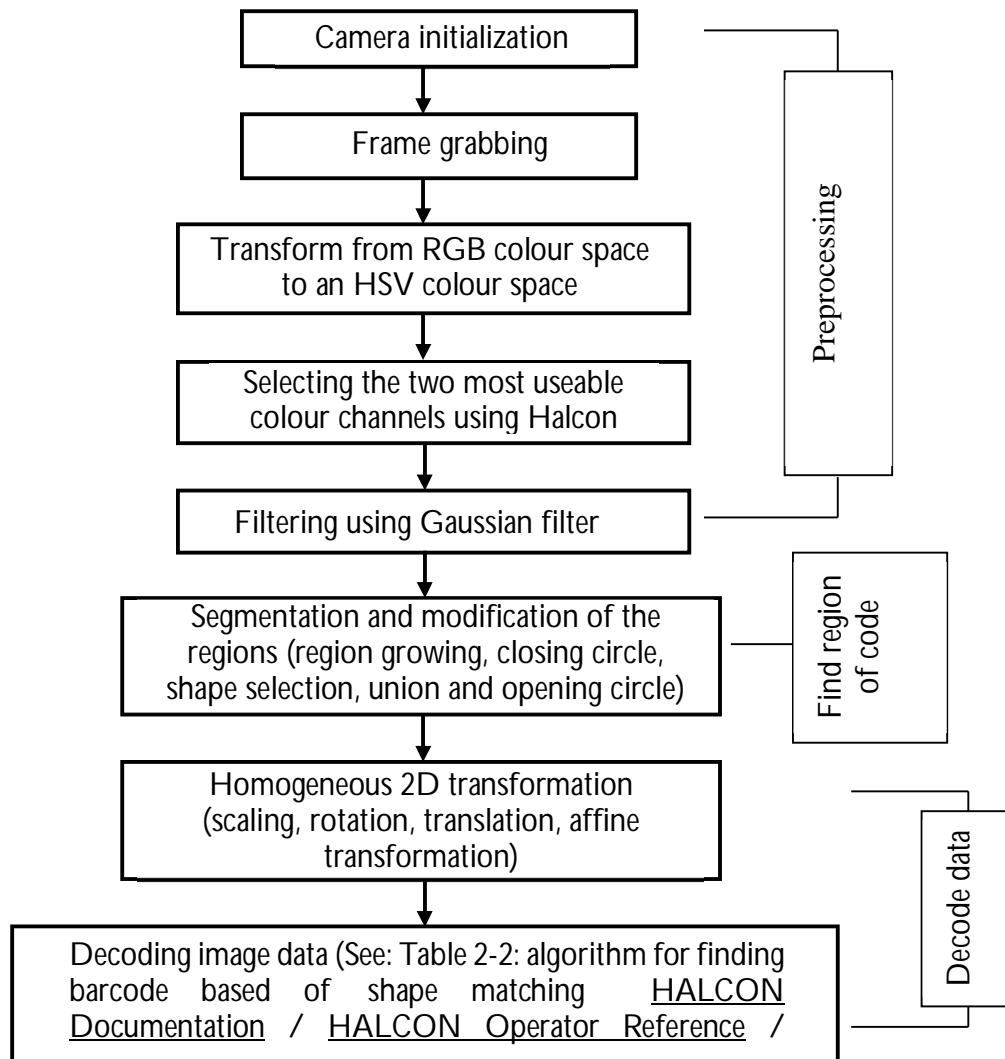


Figure 4-4: Flow chart of the image processing system

4.4 Results and discussion

4.4.1 Influence of speed and angle placement and other factors on barcode detection

The experiment to determine the effect of speed and angle placement on barcode detection used 7 different speeds with 0 m/s indicating a stationary barcode. Three different angle combinations (60°, 75° and 90°) and 400 replications were used. The colour chart (Figure 4-5) shows the influence of different speeds and angle placements on detection and reading of clean plant barcodes (PB). Also shown is the result for static barcodes at various angle combinations. The most critical angle is the rotation in the z-plane. Z-plane rotation decreases the apparent size of the barcode for the camera, which is a critical consideration when dealing with barcode reading by image processing. The system detected 100% of the barcodes in a static position (Figure 4-5). At angle combinations of 90°.90°.90° where the barcode was held perpendicular to the camera, there was 100% detection for speeds of 0.03, 0.07, 0.11, 0.17 and 0.21 m/s. There was 95% detection at the highest speed, 0.30 m/s (Figure 4-6). This demonstrated that speed did not significantly affect readings at this combination of angles. However, at angle combinations of 60°.60°.60°, 75°.75°.75°, 60°.90°.75° and 60°.60°.75° there was successful detection only at the lowest speed of 0.03 m/s (Figure 4-5). Thus, as speed increases and the angle of inclination of the barcodes in relation to the camera decreases from 90° to 60°, the percentage of success of barcode detection decreases. Conversely as speed decreases and the angle increases, the rate of successful detection improves.

Static and dynamic (in motion) experiments have been conducted for barcode detection using an omnidirectional camera for automated guided vehicle (AGV) with different barcode sizes (Taha et al., 2012). The dynamic experiments were conducted with multiple runs where the algorithm must decode four different barcodes located along the pathway of the AGV. Due to the slower frame rate of the omnidirectional camera, the speed of the AGV was limited to 0.32 m/s resulting in a longer processing time of the algorithm, even though the AGV could move at a speed of 2.2 m/s (Taha et al., 2012). 100% of the largest size of barcode was detected while the AGV was in motion for the 4 different runs. The detection and score decrease for smaller barcodes, with no detection for the smallest barcode size. The dynamic experiments showed that the frame rate of the camera, the barcode size and the processing time affected the detection of the barcodes (Taha et al., 2012; Mehta, 2015; Dutta

et al., 2016). In our dynamic experiments, as the speed increased above 0.21 m/s the detection rate decreased (Figure 4-6).

The static experiments conducted with the barcodes placed in front of and on the right or left sides of the AGV with the barcodes either lying flat or standing showed that larger barcode sizes had better detection rates than smaller barcode sizes. 100% of the bigger barcode sizes placed at the side of the AGV were detected. 0% of the smallest barcode sizes were detected. For barcodes placed in front of the AGV there was 100% detection for only the biggest barcode size. There was no detection for the rest of the barcode sizes. Therefore, size affects the speed of detection of the barcode. Also, larger barcodes have wider bar arrangements and even in the midst of noise are clearly mapped into image pixels, resulting in better detection compared to the other sizes (Taha et al., 2012; Mehta, 2015; Dutta et al., 2016). In our static experiments the width and size of the scan lines of the barcodes did not affect detection although the size of the plant barcodes (PB) (31 mm × 7 mm) was slightly smaller than that of the personnel number barcodes (34 mm × 10 mm).

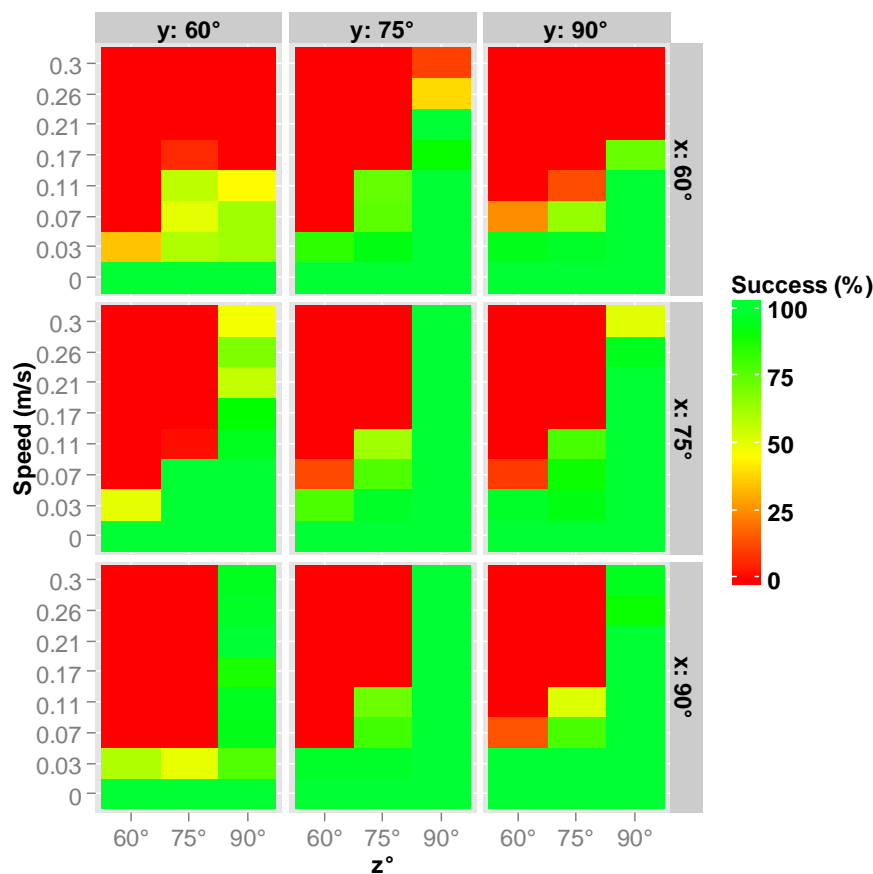


Figure 4-5: The effect of speed and angle of barcode placement on barcode detection (n= 400)

4.4.2 Influence of speed on automated image-based barcode detection in the laboratory and the company

Various speed treatments were tried to see how they affect barcode detection with the image-based detection system in the laboratory and in real production conditions. The bar chart (Figure 4-6) shows the percentage of successfully decoded barcodes in the laboratory and company. As the speed increases the success of barcode detection decreases for both types of barcodes (PB and PNB). Figure 4-6 shows the influence of different speeds on barcode detection of clean PB (laboratory and company experiment) and PNB (company experiment) labels. The Pearson Chi² test using the Holm-adjustment method for multiple comparison tests showed that there were no significant differences among all the clean barcodes in the laboratory and the two types of barcodes used in the company at 0.03, 0.07 and 0.11 m/s. However, there were significant differences among the results in the laboratory and company at 0.17, 0.21, 0.26 and 0.30 m/s. As the speed of the automated image-based barcode detection system in both the laboratory and company increased the detection of the barcodes decreased significantly.

There was 100% detection of clean PB at more of the operating speeds of the system used in the laboratory than in the company. The system of the company is inclined at an angle approximately 45° as the planting tray passes in the FOV (field of view) of the camera. However, in the laboratory, the operating system is not inclined and thus the barcode image is perpendicular to the FOV of the camera. Barcode orientation and inclination has been known to affect detection of 1D barcodes. Therefore, as speed increased detection decreased and the greater success in detecting barcodes in the laboratory as compared to the company, can be attributed to this (Qi et al., 2014; Namane and Arezki, 2017). Also due to the wider bar arrangement of scan lines of the PNB as compared to the PB (Figure 4-1) used in the company, there was better detection of PNB in the company at the various operating speeds (Figure 4-6). Consequently, as speed increases there was a better detection of the PNB (Taha et al., 2012; Diazgranados and Funk, 2013; Mehta, 2015; Dutta et al., 2016; Li et al., 2016).

Also the frame rate of the camera and operating system of the computer has been known to affect the speed of barcode detection in production systems. In the dynamic experiments using the omnidirectional vision system the operating speed of the AGV was limited to 0.32 m/s due to the slower frame rate of the camera resulting in a longer processing time for the image due to the computer processor (Taha et al., 2012). In our experiments, a camera with a frame rate of 15 fps and a PC with

Pentium®Dual-Core™ E5800 3.3GHz CPU, 2 GB RAM Windows 7 Enterprise 32-bit Operating System was used. This can possibly be one of the reasons why there was reduction in barcode detection in our experiments when the test speed of the automated image-based system increased from 0.21 to 0.30 m/s (Figure 4-6). A modern camera with a very high frame rate and a PC with a high speed processor should therefore be tested to see if it will result in better barcode detection. Also, external light affects the detection of the barcodes because it affects the reflection of scan lines of the barcode. Shading was done in order to prevent the influence of external light but a hundred percent shading was not achieved. This is because the system requires openings in the shading system so that the trays can pass on the conveyor belt. These openings inevitably allowed some external light to enter. How much this external light affected the detection was not measured and should be examined or studied in the nearest future.

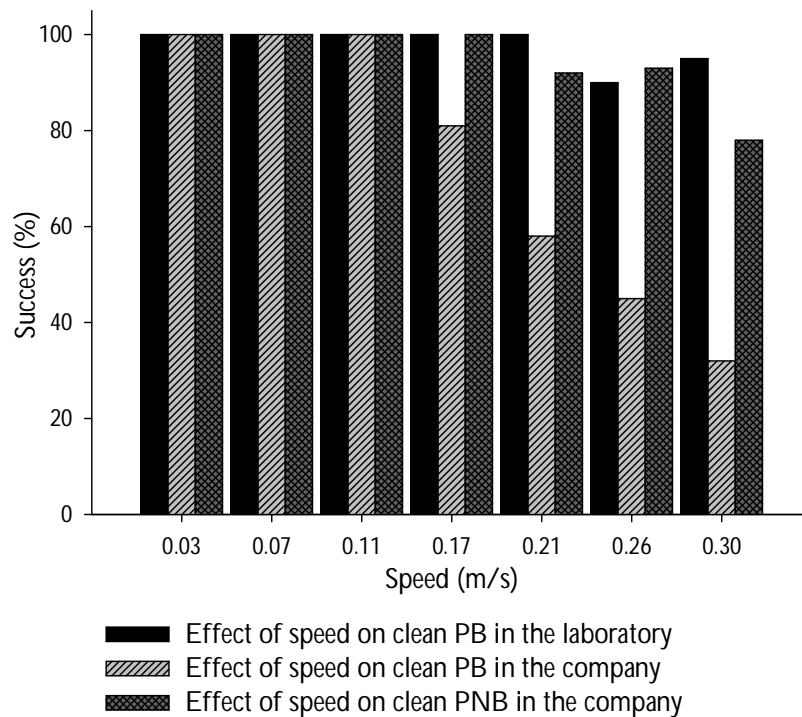


Figure 4-6: The effect of speed on barcode detection in the lab and company (n=400)

4.4.3 Robustness of the automated image-based barcode detection system

Various dirt treatments were used to see how they affect barcode detection with the automated image-based detection in real production conditions. The bar chart (Figure 4-7) shows the influence of speed, dirt and moisture on successfully decoded dirty PB and PNB in the company. Dirt and speed had an effect on the barcode detection as the barcodes that were slightly dirtied had better detection than those that were extremely dirtied. There was 100% detection for slightly dirty PB at 0.11 m/s and 90% at 0.15 m/s. For both extremely dirty PB and dirty water PB there was 90% detection at 0.11 m/s and 78% and 93% at 0.15 m/s respectively. For PNB there was 100% detection for both slightly dirty and dirty water at both speeds and 90% detection for extremely dirty at both speeds. Thus, extremely dirty barcode surfaces influenced the detection of the barcodes while moisture and slightly dirty barcode surfaces did not significantly affect detection. Table 4-3 below shows the comparison among the various dirt treatments, barcode types (PB and PNB) and the two speeds (0.11 and 0.15 m/s) used in the company. The Pearson Chi² test using the Holm-adjustment method for multiple comparison tests showed that there were significant differences among slightly dirty (SD) and dirty water (DW) and SD and extremely dirty (ED) at 0.11 m/s when PB were used. There was no significant difference between ED and DW at 0.11 m/s when PB was used. At 0.15 m/s there were significant differences among all the dirt treatments of PB. For PNB at 0.11 and 0.15 m/s there was no significant difference between SD and DW but there were significant differences among ED and DW and SD and ED. This showed that dirt on the surface of the barcode and speed of the automated image-based barcode detection system in company significantly affects barcode detection. For nearly all the treatments there was either no difference at all or the observed differences were so highly significant that the p-values are practically equal to 0 (Table 4-3). PNB had the best detection at the two speeds of all the dirt treatments which could be due to its slightly wider bar arrangement and size compared to that of the PB (Pihir et al., 2011; Huang and Zhao, 2011; Fang et al., 2012; Qi et al., 2014; Mehta, 2015; Şimşekli and Birdal, 2015; Dutta et al., 2016).

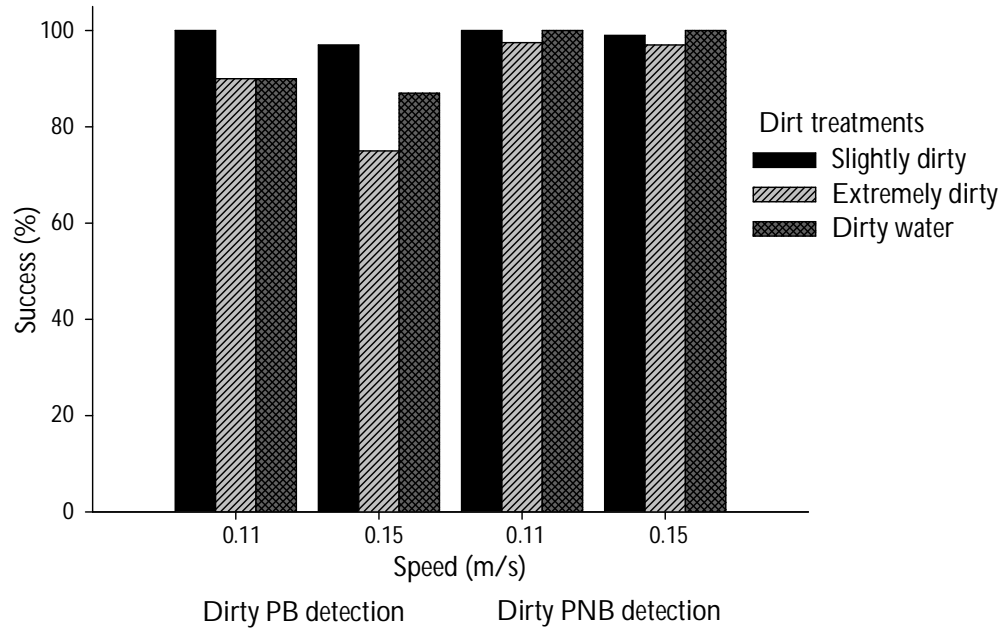


Figure 4-7: The effects of dirt and speed on barcode detection in the company (n=400)

Table 4-3: Comparison of dirt treatments of the plant barcodes (PB), worker barcodes (PNB) and speed at 95% confidence intervals using Pearson Chi2 test and the Holm-adjustment method for multiple comparison tests

p.val.adj	p.val.raw	comparison	barcode	speed (m/s)
1.000	0.9057	ED-DW	PB	0.11
0	0	SD-DW	PB	0.11
0	0	SD-ED	PB	0.11
0.0377	0.0063	ED-DW	PNB	0.11
1.0000	1.0000	SD-DW	PNB	0.11
0.0377	0.0063	SD-ED	PNB	0.11
0.0003	0	ED-DW	PB	0.15
0	0	SD-DW	PB	0.15
0	0	SD-ED	PB	0.15
0.0147	0.0021	ED-DW	PNB	0.15
1.0000	0.5630	SD-DW	PNB	0.15
0.0759	0.0190	SD-ED	PNB	0.15

NB: SD = Slightly Dirty, ED= Extremely Dirty, DW= Dirty Water

Operational errors such as distorted labels and wrong position of barcodes also play a significant role in automated barcode detection systems. Operational errors from handling of the barcodes, such as improper fixing of barcodes, dirt on the barcodes and the use of wrong barcodes, i.e., barcodes without scan lines (as some are used in the company for labeling), all affect successful automated barcode detection. Operational errors can lead to 64% reduction in barcode detection (Kuroki et al., 1997). This is a significant loss in barcode detection and as such during production all efforts must be put in place to minimize these errors as it affects the profit of the production system. There was always a 100% detection of barcodes using the Datalogic Memor X3 mobile barcode scanner irrespective of the treatments used although the more extreme the treatment (extremely dirty) the longer it took to detect the barcode. Readings for the barcodes using the hand laser scanner ranged between 1 to 5 seconds depending on the treatment on the barcode, as line of sight is required for successful scanning. However, for the automated image-based system it took 1 second for readings to be detected as there was no need for a direct line of sight to the barcode before detection. The proposed system was robust and faster in detecting dirty barcodes than with the hand laser scanner.

4.5 Conclusions

The image-based barcode detection system demonstrated that both clean and dirty barcodes can be successfully decoded in real production conditions at the company's production speed of 0.11 m/s. However, extremely dirty barcodes affected the detection of the plant barcodes more than the personnel number barcodes. The automated image-based barcode system has good future prospects over the hand-based system. Automated image-based barcode detection and reading can be implemented at a speed range of 0.11 to 15 m/s in a horticultural production system to increase the productivity and profitability of the company. For a successful implementation of the image-based system for automation, the following points must all be considered for reliable and stable results: a good lighting system, shading from interaction of external light and angle of inclination of barcodes in relation to the camera, barcode size, camera resolution and frame rate, width of the bar arrangement on the barcode and operational errors from workers. QR Codes are now widely used in horticulture production and carry a lot of information with a high data capacity. Future studies using QR Code should also be carried out using the image-based system and compared to the 1D (Code 128) barcode to see which works best with the image-based system. This will help small flower producing companies

save costs as printing of QR Codes is much cheaper than using RFID. There are plans to implement the proposed system in the flower production company, Brandkamp GmbH in the near future.

Chapter 5

5.1 General discussion

This doctoral thesis is a product of the analysis of computer vision reading on stickers and direct part marking on complex backgrounds. The project was developed to help solve the problems of automation in the nursery of the flower producing company Brandkamp GmbH, also to provide insight on the use of direct part marking on various horticultural products. Three main research questions were put forward and different datasets and approaches were adopted to help fulfill the purpose of this thesis. The first objective, which has its analysis presented in chapter 4, was to solve the problems associated with using hand-based laser detection systems. The proposed solution is the use of an image-based barcode detection system. The data sets from the laboratory of the Leibniz University of Hannover and Brandkamp GmbH were statistically analysed to make logical conclusions. From the investigations, it was deduced that the image-based barcode detection system provided more reliable, stable and faster results as compared to the use of the hand laser readers. The problem of direct line of sight for detection is solved by using this system. Also, multiple barcodes can be detected. This showed that barcodes can be successfully used in automation of flower production in greenhouses. Increase in speed above the company's production speed resulted in a decrease in the successful detection of the barcodes. Dirty and smeared barcodes can also be decoded by the image-based barcode system. The rate of successful detection however, decreases with the increase of dirt on the barcode surface.

Furthermore, water did not affect barcode detection, showing that there is no interference from moisture in the greenhouse when the image-based barcode system is used. Operational errors, like using stickers without barcodes, as used in the company, would result in loss of barcode detection if the image-based system is used. This will affect the production process when the data is used for analysis. Therefore, training is required on handling of barcodes during the production system when using this technology. The proposed system can be analysed and evaluated for real horticultural production systems. There are plans to implement this system in the flower production company Brandkamp GmbH in the near future. Also, the first part of the third objective of the research was

addressed with the proposed algorithm to decode 1D barcodes (Appendix I). The proposed algorithm for decoding the Code 128 barcodes in both the laboratory and company was successful in reading the barcodes at various speeds and angle of placement. The proposed algorithm was successful in detecting all the clean and slightly dirty barcodes and barcodes with dirty water of both PB and PNB at the company's production speed. Only the extremely dirty barcodes were not successfully detected at this speed. The proposed algorithm can be successfully implemented in real production systems at the company's production speed.

The second research question of this thesis, which sought to investigate the effect of low laser marking energy by considering its effect on print growth and the effect of barcode size and contrast on the quality and readability of 2D Data Matrix codes on apples was presented in chapter 3. The investigations showed that the laser energy, print growth, barcode size, type of product, contrast between the markings and the colour of the products, the days in storage and the inertia of the laser system all singularly or in combination with each other affected the laser marking and detection of the Data Matrix codes on apples. High laser marking energy resulted in ablation, browning and carbonisation, which resulted in decreased detection of the Data Matrix code. There was no detection for all the apples at the lowest marking energy. There was better detection of the barcodes on the Golden Delicious apples as compared to Red Jonaprince and Kanzi. This was attributed to the contrast between the markings and the background colour of Golden Delicious and the print growth. The better contrast of the markings on the Golden Delicious compared to the other apples was due to the increase in oxidation around the markings as the days of storage increased resulting in a better detection. Finally, the print growth of the Data Matrix code was affected by the working direction of the laser beam as the initial marking energy was higher than the final marking energy.

Also, the final part of the third objective of the research to propose an algorithm for detecting 2D Data Matrix code directly marked on horticultural products was addressed with the proposed algorithm (Appendix II). There was 100% detection on Golden Delicious for 10 days with some success with Red Jonaprince and Kanzi apples. This showed that there is a future prospect of directly identifying barcodes on apples in real production systems.

5.2 Future research needs

The study showed that due to the complex background and nature of horticultural products there is still a lot of work to be done in direct part marking of 2D barcodes. However, due to the numerous benefits of using DPM, more companies are willing to invest in this field to achieve the necessary results. There is always going to be room for improvement due to the advancement in product marking technology and the desire for companies to increase productivity and profitability. Therefore, the following experiments should be carried out to see how the barcode and laser marking technologies can be improved for future use: Experiments using Data Matrix code and QR code containing various information regarding the plant cuttings using the image-based barcode detection system, since these codes are now widely used in horticulture production and carry a lot of information with a high data capacity. These barcodes are currently not being used in the company's nursery production.

Also, since there are modern cameras with high frame rates and field of view; experiments should be conducted with these cameras to see how they detect 1D barcodes in horticulture production systems. Image processing algorithms to detect multiple products should be developed since detection of Data Matrix code on horticultural products is still product specific. The algorithm developed is currently working successfully on Golden Delicious and able to read some markings on Red Jonaprince and Kanzi apples. Therefore, more varieties of apples and other horticultural products have to be analyzed with the proposed algorithm to see if it also works on some of them.

References

- Ahmed, S.A., Dey, S. and Sarma, K.K. (2011). Image texture classification using artificial neural network (ANN). 2nd National Conference on Emerging Trends and Applications in Computer Science (NCETACS), 1-4.
- Ahson, S. and Ilyas, M. (2017). RFID handbook: Applications technology security and privacy, FL, Boca Raton: CRC Press, 2017.
- Alkoffash, M.S., Bawaneh, M.J., Muaidi, H., Alqrainy, S. and Alzghool, M. (2014). A survey of digital image processing techniques in character recognition. *International Journal of Computer Science and Network Security*, 14(3), 65-71.
- Andrade-Sanchez, P., Pierce, F.J. and Elliot, T.V. (2007). Performance assessment of wireless sensor networks in agricultural settings. 2007 ASABE Annual International Meeting Minneapolis, MN, USA.
- Azad, M., Hasan, M. and Naseer, M.K. (2017). Colour image processing in digital image. *International Journal of New Technology and Research*, 3(3), 56-62.
- Babu, K.M. and Sulthana, A. (2017). Fruit classification system using computer vision: A review. *International Journal for Innovative Engineering and Management Research*, 6(3), 739-748.
- Badia-Melis, R., Mishra, P. and Ruiz-García, L. (2015). Food traceability: New trends and recent advances. *Food Control*, 57, 393-401.
- Bali, A. and Singh, S.N. (2015). A review on the strategies and techniques of image segmentation. Fifth international conference on advanced computing and communication technologies, 113-120.
- Bansal, B., Saini, J.S., Bansal, V. and Kaur, G. (2012). Comparison of various edge detection techniques. *Journal of Information and Operations Management*, 3(1), 103-106.
- Barbosa, D., Dietenbeck, T., Schaerer, J., D'hooge, J., Friboulet, D. and Bernard, O. (2012). B-spline explicit active surfaces: An efficient framework for Real-time 3-D region-based segmentation. *IEEE Transactions on Image Processing*, 21, 241-251.
- Barcikowski, S., Koch, G. and Odermatt, J. (2006). Characterisation and modification of the heat affected zone during laser material processing of wood and wood composites. *Holz als Roh- und Werkstoff*, 64, 94-103.
- Bassoli, E. (2018). Direct part marking of inconel 718. *International Journal of Applied Engineering Research*, 13(5), 2235-2241.

- Becker, W. (2015). Hein Lühs ist Entdecker des Bikini-Effektes und Erfinder des Laser-Apfels. Business and People, 07.06.2015. Available at: <https://www.business-people-magazin.de/2015/07-2015/bei-ihm-wachsen-aepfel-mit-herz-2060/>. Accessed on 15th January 2020.
- Bernsen, J. (1986). Dynamic thresholding of gray level images. Proceedings of International Conference on Pattern Recognition (ICPR), 1251–1255.
- Bodnár, P. and Nyúl, L.G. (2012a). Barcode detection with morphological operations and clustering. Proceedings of the Ninth IASTED International Conference on Signal Processing, Pattern Recognition and Applications, 51-57.
- Bodnár, P. and Nyúl, L.G. (2012b). Improving barcode detection with combination of simple detectors. Proceedings of the Eighth International Conference on Signal Image Technology and Internet Based Systems, 300-306.
- Bodnár, P. and Nyúl, L.G. (2013). A novel method for barcode localization in image domain. *Image Analysis and Recognition*, 7950, 189-196.
- Bodnár, P., Grósz, T., Tóth, L. and Nyúl, L.G. (2018). Efficient visual code localization with neural networks. *Pattern Analysis Applications*, 21(1), 249–260.
- Borgohain, T., Kumar, U. and Sanyal, S. (2015). Survey of security and privacy issues of internet of things. *International Journal of Advanced Network Applications*, 6(4), 2372–2378.
- Boyat, A.K. and Joshi, B.K. (2015). A review paper: Noise models in digital image processing. *International Journal on Signal and Image Processing*, 6(2), 63-75.
- Chai, D. (2005). Locating and decoding EAN-13 barcodes from images captured by digital cameras. Fifth International Conference on Information, Communications and Signal Processing, 1595-1599.
- Chen, G., Hu, T., Guo, X. and Meng, X. (2009). A fast region-based image segmentation based on least square method. IEEE International Conference on Systems, Man and Cybernetics, SMC, 972-977.
- Cheng, H.D., Jiang, X. H., Sun, Y. and Wang, J. (2001). Color image segmentation: Advances and prospects. *Pattern Recognition*, 34(12), 2259-2281.
- Chen, C., He, B-W., Zhang, L-W. and Yan, P-Q. (2017). Autonomous recognition system for barcode detection in complex scenes. ITM Web of Conferences, The 4th Annual International Conference on Information Technology and Applications (ITA 2017), Guangzhou, China,

- May 26-28, 2017, 12(04106) Available at: <https://doi.org/10.1051/itmconf/20171204016>. Accessed on 15th February 2020.
- Chernov, V., Alander, J. and Bochko, V. (2015). Integer-based accurate conversion between RGB and HSV color spaces. *Computers and Electrical Engineering*, 46, 328-337.
- Chitradevi, B. and Srimathi, P. (2014). An overview of image processing techniques. *International Journal of Innovative Research in Computer and Communication Engineering*, 2(11), 6466-6472.
- Chowdhury, A.I., Rahman, M.S. and Sakib, N. (2019). A study of multiple barcode detection from an image in business system. *International Journal of Computer Applications*, 181(37), 30–37.
- Cook, N. (2017). Key considerations when using lasers to code fruit and vegetables. Available at: <https://packagingeurope.com/key-considerations-for-lasers-to-code-fruit-and-vegetables/> Accessed on 3rd January, 2020.
- Creusot, C. and Munawar, A. (2015). Real-time barcode detection in the wild. IEEE Winter Conference on Applications of Computer Vision (WACV), Waikoloa Beach, Hawaii, January 6-9, 239–245.
- Cui, W. and Zhang, Y. (2010). Graph based multispectral high resolution image segmentation. Proceedings of International Conference on Multimedia Technology (ICMT), 1-5.
- Curry, A. (2010). BASF Subsidiary Develops Better Crops Through RFID. Available at: <http://www.rfidjournal.com/article/print/7664>. Accessed on 16th February 2020.
- Danyluk, M., Interiano, L., Friedrich, L., Schneider, K. and Etxeberria, E. (2010). Natural-light labeling of tomatoes does not facilitate growth or penetration of Salmonella into the fruit. *Journal of Food Protection*, 73, 2276-2280.
- Danyluk, M., Friedrich, L., Sood, P. and Etxeberria, E. (2013). Growth or penetration of Salmonella into citrus fruit is not facilitated by natural-light labels. *Food Control*, 34, 398-403.
- Das, S. (2016). Comparison of various edge detection technique. *International Journal of Signal Processing, Image Processing and Pattern Recognition*, 9(2), 143-158.
- Dass, R., Priyanka, P. and Devi, S. (2012). Image segmentation techniques. *International Journal of Electronic Communication and Technology*, 3(1), 66-70.
- Darwish, A. (2018). Automatic plant recognition and diseases identification methods based on image processing techniques. *Journal of the Egyptian Mathematical Society*, 26(2), 297-310.
- Datalogic. (2013). White paper on direct part marking: More than just a code on a surface.
- David, B.L.O., Macatuno, P.M.D., Valdez, M.L.C., Yau, R.D.N., Sybingco., E. and Sapang, O. (2015). Design and application of automated sales scanning and recording of apparel swing tags. 8th

- IEEE International Conference Humanoid, Nanotechnology, Information Technology Communication and Control, Environment and Management (HNICEM), Cebu City, Philippines, December 9-12, 1-7.
- Daw-Tung, L., Min-Chueh, L. and Kai-Yung, H. (2011). Real-time automatic recognition of omnidirectional multiple barcodes and dsp implementation. *Machine Vision and Applications*, 22, 409-419.
- Denkena, B., Grove, T. and Seibel, A. (2016). Direct part marking by vibration assisted face milling. 3rd International Conference on System-integrated Intelligence: New Challenges for Product and Production Engineering, SysInt (2016). *Procedia Technology*, 26, 185-191.
- Dhankhar, P. and Sahu, N. (2013). A review and research of edge detection techniques for image segmentation. *International Journal of Computer Science and Mobile Computing*, July 2013, 2(7), 86-92.
- Diazgranados, M. and Funk, V. A. (2013). Utility of QR codes in biological collections. *PhytoKeys*, 25, 21-34.
- Dinesh, R., Kiran, R.G. and Veena, M. (2013). Classification and decoding of barcodes: An image processing approach. *Multimedia Processing, Communication and Computing Applications*, 293-307.
- Drouilliard, G. and R.W. Rowland. (1997). Method of laser marking of produce. U.S. Patent No. 5660747. U.S. Dept. of Commerce, Patent and Trademark Office, Washington, DC.
- Drouilliard, G. and Kanner, R. W. (1999). Produce marking system. U.S. Patent No. 5897797. U.S. Dept. of Commerce, Patent and Trademark Office, Washington, DC.
- Duda, R.O. and Hart, P.E. (1972). Use of the Hough transformation to detect lines and curves in pictures. *Communications of the ACM*, 15(1), 11-15.
- Dutta, K., Gupta, S. and Kaur, M. (2016). Fast algorithm for recognition of 2D barcode: A review. *International Journal of Emerging Trends in Science and Technology*, 2(7), 4334-4339.
- Dwinell, J., Peng, B. and Long Xiang, B. (2012). Robust recognition of 1D barcodes using Hough transform. *Proceedings of SPIE 8300, Image Processing: Machine Vision Applications V*, 83000K. Available at: <https://doi.org/10.1117/12.907598>. Accessed on 16th February 2020.
- Eppenberger, D. (2018). Weniger Verpackung dank Laser-Markierung. Available at: <https://www.gabot.de/ansicht/news/detail/News/neu-weniger-verpackung-dank-laser-markierung-390200.html>. Accessed on 4th January 2020.

- Etxeberria, E., Miller, W. M. and Achor, D. (2006). Anatomical and morphological characteristics of laser etching depressions for fruit labeling. *Hort Technology*, 16(3), 527-532.
- Etxeberria, E., Narciso, C., Sood, P., Gonzalez, P. and Narciso, J. (2009). The anatomy of a laser label. *Proceedings of Florida State Horticultural Society*, 122, 347-349.
- Etxeberria, E. and Gonzalez, P. (2014). The use of laser light to enhance penetration of antimicrobials into citrus leaves. *Proceedings of the Florida State Horticultural Society*, 127, 75-77.
- Etxeberria, E., Gonzalez, P., Borges, A. and Brodersen, C. (2016). The use of laser light to enhance the uptake of foliar applied substances into citrus (*Citrus sinensis*) leaves. *Applications in Plant Sciences*, 4(1), 1500106.
- EU Regulation for Laser Marking of Fruits. (2013). Official Journal of the European Union L 150/17. Available at: <http://www.freshplaza.com/article/109960/EU-New-regulation-approves-laser-etching-on-fruit>. Accessed on 5th February 2020.
- Fabijanska, A. (2011). Variance filter for edge detection and edge-based image segmentation. *Proceedings of International Conference on Perspective Technologies and Methods in MEMS Design (MEMSTECH)*, 151-154.
- Fang, J.P., Chang, Y., Chu, W. and Chen, K.W. (2012). Incomplete barcode reading mechanism with remote database access. *Recent Advances in Computer Science and Information Engineering Lecture Notes in Electrical Engineering*, 124, 705–710.
- Farooque, M.A. and Rohankar, J.S. (2013). Survey on various noises and techniques for denoising the color image. *International Journal of Application or Innovation in Engineering and Management*, 2(11), 217-221.
- Fatima, R., Mirajkar, F.D. and Begum, H. (2017). An extensive survey on edge detection techniques. *International Journal of Engineering and Techniques*, 3(6), 63-69.
- Fröschle, H.K., Gonzales-Barron, U., McDonnell, K. and Ward, S. (2009). Investigation of the potential use of e-tracking and tracing of poultry using linear and 2D barcodes. *Computers and Electronics in Agriculture*, 66, 126-132.
- Furness, A. (2000). Machine-readable data carriers - A brief introduction to automatic identification and data capture. *Assembly Automation*, 20(1), 28-34.
- Gao, J.Z., Prakash, L. and Jagatesan, R. (2007). Understanding 2D-barcode technology and application in m-commerce-design and implementation of a 2D barcode processing solution. *Computer Software Applications Conference*, 49-56.

- Gaur, P. and Tiwari, S. (2014). Recognition of 2D barcode images using edge detection and morphological operation. *International Journal of Computer Science and Mobile Computing*, 3(4), 1277-1282.
- Gayathri, R.N. and Vinoth, J. (2012). Barcode recognition from video by combining image processing and xilinx. International Conference on Modelling, Optimisation and Computing. *Procedia Engineering*, 38, 2140-2146.
- Gelman, A. and Yu-Sung, S. (2016). Data analysis using regression and multilevel/hierarchical models. R package version 1.9-3. Available at: <https://CRAN.R-project.org/package=arm>. Accessed on 20th January 2020.
- Georgieva, L., Dimitrova, T. and Angelov, N. (2005). RGB and HSV color models in color identification of digital traumas images. International Conference on Computer Systems and Technologies, 121-126.
- Gonzalez, R.C., and Woods, R.E. (2018). Digital Image Processing. Fourth Edition. Prentice-Hall, Inc. Upper Saddle River New Jersey.
- Griffiths, M.J. and Fox, Y.E. (2011). Method and apparatus for laser marking objects. U.S. Patent No. 8084712.
- GS1. (2015). GS1 2D barcode verification process implementation guideline. Available at: https://www.gs1.org/docs/barcodes/2D_Barcode_Verification_Process_Implementation_Guideline.pdf. Accessed on 20th January 2020.
- GS1. (2018). GS1 Data Matrix Guideline. Available at: https://www.gs1.org/docs/barcodes/GS1_DataMatrix_Guideline.pdf. Accessed on 20th January 2020.
- Hameed, M., Sharif, M., Raza, M., Haider, S.W. and Iqbal, M. (2013). Framework for the comparison of classifiers for medical image segmentation with transform and moment based features. *Research Journal of Recent Sciences*, 2(6), 1-10.
- Hansen, J.P. (2012) Using QR codes for context specific support around the farm. AFITA/WCCA 2012 Taipei/Taiwan, September 3-6, 1-5.
- He, D. and Joseph, E.B. (2017). System for and method of controlling illumination of direct part marking (DPM) target to be read by image capture. U.S. Patent No. 9792477B1.
- Heck, R.D., Gutierrez Ibarra, J. and Sheffler, J.B. (2007). Method and apparatus for non-invasive laser based labeling of plant products. U.S. Patent No 2007/0252006.

- Hinds, S., Fisher, J. and D'Amato, D. (1990). A document skew detection method using run-length encoding and the Hough transform. Proceedings of the 10th Conference on Pattern Recognition, Atlantic City, 464-468.
- Hodgson, S., Nabhani, F. and Zarei, S. (2010). AIDC feasibility within a manufacturing SME. *Assembly Automation*, 30(2), 109-116.
- Hoult, A. (2017). System and method of laser marking produce. U.S. Patent No. 20170239754A1.
- Howlett, R.J., Berthier, S. and Awcock, G.J. (1997). Determining the location of industrial bar-codes using neural networks. Sixth International Conference on Image Processing and Its Applications, 2, 511-515.
- Hua, Z., Li, Y. and Li, J. (2010). Image segmentation algorithm based on improved visual attention model and region growing. 6th International Conference on Wireless Communications Networking and Mobile Computing (WiCOM), 1-4.
- Huang, Y. and Zhao, S. (2011). Automatic localization algorithm of multiple barcodes. *Advanced Materials Research*, 317-319, 859-864.
- Ibraheem, N.A., Hasan, M. M., Khan, R.Z. and Mishra, P.K. (2012). Understanding color models: A review. *ARPN Journal of Science and Technology*, 2(3), 265-275.
- Illingworth, J. and Kittler, J. (1988). A survey of Hough transform. *Computer Graphics and Image Processing*, 44, 87-116.
- Islam, M.J., Basalamah, S., Ahmadi, M. and Ahmed, M.A.S. (2011). Capsule image segmentation in pharmaceutical applications using edge-based techniques. IEEE International Conference on Electro/Information Technology (EIT), 1-5.
- Jähne, B., Scharr, H., and Körkel, S. (1999). Principles of filter design. In Handbook of computer vision and applications. Academic Press.
- Jain, P. and Tyagi, V. (2016). A survey of edge-preserving image denoising methods. *Information Systems Frontiers*, 18(1), 159-170.
- Jangsombatsiri, W. and Porter, D.J. (2006). Artificial neural network approach to data matrix laser direct part marking. *Journal of Intelligent Manufacturing*, 17, 133-147.
- Jangsombatsiri, W. and Porter, D.J. (2007). Laser direct part marking of data matrix symbols on carbon steel substrates. *Journal of Manufacturing Science and Engineering*, 129, 583-591.
- Jhuria, M., Borse, R. and Kumar, A. (2013). Image processing for smart farming detection of disease and fruit grading. Proceeding of the IEEE Second International Conference on Image Information Processing (ICIIP), 521-526.

- Jiang, F., Frater, M.R. and Pickering, M. (2012). Threshold-based image segmentation through an improved particle swarm optimisation. Proceedings on International Conference on Digital Image Computing Techniques and Applications (DICTA), 1-5.
- Jeyavathana, R.B., Balasubramanian, R. and Pandian, A.A. (2016). A survey: Analysis on pre-processing and segmentation techniques for medical images. *International Journal of Research and Scientific Innovation*, 3(6), 113-120.
- Jyotsna, B., Shivani, C., Ekta, S. and Amit, D. (2016). Binarization techniques for degraded document images – A review. 5th International Conference on Reliability, Infocom Technologies and Optimization (ICRITO) (Trends and Future Directions), Sep. 7-9, 2016, AIIT, Amity University Uttar Pradesh, Noida, India, 163-166.
- Juett, J. and Qi, X. (2005). Barcode localization using bottom-hat filter. Nsf research experience for undergraduates.
- Kaihua, W. and Tao, B. (2011). Optimal threshold image segmentation method based on genetic algorithm in wheel set online measurement. Third International Conference on Measuring Technology and Mechatronics Automation (ICMTMA), 799-802.
- Kang, Y-S. and Lee, Y-H. (2013). Development of generic RFID traceability services. *Computers in Industry*, 64(5), 609-23.
- Katona, M. and Nyúl, L.G. (2012). A novel method for accurate and efficient barcode detection with morphological operations. The 8th International Conference on Signal Image Technology (SITIS 2012), 307–314.
- Katona, M. and Nyúl, L.G. (2013). Efficient 1d and 2d barcode detection using mathematical morphology. Proceedings in International Symposium on Mathematical Morphology and Its Applications to Signal and Image Processing, 464-475.
- Kato, H. and Tan, K. (2007). Pervasive 2D barcodes for camera phone applications. *IEEE Pervasive Computing: Mobile and Ubiquitous Systems*, 6(4), 76-85.
- Kato, H., Tan, Keng. T. and Chai, D. (2010). Barcodes for mobile devices. Cambridge University Press, New York, USA.
- Kaur, J., Agrawal, S. and Vig, R. (2012). A comparative analysis of thresholding and edge detection segmentation techniques. *International Journal of Computer Applications*, 39(15), 29-34.
- Kaur, D. and Kaur, Y. (2014). Various image segmentation techniques: A review. *International Journal of Computer Science and Mobile Computing*, 3(5), 809-814.

- Kaur, S. and Maini, R. (2014). Implementation of barcode localization technique using morphological operations. *International Journal of Computer Applications*, 97(13), 42-47.
- Kemény, Z., Bozóki, S., Ilie-Zudor, E. and Monostori, L. (2014). Low-cost extension of information transparency throughout the product life-cycle via optical identification and quality indication. *Procedia CIRP*, 25, 106-113.
- Khan, W. (2013). Image segmentation techniques: A survey. *Journal of Image and Graphics*, 1(4), 166-170.
- Khan, M. S. (2014). A survey: Image segmentation techniques. *International Journal of Future Computer and Communication*, 3(2), 89-93.
- Khirade, S.D. and Patil, A.B. (2015). Plant disease detection using image processing. International Conference on Computing Communication Control and Automation, 768-771.
- Kim, Y.J. and Lee, J.Y. (2016). Algorithm of a perspective transform-based PDF417 barcode recognition. *Wireless Personal Communications*, 89(3), 893-991.
- Kobylin, O. and Lyashenko, V. (2014). Comparison of standard image edge detection techniques and of method based on wavelet transform. *International Journal of Advanced Research*, 2(8), 572-580.
- Kondo, N. (2010). Automation on fruit and vegetable grading system and food traceability. *Trends in Food Science and Technology*, 21(3), 145-152.
- Kumar, G. and Bhatia, P.K. (2014). A detailed review of feature extraction in image processing systems. Fourth International Conference on Advanced Computing and Communication Technologies, 5-12.
- Kumar, T. and Verma, K. (2010). A theory based on conversion of RGB image to gray image. *International Journal of Computer Applications*, 7(2), 7-10.
- Kumar, M.J., Kumar, R.GVS. and Reddy, R.V.K. (2014). Review on image segmentation techniques. *International Journal of Scientific Research Engineering and Technology*, 3(6), 992-997.
- Kumari, L., Narsaiah, K., Grewal, M.K. and Anurag, R.K. (2015). Application of RFID in agri-food sector. *Trends Food Science Technology*, 43(2), 144-161.
- Kumari, A. and Chadha, P.D. (2014). A survey on filtering technique for denoising images in digital image processing. *International Journal of Advanced Research in Computer Science and Software Engineering*, 4(8), 612-614.
- Kuroki, M., Yoneoka, T., Satou, T., Takagi, Y., Kitamura, T. and Kayamori, N. (1997). Barcode recognition system using image processing. 6th International Conference on Emerging Technologies and Factory Automation Proceedings, September 9-12, 568-572.

- Kurtz, C., Desjardins, G.E. and Sanchez, S.J. (2007). Self checkout system with automated transportation conveyor. US Patent 7204346.
- Lenth, R.V. (2016). Least-squares means: The R package lsmmeans. *Journal of Statistical Software*, 69(1), 1-33. Available at: DOI:10.18637/jss.v069.i01. Accessed on 4th January, 2020.
- Liao, H-Y., Liu, S-J., Chen, L-H. and Tyan, H-R. (1995). Bar-code recognition system using back propagation neural networks. *Journal of Engineering Applications in Artificial Intelligence*, 8(1), 81-90.
- Li, J., Zhao, Q., Tan, X., Luo, Z. and Tang, Z. (2017). Using deep ConvNet for robust 1D barcode detection. International Conference on Intelligent and Interactive Systems and Applications, 261–267.
- Li, J-H., Wang, W-H., Rao, T-T., Zhu, W-B. and Liu, C-J. Morphological segmentation of 2D barcode gray scale image. International Conference on Information System and Artificial Intelligence, 62-68.
- Li, S., Visich, J.K., Khumawala, B.M. and Zhang, C. (2006). Radio frequency identification technology: applications, technical challenges and strategies. *Sensor Review*, 26(3), pp.193-202, Available at: <https://doi.org/10.1108/02602280610675474>. Accessed on 12th January 2020.
- Li, X-S., He, W-P., Lei, L., Wang, J., Guo, G-F., Zhang, T-Y. and Yue, T. (2016). Laser direct marking applied to rasterizing miniature Data Matrix code on aluminum alloy. *Optics and Laser Technology*, 77, 31–39.
- Lin, D.T., Lin, M.C. and Huang, K.Y. (2011). Real-time automatic recognition of omnidirectional multiple barcodes and dsp implementation. *Machine Vision and Applications*, 22, 409-419.
- Chih-Hsing, L., Ta-Lun, C., Tzu-Yang, P., Chen-Hua, C., Wei-Geng, P. and Chi-Chun, W. (2019). An intelligent robotic system for handling and laser marking fruits. *Technologies and Eco-innovation Towards Sustainability*, 75-88.
- Liu, F. (2010). Research on PDF417 barcode recognition method. CA: National University of Defense and Technology.
- Liu, F., Yin, J., Li, K. and Liu, Q. (2010). An improved recognition method of PDF417 barcode. Chinese Conference on Pattern Recognition (CCPR), 1-5.
- Liukkonen., M. and Tsai., T. (2016). Toward decentralized intelligence in manufacturing: recent trends in automatic identification of things. *The International Journal of Advanced Manufacturing Technology*, 1-23.

- Loesdau, M., Chabrier, S. and Gabillon, A. (2014). Hue and saturation in the RGB color space. Proceedings of the 6th International Conference on Image and Signal Processing, Lecture Notes in Computer Science, 8509, 203-212.
- Longobardi, R. (2007). Process and device for the marking of fruits through laser with, before the marking, cleaning/drying step and, after the marking, a sealing of the marked area. European Patent No. EP1747838.
- Mahbubun, N. and Sujana, A. (2014). An improved approach for digital image edge detection. *International Journal of Recent Development in Engineering and Technology*, 2(3), 14-20.
- Marx, C., Hustedt, M., Hoja, H., Winkelmann, T. and Rath, T. (2013). Investigations of laser marking of plants and fruits. *Biosystems Engineering*, 116(4), 436-446.
- McGarry, K., Wermter, S. and MacIntyre, J. (1999). Hybrid neural systems: from simple coupling to fully integrated neural networks. *Neural Computing Surveys*, 2(1), 62-93.
- Mc Inerney, B., Corkery, G., Ayalew, G., Ward, S. and Mc Donnell, K. (2011a). Preliminary in vivo study on the potential application of a novel method of e-tracking to facilitate traceability in the poultry food chain. *Computers and Electronics in Agriculture*, 77, 1-6.
- Mc Inerney, B., Corkery, G., Ayalew, G., Ward, S., and Mc Donnell, K. (2011b). A preliminary in vivo study on the potential application of a novel method of e-tracking in the poultry food chain and its potential impact on animal welfare. *Computers and Electronics in Agriculture*, 79, 51-62.
- Mehta, A. (2015). QR code recognition from image. *International Journal of Advanced Research in Computer Science and Software Engineering*, 5(12), 781-785.
- Minakshi, S. and Sourabh, M. (2013). Fuzzy C-means and snake model for segmenting astrocytoma – A type of brain tumor. *International Journal of Advances in Engineering Sciences*, 3(3), 30-35.
- Mishra, Y., Kaur, G. and Verma, S. (2015). Arduino based smart RFID and attendance system with audio acknowledgement. *International Journal of Engineering Research and Technology*, 4, 363-367.
- Mitsuru, I., Reiko, M. and Kuniharu, I. (2012). A new evaluation method for image noise reduction and usefulness of the spatially adaptive wavelet thresholding method for CT images. *Australasian Physical and Engineering Sciences in Medicine*, 35(4), 475-483.
- Mizushima, A. and Lu, R. (2013). An image segmentation method for apple sorting and grading using support vector machine and Otsu's method. *Computers and Electronics in Agriculture*, 94, 29-37.
- Moeslund, T.B. (2012). Introduction to video and image processing, undergraduate topics in computer science. Springer-Verlag London Limited, 7-24.

- Monga, M.P. and Ghogare, S.A. (2015). Scrutiny on image processing. *International Journal of Advanced Research in Computer Science and Software Engineering*, 5(1), 411-416.
- Monteiro, F.C. and Campilho, A. (2008). Watershed framework to region-based image segmentation. 19th Proceedings on International Conference on Pattern Recognition (ICPR), 1-4.
- Mukhopadhyay, P. and Chaudhuri, B.B. (2015). A survey of Hough transform. *Pattern Recognition*, 48, 993-1010.
- Musa, A., Gunasekaran, A., Yusuf, Y. and Abdelazim, A. (2014). Embedded devices for supply chain applications: Towards hardware integration of disparate technologies. *Expert Systems with Applications*, 41, 137-155.
- MVTec Software GmbH. (2012). HALCON/HDevelop 11.0.1 Reference Manual, München, Germany.
- Namane, A. and Arezki, M. (2017). Fast real time 1D barcode detection from webcam images using the bars detection method. Proceedings of the World Congress on Engineering (WCE), London, U.K, July 5-7, 1, 501–507.
- Nasution, I.S. and Rath, T. (2017). Optimal laser marking of 2D Data Matrix code on Cavendish banana. *Research in Agricultural Engineering*, 63(4), 172-179.
- Nasution, I.S. and Rath, T. (2015). Studies of laser marking on Cavendish banana. DGG-Proceedings, December 2015, 5(18), 1-5. Available at: DOI: 10.5288/dgg-pr-05-18-in-2015. Accessed on 20th January 2020.
- Niblack, W. (1986). An introduction to digital image processing. Prentice Hall, Eaglewood Cliffs, 115–116.
- O’Gormann, L. and Kasturi, R. (1995). Document image analysis. IEEE Computer Society Press, Los Alamitos.
- Ojha, S. and Sakhare, S. (2015). Image processing techniques for object tracking in video surveillance – A survey. IEEE International Conference on Pervasive Computing and Communications (ICPC), March 23-27, St. Louis, Missouri, USA, 1-6.
- Parker, B.E. (2011). Method and apparatus for marking an egg with an advertisement, a freshness date and a traceability code. U.S. Patent No. 7951409.
- Patil, J. and Jadhav, S. (2013). A comparative study of image denoising techniques. *International Journal of Innovative Research in Science, Engineering and Technology*, 2(3), 787-794.
- Pihir, I., Pihir, V. and Vidačić, S. (2011). Improvement of warehouse operations through implementation of mobile barcode systems aimed at advancing sales process. Proceedings of

- the ITI 2011 33rd International Conference on Information Technology Interfaces, June 27-30, 2011, Cavtat, Croatia, 433-438.
- Powers, J.R. and Reddy, V.M. (2014). System and method for recognizing deformed linear barcodes from a stream of varied-focus video frames. US Patent No. 8851378B2.
- Prakash, K., Saravanamoorthi, P., Sathishkumar, R. and Parimala, M. (2017). A study of image processing in agriculture. *International Journal of Advanced Networking and Applications*, 9(1), 3311-3315.
- Prasad, R., Kumar, V. and Prasad, K.S. (2014). Nanotechnology in sustainable agriculture: Present concerns and future aspects. *African Journal of Biotechnology*, 13(6), 705-713.
- Pullman, N. (2017). Swedish supermarkets replace sticky labels with laser marking. Available at: <https://www.theguardian.com/sustainable-business/2017/jan/16/ms-and-swedish-supermarkets-ditch-sticky-labels-for-natural-branding>. Accessed on 21st January 2020.
- Puneet, G.B. and Naresh, K.G. (2013). Binarization techniques used for grey scale images. *International Journal of Computer Applications*, Vol. 71(1), 8-11.
- Qian, J-P., Yang, X-T., Wu, X-M., Zhao, L., Fan, B-L. and Xing, B. (2012). A traceability system incorporating 2D barcode and RFID technology for wheat flour mills. *Computers and Electronics in Agriculture*, 89, 76-85.
- Qi, Y., Li, Y., Wang, C. and Lu, L. (2014). A fast algorithm detection for barcode inclination defect. *Applied Mechanics and Materials*, 644-650, 1172-1175.
- Raj, A.S.B. (2001). Bar codes - technology and implementation. Tata McGraw-Hill Publishing Company Limited, New Delhi, India.
- Ravi, S. and Khan, A.M. (2013). Morphological operations for image processing: Understanding and its applications. Proceedings on 2nd National Conference on VLSI, Signal Processing and Communications NCVSComs-13, December 11-12, 2013, 17-19.
- R Core Team. (2018). R: A language and environment for statistical computing. R Foundation for Statistical Computing, Vienna, Austria. Available at: <http://www.R-project.org/>. Accessed on 22nd January, 2020.
- Rolls-Royce. (2004). Direct part marking, implementation guide. Issue 1, June 2004-Vcom 9897.
- Samantaray, R.K., Panda, S. and Pradhan, D. (2011). Application of digital image processing and analysis in healthcare based on medical palmistry. *IJCA Special Issue on Intelligent Systems and Data Processing*, 56-59.

- Saravanan, C. (2010). Color image to grayscale image conversion. Second International Conference on Computer Engineering and Applications (ICCEA), 19-21 March, Bali Island, Indonesia, 196-199.
- Saravanan, G., Yamuna, G. and Nandhini, S. (2016). Real time implementation of RGB to HSV/HIS/HSL and its reverse color space models. International Conference on Communication and Signal Processing (ICCSP), 0462-0466.
- Sauvola, J. and Pietikainen, M. (2000). Adaptive document image binarization. *Pattern Recognition*, 33(2), 225–236.
- Savant, S. (2014). A review on edge detection techniques for image segmentation. *International Journal of Computer Science and Information Technologies*, 5(4), 5898-5900.
- Saxena, C. and Kourav, D. (2014). Noises and image denoising techniques: A brief survey. *International Journal of Emerging Technology and Advanced Engineering*, 4(3), 878-885.
- Schlösser, U., Dedden, L. and Boxser, D. (2002). Label for plants which can be inserted into the soil. U.S. Patent No 6460480B1.
- Sentilkumaran, N. and Rajesh, R. (2009). Edge detection techniques for image segmentation – A survey of soft computing approaches. *International Journal of Recent Trends in Engineering*, 1(2), 250-254.
- Shah, K., Patel, K. and Prajapati, G.I. (2013). Various edge detection techniques: survey, implementation and comparison. *International Journal of Advanced Research in Computer Science*, 4(4), 109-113.
- Shapiro, S.D. (1978a). Properties of transformation for the detection of curves in noisy pictures. *Computer Vision and Graphics Image Process*, 8, 219-236.
- Shapiro, S.D. (1978b). Feature space transforms for curve detection. *Pattern Recognition*, 10, 129-143.
- Sharif, M., Jamal, M.J., Javed, M.Y. and Raza, M. (2011). Face recognition for disguised variations using Gabor feature extraction. *Australian Journal of Basic and Applied Sciences*, 5, 1648-1656.
- Sharif, M., Raza, M. and Mohsin, S. (2011). Face recognition using edge information and DCT. *Sindh University Resource Journal (Science Series)*, 43(2), 209-214.
- Sharif, M., Mohsin, S., Javed, M.Y. and Ali, M.A. (2012). Single image face recognition using Laplacian of Gaussian and discrete cosine transforms. *International Arab Journal of Information Technology*, 9, 562-570.

- Şimşekli, U. and Birdal, T. (2015). A unified probabilistic framework for robust decoding of linear barcodes. IEEE International Conference on Acoustics, Speech and Signal Processing (ICASSP), Brisbane, QLD, Australia, April 19-24, 1946-1950.
- Singh, S. and Datar, A. (2013). Edge detection techniques using Hough transform. *International Journal of Emerging Technology and Advanced Engineering*, 3(6), 333-337.
- Singh, S., Kumar, N. and Kaur, N. (2014). Design and development of RFID based intelligent security system. *International Journal of Advanced Research in Computer Engineering and Technology*, 3(1), 62-65.
- Singh, V. and Misra, A.K. (2017). Detection of plant leaf diseases using image segmentation and soft computing techniques. *Information Processing in Agriculture*, 4, 41-49.
- Sofu, M.M., Er, O., Kayacan, M.C. and Cetişli, B. (2016). Design of an automatic apple sorting system using machine vision. *Computers and Electronics in Agriculture*, 127, 395-405.
- Sood, P., Ference, C., Narciso, J. and Etxeberria, E. (2008). Effects of laser labeling on the quality of tangerines during storage. Proceedings of the annual meeting of the Florida State Horticultural Society, 297-300.
- Sood, P., Ference, C., Narciso, J. and Etxeberria, E. (2009a). Laser marking: a novel technology to label Florida grapefruit. *Horttechnology*, 19, 504-510.
- Sood, P., Ference, C., Narciso, J. and Etxeberria, E. (2009b). Laser labeling, a safe technology to label produce. Florida State Horticultural Society Meeting. Paper No. HP14.
- Stergiou, C. and Siganos, D. (1996). Neural networks. Available at: http://www.doc.ic.ac.uk/~nd/surprise_96/journal/vol4/cs11/report.html. Accessed on 2nd January 2020.
- Swedberg, C. (2009). RFID raises profits at plant nursery. Available at: <http://www.rfidjournal.com/article/view/4933>. Accessed on 16th February 2020.
- Swedberg, C. (2010). Dutch horticultural supply chain tests RFID "from plant to customer". Available at: <http://www.rfidjournal.com/article/view/7970>. Accessed on 16th February 2020.
- Synrad. (2012). WinMarkpro[®] Laser marking software user guide version 6.3. Mukilteo, USA.
- Taha, Z., Mat-Jizat, J.A. and Ishak, I. (2012). Bar code detection using omnidirectional vision for automated guided vehicle navigation. International Conference on Automatic Control and Artificial Intelligence, 589-592.

- Tate, R.F., Hebel, M.A. and Watson, D.G. (2008). WSN link budget analysis for precision agriculture. 2008 ASABE Annual International Meeting, 29th June – 2 July, Providence, Rhode Island, USA, 11, 6786.
- Tekin, E. (2014). A method for traceability and “as-built product structure” in aerospace industry. *Procedia CIRP*, 17, 351-355.
- Trappey, A.J.C., Trappey, C.V., Govindarajan, U.H., Sun, J.J. and Chuang, A.C. (2017). A review of essential standards and patent landscapes for the internet of things: A key enabler for industry 4.0. *Advanced Engineering Informatics*, 33, 208-229.
- Tuinstra, T.R. (2006). Reading barcodes from digital imagery. PhD thesis, Cedarville University.
- Várallyai, L. (2012). From barcode to QR code applications. *Journal of Agricultural Informatics*, 3(2), 9-17.
- Varshney, S. and Dalal, T. (2016). Plant disease prediction using image processing techniques - A review. *International Journal of Computer Science and Mobile Computing*, 5(5), 394-398.
- Velusamy, V., Karnan, M., Shivakumar, R. and Nandhagopal, N. (2014). Enhancement techniques and methods for MRI - A review. *International Journal of Computer Science and Information Technologies*, 5(1), 397-403.
- Ventura, C., Aroca, R., Antonialli, A., Abrão, A., Campos, R.J. and Câmara, M. (2016). Towards part lifetime traceability using machined Quick Response codes. *Procedia Technology*, 6, 89-96.
- Vieira, G., Reis, L., Varela, M.L.R., Machado, J. and Trojanowska, J. (2016). Integrated platform for real-time control and production and productivity monitoring and analysis. *Romanian Review Precision Mechanics, Optics and Mechatronics*, 50, 119-127.
- Wang, M.X. and Madej, D.J. (2014). Apparatus for and method of electro-optically reading direct part marking indicia by image capture. Patent No. 8690063B2. U.S. Dept. of Commerce, Patent and Trademark Office, Washington, DC.
- Wang, Z., Chen, A., Li, J., Yao, Y. and Luo, Z. (2016). 1D barcode region detection based on the Hough transform and support vector machine. *International Conference on Multimedia Modeling*, 79–90.
- White, L. (2008). Laser leaves mark on fruit. *Weekly Times Now*. Melbourne, Australia: Herald & Weekly Times Pty. Ltd.
- Wickham, H. (2009). *ggplot2: Elegant graphics for data analysis*. Springer-Verlag New York, 2009. Available at: <http://ggplot2.org>. Accessed on 20th January 2020.

- Woollaston, V. (2013). Is this the end of sticky labels on fruit? New laser 'tattoos' that mark the skin are approved by the EU. Available at: <http://www.dailymail.co.uk/sciencetech/article-2343704/Is-end-sticky-labels-fruit-New-laser-tattoos-mark-skin-approved-EU.html>. Accessed on 15th February 2020.
- Xu, A., Wang, L., Feng, S. and Qu, Y. (2010). Threshold-based level set method of image segmentation. Third International Conference on Intelligent Networks and Intelligent Systems (ICINIS), 703-706.
- Yashmin, M., Sharif, M., Masood, S., Raza, M. and Mohsin, S. (2012). Brain image enhancement – A survey. *World Applied Sciences Journal*, 17, 1192-1204.
- Yasmin, M., Sharif, M. and Mohsin, S. (2013). Neural networks in medical imaging applications: A survey. *World Applied Sciences Journal*, 22, 85-96.
- Youssef, S.M. and Salem, R.M. (2007). Automated barcode recognition for smart identification and inspection automation. *Expert Systems with Applications* 33, 968-977.
- Yuk, H., Warren, B. and Schneider, K. (2007). Infiltration and survival of Salmonella spp. on tomato surfaces labeled using a low-energy carbon dioxide laser device. *HortTechnology*, 17, 67-71.
- Zamberletti, A., Gallo, I. and Albertini, S. (2013). Robust angle invariant 1D barcode detection. 2nd IAPR Asian Conference on Pattern Recognition (ACPR), 160-164.
- Zamberletti, A., Gallo, I., Albertini, S. and Noce, L. (2015). Neural 1D barcode detection using the Hough transform. *Information and Media Technologies*, 10(1), 157-165.
- Zhang, L. and Deng, X. (2010). The research of image segmentation based on improved neural network algorithm. Sixth International Conference on Semantics Knowledge and Grid (SKG), 395-397.
- Zhang, H., Shi, G., Liu, L., Zhao, M. and Liang, Z. (2018). Detection and identification method of medical label barcode based on deep learning. Eighth International Conference on Image Processing Theory, Tools and Applications (IPTA), Xi'an, China 7-10 November, 2018. Available at: DOI: 10.1109/IPTA.2018.8608144. Accessed on 14th January 2020.
- Zhao, W., Zhang, J., Li, P. and Li, Y. (2010). Study of image segmentation algorithm based on textural features and neural network. International Conference on Intelligent Computing and Cognitive Informatics (ICICCI), 300-303.
- Zhou, R. and Guo, X. (2016). A new method of angle-robust multiple ID-barcode detection. 2nd IEEE International Conference on Computer and Communications (ICCC), October 14-16, 2016, 433-438.

-
- Zhu, S., Xia, X., Zhang, Q. and Belloulata, K. (2007). An image segmentation algorithm in image processing based on threshold segmentation. Third International IEEE Conference on Signal-Image Technologies and Internet-Based System (SITIS), 673-678.
- Zigelboim, M.S. (2015). Method and apparatus for marking coconuts and similar food products. U.S. Patent No. 0030731A1.

Appendices

Appendix I: Algorithm for Code 128 detection using HDEVELOP.

The following algorithm was used in all the barcode experiments in both the university and company.

1. open_framegrabber ('DirectShow', , AcqHandle)
2. grab_image_start (AcqHandle, -1)
3. dev_close_window ()
4. dev_open_window (0, 0, 1280/2, 960/2, 'black', WindowHandle)
5. set_display_font (WindowHandle, 16, 'mono', 'true', 'false')
6. dev_set_colour ('green')
7. dev_set_draw ('margin')
8. dev_set_line_width (3)
9. set_bar_code_param (BarCodeHandle, 'element_size_min', 1.5)
10. set_bar_code_param (BarCodeHandle, 'element_size_max', 16)
11. *
12. ***area of interest**
13. gen_rectangle1 (ROI,)
14. *
15. **Create a new Code128 model**
16. create_bar_code_model ([], [], BarCodeHandle)
17. *
18. **Find region of code**
19. store:='0'
20. store2:='0'
21. GrayvalStored:=[120,100,110]
22. speed:='0.11'
23. while (true)
24. grab_image_async (Image, AcqHandle, -1)
25. grab_image (Image, AcqHandle)
26. access_channel (Image, Image3, 3)
27. bin_threshold (Image3, Region)
28. gauss_image (Image3, ImageGauss,)
29. sobel_amp (Image3, EdgeAmplitude, 'sum_abs', 3)
30. gen_struct_elements (StructElement1, 'noise', ,)
31. dilation1 (ROI, StructElement1, RegionDilation,)
32. connection (RegionDilation, ConnectedRegions)
33. select_shape (ConnectedRegions, SelectedRegions, 'area', 'and',)
34. union1 (SelectedRegions, RegionUnion)
35. fill_up (RegionUnion, RegionFillUp)
36. gen_struct_elements (StructElement2, 'noise',)
37. erosion1 (ROI, StructElement2, RegionErosion,)
38. connection (RegionErosion, ConnectedRegions1)
39. select_shape (ConnectedRegions1, SelectedRegions1, 'area', 'and',)
40. union1 (SelectedRegions1, RegionUnion1)
41. fill_up (RegionUnion1, RegionFillUp1)

```

42. gen_struct_elements (StructElement3, 'noise', , )
43. dilation2 (ROI, StructElement3, RegionDilation2, 1)
44. connection (RegionDilation2, ConnectedRegions)
45. gen_struct_elements (StructElement4, 'noise', , )
46. erosion2 (ROI, StructElement4, RegionErosion2, 1)
47. connection (RegionDilation2, ConnectedRegions)
48. *
49. Find codes
50. find_bar_code (Image, SymbolRegions, BarCodeHandle, 'Code 128', DecodedDataStrings)
51. *
52. Prepare output
53. tuple_strlen (DecodedDataStrings, Length1)
54. area_center (SymbolRegions, Area, Row, Column)
55. dev_display (Image)
56. dev_display (SymbolRegions)
57. disp_message (WindowHandle, DecodedDataStrings, 'image', 30, 90, 'black', 'true')
58. get_image_time (Image, MSecond, Second, Minute, Hour, Day, YDay, Month, Year)
59. tuple_string (Month, '.2d', Month)
60. tuple_string (Day, '.2d', Day)
61. tuple_string (Hour, '.2d', Hour)
62. tuple_string (Minute, '.2d', Minute)
63. tuple_string (Second, '.2d', Second)
64. tuple_strlen(store, Length2)
65. tuple_strlen(store2, Length3)
66. get_grayval (Image, 462, 729, Grayval)
67. if (Grayval[1]>GrayvalStored[1]+100)
68. *dump_window (WindowHandle, 'jpeg 100',
69. 'path.....'+Year+Month+Day+' '+Hour+' '+Minute+' '+Second+' '+speed)
70. write_image (Image, 'jpeg 100', 0,
71. 'path.....'+Year+Month+Day+' '+Hour+' '+Minute+' '+Second+' '+speed)
72. endif
73. GrayvalStored:=Grayval
74. if (DecodedDataStrings # store)
75. open_file ('path.....'+Year+Month+Day+'.txt','append',FileHandle)
76. if (Length1=8)
77. if (Length3=8)
    a. if(DecodedDataStrings # store2)
    b. fnew_line(FileHandle)
    c. send1:='BR;20;'+Year+Month+Day+' '+Hour+Minute+Second+' '+DecodedDataStrings+'
      ;'
    d. fwrite_string(FileHandle,send1)
    e. endif
78. else
79. send2:='BR;20;'+Year+Month+Day+' '+Hour+Minute+Second+'
80. fwrite_string(FileHandle,send2)
81. send3:=DecodedDataStrings+'
82. fwrite_string (FileHandle, send3)
83. endif
84. store2:=DecodedDataStrings
85. endif
86. if (Length1=3)
87. if (Length3=3)

```

```
    a. if(DecodedDataStrings # store2)
88. send4:='BR;20;' + Year + Month + Day + ';' + Hour + Minute + Second + ';' + 'xxxxxxx' + ';' + DecodedDataSt
    rings
    a. fwrite_string(FileHandle,send4)
    b. fnew_line(FileHandle)
    c. endif
89. else
90. send5:=DecodedDataStrings
91. fwrite_string (FileHandle, send5)
92. fnew_line (FileHandle)
93. endif
94. store2:=DecodedDataStrings
95. endif
96. close_file(FileHandle)
97. endif
98. store:=DecodedDataStrings
99. endwhile
100. close_framegrabber (AcqHandle)
```


Appendix II: Algorithm for decoding of Data Matrix code on Apples using HDEVELOP.

1. dev_update_off ()
2. dev_close_window()
3. list_image_files ("", [], [], ImageFiles)
4. read_image (Image, ImageFiles[0])
5. dev_open_window_fit_image (Image, 0, 0, -1, -1, WindowHandle)
6. get_image_size (Image, IWidth, IHeight)
7. set_display_font (WindowHandle, 14, 'mono', 'true', 'false')
8. dev_set_draw ('margin')
9. dev_set_line_width (2)
10. dev_set_coloured (12)
11. *
12. **Area of interest**
13. gen_rectangle1 (ROI_0,)
14. reduce_domain (Image, ROI_0, ImageReduced)
15. *
16. set_display_font (WindowHandle, 16, 'mono', 'true', 'false')
17. create_data_code_2d_model ('Data Matrix ECC 200', 'default_parameters', 'enhanced_recognition', DataCodeHandle)
18. set_data_code_2d_param (DataCodeHandle, ['module_gap_min', 'module_gap_max'], ['no', 'big'])
19. set_data_code_2d_param (DataCodeHandle, 'polarity', 'dark_on_light')
20. *
21. **Perform the training**
22. for Index: = 0 to |ImageFiles| - 1 by 1
23. read_image (Image, ImageFiles[Index])
24. reduce_domain (Image, ROI_0, ImageReduced)
25. *
26. **Detect edges (amplitude and direction) using the Sobel operator**
27. sobel_dir (ImageReduced, EdgeAmplitude, EdgeDirection, 'sum_abs', 3)
28. threshold (EdgeAmplitude, Region, 30, 255)
29. **Reduce the direction image to the edge region**
30. reduce_domain (EdgeDirection, Region, EdgeDirectionReduced)
31. **Start the Hough transform using the edge direction information**
32. hough_lines_dir (EdgeDirectionReduced, HoughImage, Lines, 2, 1, 'gauss', 5, 10, 5, 5, 'true', Angle, Dist)
33. gen_region_hline (Regions, 0, 100)
34. **Preprocess with grey value morphology**
35. gray_opening_shape (ImageReduced, ImageOpening, 7, 7, 'rectangle')
36. *
37. **Median filtering**
38. median_image (ImageReduced, ImageMedian, 'circle', 3, 'continued')
39. *
40. ***Find region of code**
41. decompose3 (ImageReduced, Image1, Image2, Image3)
42. add_image (Image2, Image3, ImageResult, 0.5, 0)
43. regiongrowing (ImageResult, Regions,)
44. difference (ROI_0, Regions, RegionDifference)
45. closing_circle (RegionDifference, RegionClosing1,)
46. connection (RegionClosing1, ConnectedRegions)

47. select_shape (ConnectedRegions, SelectedRegions, 'area', 'and',)
48. union1 (SelectedRegions, RegionUnion)
49. fill_up (RegionUnion, RegionFillUp)
50. opening_circle (RegionFillUp, RegionOpening,)
51. connection (RegionOpening, ConnectedRegions2)
52. select_shape (ConnectedRegions2, SelectedRegions2, 'area', 'and',)
53. union1 (SelectedRegions2, RegionUnion1)
54. smallest_rectangle2 (RegionUnion1, Row, Column, Phi, Length1, Length2)
55. gen_rectangle2 (Rectangle, Row, Column, Phi, Length1, Length2)
56. *
57. **Affine transformation of code**
58. vector_angle_to_rigid (Row, Column, Phi, Row, Column,0, HomMat2D)
59. affine_trans_image (ImageReduced, ImageAffinTrans, HomMat2D, 'bilinear', 'false')
60. affine_trans_region (Rectangle, RegionAffineTrans, HomMat2D, 'nearest_neighbor')
61. dilation_rectangle1 (RegionAffineTrans, RegionDilation,)
62. reduce_domain (ImageAffinTrans, RegionDilation, ImageReduced2)
63. *
64. **Homogenize colour**
65. decompose3 (ImageReduced2, ImageR, ImageG, ImageB)
66. trans_from_rgb (ImageR, ImageG, ImageB, ImageResult1, ImageResult2, ImageResult3, 'hsv')
67. add_image (ImageResult2, ImageResult3, ImageResult,)
68. *
69. **Rectification of data code**
70. gray_dilation_rect (ImageResult, ImageMax,)
71. scale_image (ImageMax, ImageScaled,)
72. *
73. find_data_code_2d (ImageResult, SymbolXLDs, DataCodeHandle, [], [], ResultHandles, DecodedDataStrings)
74. *
75. **Prepare output**
76. hom_mat2d_invert (HomMat2D, HomMat2DInvert)
77. affine_trans_contour_xld (SymbolXLDs, ContoursAffinTrans, HomMat2DInvert)
78. dev_display (Image)
79. dev_display (SymbolXLDs)
80. disp_message (WindowHandle, DecodedDataStrings, 'window', 12, 12, 'black', 'true')
81. stop ()
82. endfor
83. dev_clear_window()
84. disp_message (WindowHandle, 'No more lines to execute', 'window', 12, 12, 'black', 'true')
85. *
86. *
87. **Clear the data code model**
88. clear_data_code_2d_model (DataCodeHandle)

Appendix III: Algorithm for grading the quality of the Data Matrix code on horticultural products using HDEVELOP.

1. dev_update_off ()
2. dev_close_window()
3. list_image_files ("", [], [], ImageFiles)
4. read_image (Image, ImageFiles[0])
5. dev_open_window_fit_image (Image, 0, 0, -1, -1, WindowHandle)
6. get_image_size (Image, IWidth, IHeight)
7. set_display_font (WindowHandle, 14, 'mono', 'true', 'false')
8. dev_set_draw ('margin')
9. dev_set_line_width (2)
10. dev_set_coloured (12)
11. *
12. *area of interest
13. gen_rectangle1 (ROI_0,)
14. reduce_domain (Image, ROI_0, ImageReduced)
15. set_display_font (WindowHandle, 16, 'mono', 'true', 'false')
16. create_data_code_2d_model ('Data Matrix ECC 200', [], [], DataCodeHandle)
17. set_data_code_2d_param (DataCodeHandle, 'default_parameters', 'enhanced_recognition')
18. set_data_code_2d_param (DataCodeHandle, 'persistence', 1)
19. set_data_code_2d_param (DataCodeHandle, 'polarity', 'dark_on_light')
20. *
21. Constants for quality grade access
22. *
23. GRADE_CONTRAST: = 1
24. GRADE_MODULATION: = 2
25. GRADE_FIXED_PATTERN_DAMAGE: = 3
26. GRADE_DECODE: = 4
27. GRADE_AXIAL_NON_UNIFORMITY: = 5
28. GRADE_GRID_NON_UNIFORMITY: = 6
29. GRADE_UNUSED_ERROR_CORRECTION: = 7
30. get_data_code_2d_results (DataCodeHandle, 'general', 'quality_isoiec15415_labels', Labels)
31. *
32. Example: Contrast
33. for Index: = 0 to | ImageFiles | - 1 by 1
34. read_image (Image, ImageFiles[Index])
35. reduce_domain (Image, ROI_0, ImageReduced)
36. *
37. Detect edges (amplitude and direction) using the Sobel operator
38. sobel_dir (ImageReduced, EdgeAmplitude, EdgeDirection, 'sum_abs', 3)
39. threshold (EdgeAmplitude, Region, 0, 255)
40. Reduce the direction image to the edge region
41. reduce_domain (EdgeDirection, Region, EdgeDirectionReduced)
42. Start the Hough transform using the edge direction information
43. hough_lines_dir (EdgeDirectionReduced, HoughImage, Lines, 2, 1, 'gauss', 5, 10, 5, 5, 'true', Angle, Dist)
44. gen_region_hline (Regions, 0, 100)
45. Preprocess with grey value morphology
46. gray_opening_shape (ImageReduced, ImageOpening, 7, 7, 'rectangle')

47. *
48. Median filtering
49. median_image (ImageReduced, ImageMedian, 'circle', 3, 'continued')
50. *
51. *Find region of code
52. decompose3 (ImageReduced, Image1, Image2, Image3)
53. regiongrowing (Image2, Regions, 1,)
54. difference (ROI_0, Regions, RegionDifference)
55. closing_circle (RegionDifference, RegionClosing1,)
56. connection (RegionClosing1, ConnectedRegions)
57. select_shape (ConnectedRegions, SelectedRegions, 'area', 'and',)
58. union1 (SelectedRegions, RegionUnion)
59. fill_up (RegionUnion, RegionFillUp)
60. opening_circle (RegionFillUp, RegionOpening,)
61. connection (RegionOpening, ConnectedRegions2)
62. select_shape (ConnectedRegions2, SelectedRegions2, 'area', 'and',)
63. union1 (SelectedRegions2, RegionUnion1)
64. smallest_rectangle2 (RegionUnion1, Row, Column, Phi, Length1, Length2)
65. gen_rectangle2 (Rectangle, Row, Column, Phi, Length1, Length2)
66. *
67. Affine transformation of code
68. vector_angle_to_rigid (Row, Column, Phi, Row, Column,0, HomMat2D)
69. affine_trans_image (ImageReduced, ImageAffinTrans, HomMat2D, 'bilinear', 'false')
70. affine_trans_region (Rectangle, RegionAffinTrans, HomMat2D, 'nearest_neighbor')
71. dilation_rectangle1 (RegionAffinTrans, RegionDilation,)
72. reduce_domain (ImageAffinTrans, RegionDilation, ImageReduced2)
73. *
74. Homogenize colour
75. decompose3 (ImageReduced2, ImageR, ImageG, ImageB)
76. trans_from_rgb (ImageR, ImageG, ImageB, ImageResult1, ImageResult2, ImageResult3, 'hsv')
77. add_image (ImageResult2, ImageResult3, ImageResult,)
78. *
79. Rectification of data code
80. gray_dilation_rect (ImageResult, ImageMax,)
81. scale_image (ImageMax, ImageScaled,)
82. *
83. find_data_code_2d (Image2, SymbolXLDs, DataCodeHandle, [], [], ResultHandles, DecodedDataStrings)
84. get_data_code_2d_results (DataCodeHandle, ResultHandles, 'quality_isoiec15415', Quality)
85. get_data_code_2d_results (DataCodeHandle, ResultHandles, 'quality_isoiec15415_values', QualityValues)
86. gen_region_contour_xld (SymbolXLDs, Region, 'filled')
87. min_max_gray (Region, Image2, 0, Min, Max, Range)
88. Contrast: = Range / 255
89. dev_display (Image)
90. dev_set_colour ('green')
91. dev_display (SymbolXLDs)
92. grade_message_text (Labels, Quality, QualityValues, GRADE_CONTRAST, Message)
93. disp_message (WindowHandle, Message, 'window', 10, -1, 'black', 'true')
94. dev_display (Image)
95. dev_set_colour ('green')
96. dev_display (SymbolXLDs)

```
97. grade_message_text (Labels, Quality, QualityValues, GRADE_MODULATION, Message)
98. disp_message (WindowHandle, Message, 'window', 10, -1, 'black', 'true')
99. dev_display (Image)
100.dev_set_colour ('green')
101.dev_display (SymbolXLDs)
102.grade_message_text (Labels, Quality, QualityValues, GRADE_FIXED_PATTERN_DAMAGE,
    Message)
103.disp_message (WindowHandle, Message, 'window', 10, -1, 'black', 'true')
104.dev_display (Image)
105.dev_set_colour ('green')
106.dev_display (SymbolXLDs)
107.grade_message_text (Labels, Quality, QualityValues, GRADE_AXIAL_NON_UNIFORMITY,
    Message)
108.disp_message (WindowHandle, Message, 'window', 10, -1, 'black', 'true')
109.dev_display (Image)
110.dev_set_colour ('green')
111.dev_display (SymbolXLDs)
112.grade_message_text (Labels, Quality, QualityValues, GRADE_GRID_NON_UNIFORMITY,
    Message)
113.disp_message (WindowHandle, Message, 'window', 10, -1, 'black', 'true')
114.dev_display (Image)
115.dev_set_colour ('green')
116.dev_display (SymbolXLDs)
117.grade_message_text (Labels, Quality, QualityValues,
    GRADE_UNUSED_ERROR_CORRECTION, Message)
118.disp_message (WindowHandle, Message, 'window', 10, -1, 'black', 'true')
119.hom_mat2d_invert (HomMat2D, HomMat2DInvert)
120.affine_trans_contour_xld (SymbolXLDs, ContoursAffinTrans, HomMat2DInvert)
121.dev_display (Image)
122.dev_display (SymbolXLDs)
123.disp_message (WindowHandle, DecodedDataStrings, 'window', 12, 12, 'black', 'true')
124.stop ()
125.endfor
126.dev_clear_window()
127.disp_message (WindowHandle, 'No more lines to execute', 'window', 12, 12, 'black', 'true')
128.*
129.*
130.Clear the data code model
131.clear_data_code_2d_model (DataCodeHandle)
```

Appendix IV: Grade quality of Data Matrix code

Table 7-1: Summary of the test parameters and grade levels of the print quality of Data Matrix code (ISO/IEC 15415)

Parameter / Grade	Decode	Symbol Contrast	Fixed Pattern Damage	Axial Non-uniformity	Grid Non-uniformity	Modulation	Unused Error Correction
4 (A)	Pass	SC ≥ 0.70	0	AN ≤ 0.06	GN ≤ 0.38	MOD ≥ 0.50	UEC ≥ 0.62
3 (B)		SC ≥ 0.55	≤ 9%	AN ≤ 0.08	GN ≤ 0.50	MOD ≥ 0.40	UEC ≥ 0.50
2 (C)		SC ≥ 0.40	≤ 13%	AN ≤ 0.10	GN ≤ 0.63	MOD ≥ 0.30	UEC ≥ 0.37
1 (D)		SC ≥ 0.20	≤ 17%	AN ≤ 0.12	GN ≤ 0.75	MOD ≥ 0.20	UEC ≥ 0.25
0 (F)	Fail	SC < 0.20	> 17%	AN > 0.12	GN > 0.75	MOD < 0.20	UEC < 0.25

Decode: describes whether the code can be successfully be read or not

Contrast: the difference between the minimum and maximum pixel intensities (maximum amplitudes) in the 2D data code domain

Fixed Pattern Damage: shows how reliable a symbol can be located and identified in the image

Axial Non-uniformity: the squareness of the modules (normally, the distance between the module's center positions is the same in horizontal and vertical direction)

Grid Non-uniformity: quantifies the deviation of the modules from their ideal grid

Modulation: measures the uniformity of the amplitudes of the modules inside the symbol

Unused Error Correction: quantifies the reserve in error correction that is still available after reading the data code

Appendix V: Laser marking properties

Delay Properties

Due to the brief amount of time required by optical scanners to overcome the mirror inertia to get into the right position, there is a slight lag in the movement of the optical scanner when the command is entered. Delay properties are therefore essential to get the correct marking of the object. Each optical scanner has a different response time, and default delay values with the Flyer Series are faster than the FH Series marking heads (Table 7-2). Pline Start Delay (PSD), Pline End Delay (PED), Interseg Delay (ID) and Off Vector Delay (OVD) are the four types of delay properties that have to be adjusted to get the proper marking of the object (Synrad, 2012).

Table 7-2: Default delay values of Flyer and FH Series marking heads

Delay	Flyer Marking Head (μs)	FH Series Marking Head (μs)
Pline Start Delay	0	100
Pline End Delay	200	450
Interseg Delay	75	350
Off Vector Delay	250	300

Pline Start Delay

Pline Start Delay reduces hotspots (dwells) at the beginning of a polyline or a series of polyline. If PSD is set too short or small, it results in hotspots at the beginning of each polyline (Figure 7-1a). When PSD is set too long or large, it results in shortened polyline at the beginning of the marking or incomplete closing of the marking (Figure 7-1b). Finally, the correct use of PSD is to choose values that are not too small or large during the setting to get the best marking of the object without hotspots during the setting of the laser parameters (Figure 7-1c) (Synrad, 2012).

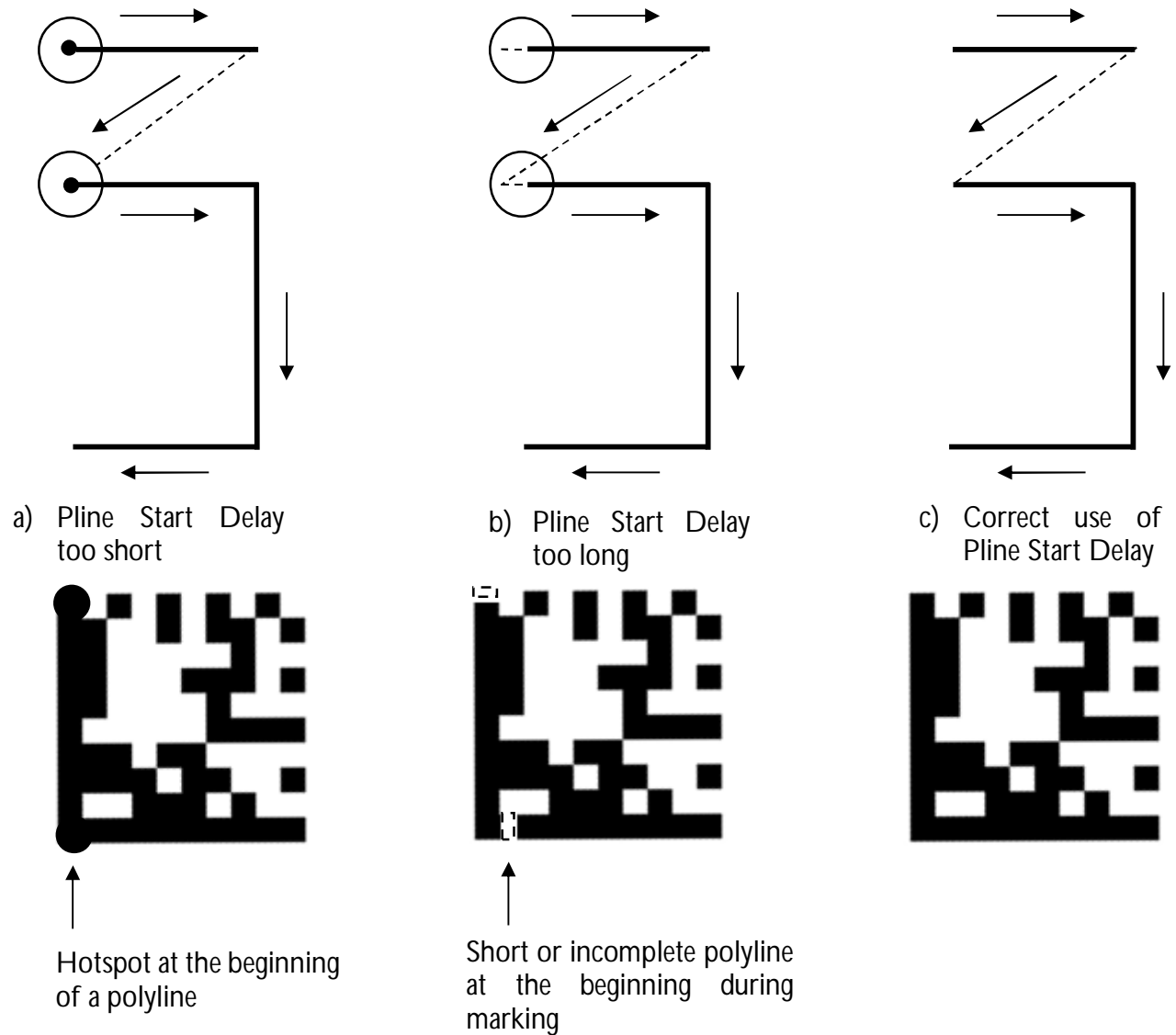


Figure 7-1: The effect of Pline Start Delay on laser marking

Pline End Delay

Pline End Delay ensures that a polyline is completed before moving onto the next one by maintaining the right beam at the end of a polyline or series of polylines. If PED is too much or long, hotspots are created at the end of polylines (Figure 7-2a). If PED is too little or short, polylines are shortened at the end of the marking or incomplete closing of the marking occurs (Figure 7-2b). Finally, the correct

use of PED is to choose values that are not too large or little during the setting to get the best marking of the object without hotspots during the setting of the laser parameters (Figure 7-2c) (Synrad, 2012).

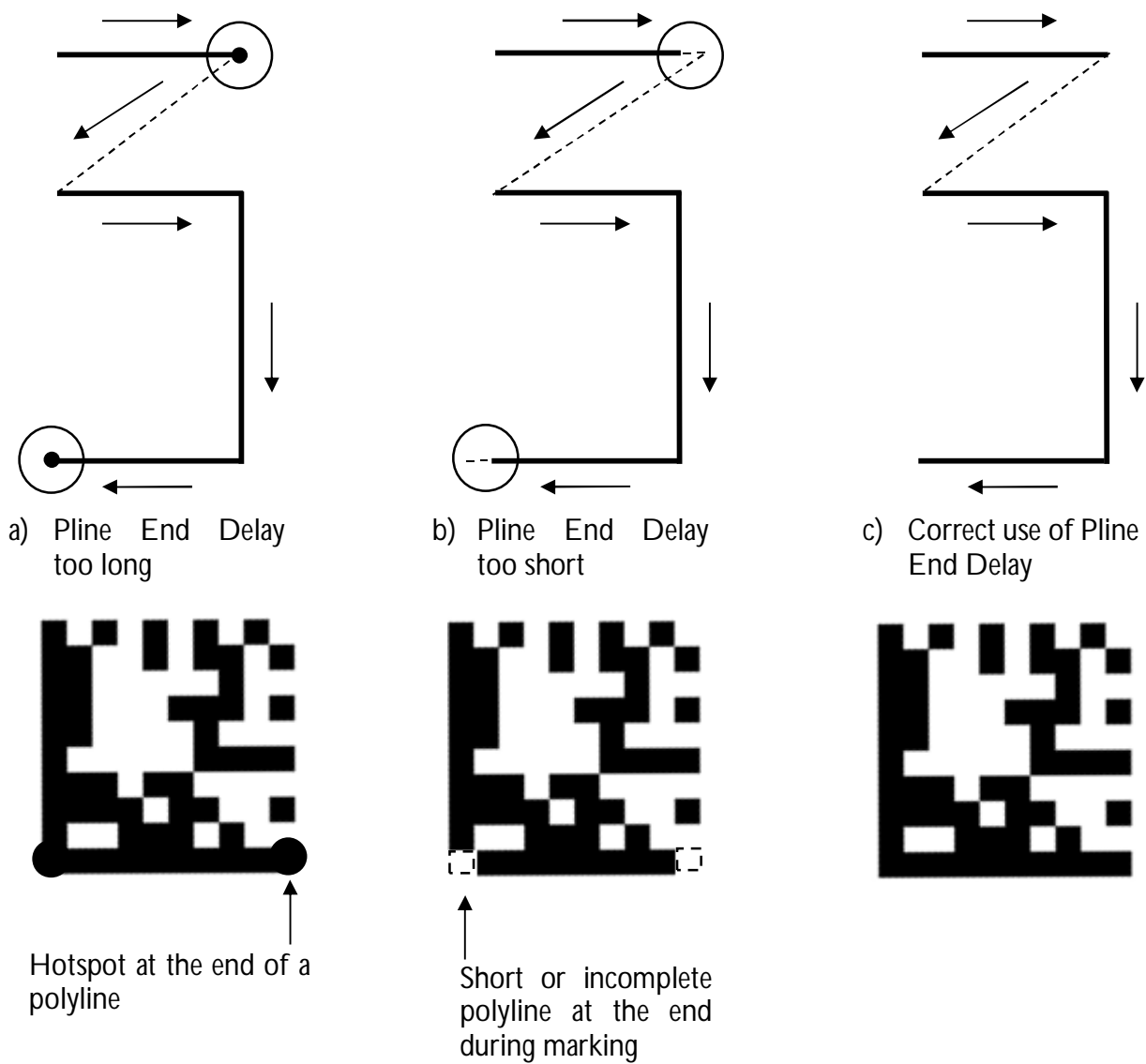


Figure 7-2: The effect of Pline End Delay on laser marking

Interseg Delay

Interseg Delay connects polylines in the object when the end point of one polyline is the start of the next polyline, by setting a delay between them. The sharpness of the points where the polylines are connected is increased by Interseg Delay. If ID is too much or long, hotspots are created at the end of the polylines (Figure 7-3a). If ID is too little or short, corners of the object are rounded (Figure 7-3b). The correct use of ID is to select values that are not too much or little during the setting of the laser parameters (Figure 7-3c) (Synrad, 2012).

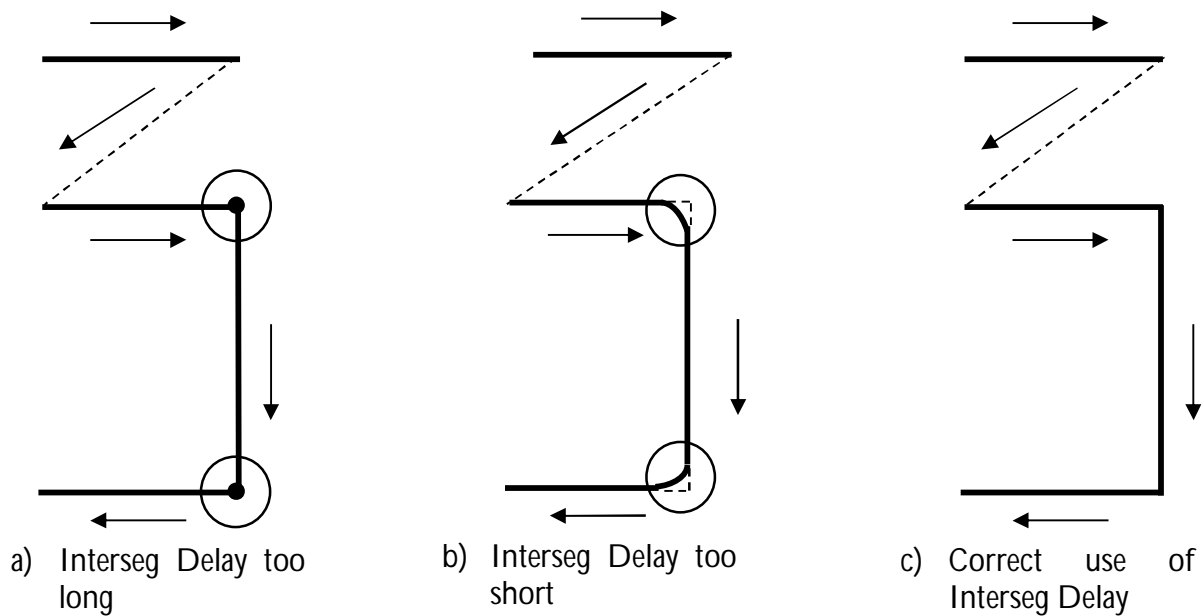


Figure 7-3: The effect of Interseg Delay on laser marking

Off Vector Delay

To remove “tails”, i.e., extension of polylines, when moving between non-connected polylines during all laser off-vector moves, Off Vector Delay is used to set a proportional delay during this process. If OVD is too much or long, a good mark is created, however, the marking cycle time (throughput) will be too long, which is unacceptable (Figure 7-4a). If OVD is too little or short, tails may be created at the beginning of polylines (Figure 7-4b). The correct use of OVD is to select values that are not too much or little during the setting of the laser parameters (Synrad, 2012).

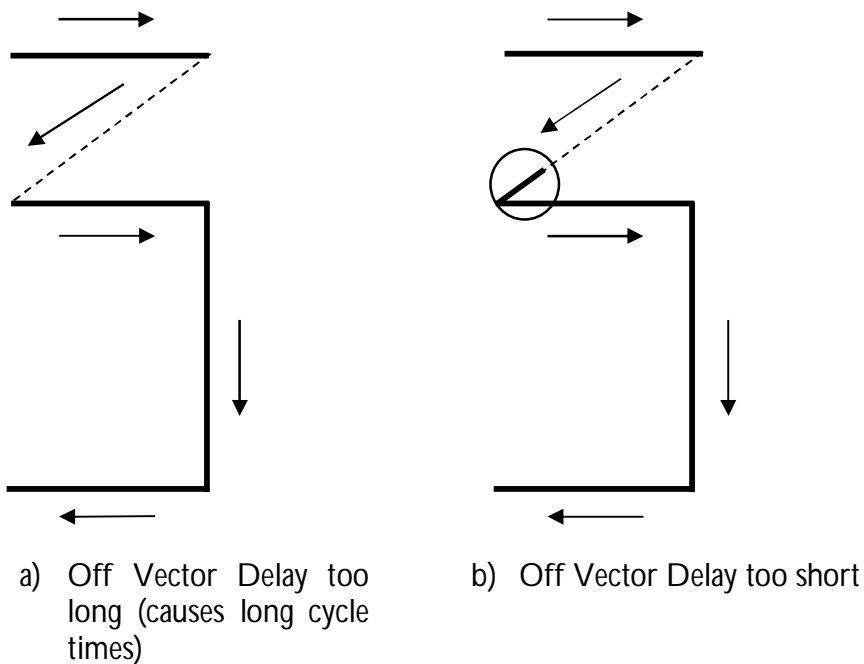
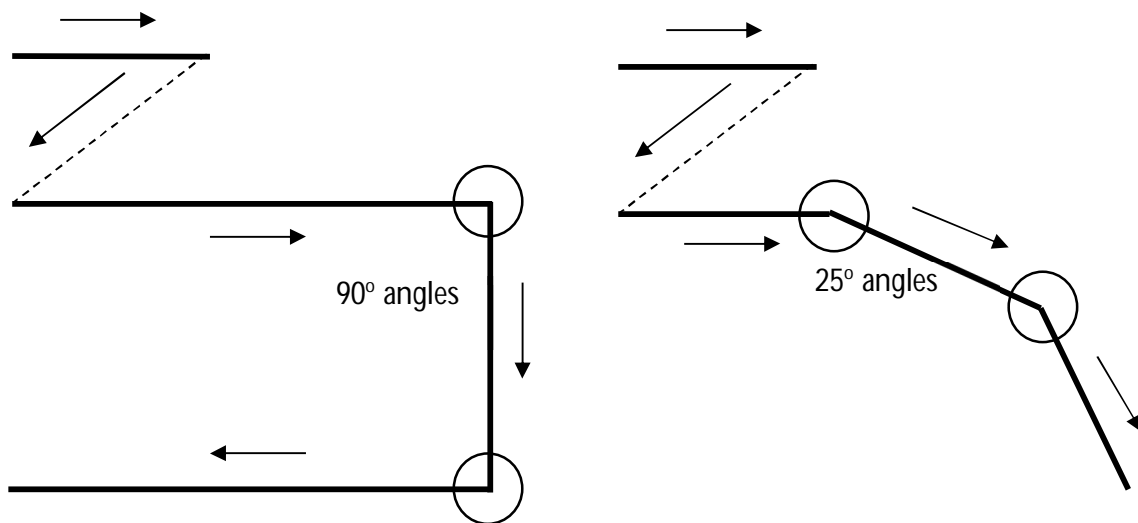


Figure 7-4: The effect of Off Vector Delay on laser marking

Interseg Break Angle (°)

Interseg Break Angle is the break angle between two connected polylines. If the angle between the polyline is greater than break angle, interseg delay is used (Figure 7-5a). However, when the angle between two marked polylines is less than the specified angle, Interseg Break Angle is not used (Figure 7-5b) (Synrad, 2012).



a) Angles are greater than the specified Interseg Break Angle. Interseg Delay is used to prevent hotspots or rounded corners.

b) Angles are less than the specified Interseg Break Angle. No Interseg Delay is used.

Figure 7-5: The effect of Interseg Break Angle on laser marking

Curriculum vitae

Personal data

Name	Felix Amenyo Eyahanyo
Date of birth	19.05.1982
Place of birth	Madina, Ghana
Marital status	Married, 2 Children

Education

04/2011 – 09/2020	Gottfried Wilhelm Leibniz Universität Hannover, Biosystems Engineering Section, Hannover, Germany: PhD studies (Dr. rer. hort.)
10/2008 – 09/2010	Gottfried Wilhelm Leibniz Universität Hannover, Biosystems Engineering Section, Hannover, Germany: M.Sc. Internal Horticulture (Major: Horticultural and Agricultural Engineering)
09/2002 – 06/2006	Kwame Nkrumah University of Science and Technology (KNUST), Kumasi, Ghana: B.Sc. Agricultural Science (Major: Agricultural Mechanization)
02/1998 – 12/2000	Presbyterian Boys' Senior High School, Legon, Ghana: WASSCE
01/1986 – 08/1997	Elican School, Mempeasem – East Legon, Accra, Ghana: BECE

Award

07/2008 – 09/2010	German Academic Exchange Service Scholarship (DAAD)
-------------------	---

Work Experience

04/2011 – 03/2017	Research Associate, Biosystems Engineering Section, Leibniz Universität Hannover, Germany
01/2008 – 05/2008	Supervisor/Assistant Application Specialist II, Directions Consult, Accra, Ghana
09/2007 – 12/2007	Assistant Application Specialist II, Centre for Remote Sensing and Geographic Information Services (CERSGIS), Legon, Accra, Ghana
09/2006 – 08/2007	National Service Personnel, Field Officer at Komenda Edina Eguafo Abirem (KEEA) District, Centre for Remote Sensing and Geographic Information Services (CERSGIS), Legon, Accra, Ghana

Lebenslauf

Persönliche Daten

Name Felix Amenyo Eyahanyo
Geboren am 19.05.1982
Geburtsort Madina, Ghana
Familienstand Verheiratet, zwei Kinder

Ausbildung

04/2011 – 09/2020 Gottfried Wilhelm Leibniz Universität Hannover, Abteilung Biosystem- technik, Hannover, Deutschland: Promotionsstudium (Dr. rer. hort.)
10/2008 – 09/2010 Gottfried Wilhelm Leibniz Universität Hannover, Abteilung Biosystem- technik, Hannover, Deutschland: M.Sc. International Gartenbau (Spezialisierung in Gartenbau-und Agraringenieur)
09/2002 – 06/2006 Kwame Nkrumah University of Science and Technology (KNUST), Kumasi, Ghana: B.Sc. Agrarwissenschaft (Spezialisierung in Landwirtschaftliche Mechanisierung)
02/1998 – 12/2000 Presbyterian Boys' Senior High School, Legon, Ghana: WASSCE
01/1986 – 08/1997 Elican School, Mempeasem – East Legon, Accra, Ghana: BECE

Auszeichnungen

07/2008 – 09/2010 Deutscher Akademischer Austauschdienst Stipendium (DAAD)

Berufliche Tätigkeit

04/2011 – 03/2017 Wissenschaftlicher Mitarbeiter, Abteilung Biosystemtechnik, Leibniz Universität Hannover, Deutschland
01/2008 – 05/2008 Betreuer / Assistent Anwendungsspezialist II, Directions Consult, Accra, Ghana
09/2007 – 12/2007 Assistent Anwendungsspezialist II, Centre for Remote Sensing and Geographic Information Services (CERSGIS), Legon, Accra, Ghana
09/2006 – 08/2007 Wehrdienst, Feldoffizier Komenda Edina Eguafio Abirem (KEEA) District, Centre for Remote Sensing and Geographic Information Services (CERSGIS), Legon, Accra, Ghana

List of publications

Under Peer-Review

a) Journal

Eyahanyo, F. and Rath, T. (2019). Comparison of manual and automatic barcode detection in rough horticultural production systems. Published in *International Journal of Agricultural and Biological Engineering (IJABE)*

b) Journal

Eyahanyo, F. and Rath, T. (2020). Investigations on the effects of low laser infrared marking energy and barcode size on 2D Data Matrix code detection on apples. Accepted in *Journal of Applied Engineering in Agriculture (ASABE)*

Abstract

Optimization of barcode and RFID technology in plant production, SHE, Angers-France, 2012

Conference Presentations

Eyahanyo, F. and Rath, T. (2011): Poster Presentation on Optimization of Barcode and RFID Technologies in Plant Production. WeGa AP3.5: Photo-elektronische Produktsiegel mit Barcode-, RFID- und Lasertechnologie: WeGa-PhD Day, 24th November 2011, Hannover

Eyahanyo, F., Grade, S. and Rath, T. (2012): Post Presentation on Optimization of Barcode Technology in Horticulture. WeGa AP3.5: Photo-elektronische Produktsiegel mit Barcode-, RFID- und Lasertechnologie. WeGa-PhD Day, Berlin, 6th September, 2012, Berlin

Eyahanyo, F. and Grade, S. (2012). Poster Presentation on Optimization of Barcode and RFID Technologies in Plant Production. 2nd Symposium on Horticulture in Europe-SHE, Angers - France, 1-5 July, 2012, <https://colloque.inra.fr/she2012>, p.74

Rath, T., **Marx, C.**, Eyahanyo, F., Britz, R. and Grade, S. (2013). Poster Presentation: WeGa AP3.5: Photo-elektronische Produktsiegel mit Barcode-, RFID- und Lasertechnologie. Evaluierung des BMBF-AgroClustEr: WeGa-Kompetenznetz Gartenbau, 21. Februar 2013, Hannover

Eyahanyo, F. and Rath, T. (2014). Comparison of manual and automatic barcode detection in horticultural production systems. 20th Workshop Computer Image Analysis in Agriculture, Hochschule Osnabrück, Germany, 26th May, 2014. Bornimer Agrartechnische Berichte, Heft 88, ISSN 0947-7314, p. 217.

Acknowledgement

First and foremost, I thank the Almighty God for His grace, favour and abundant mercies bestowed upon me for a successful completion of my studies. To God be all the Glory!

My sincere gratitude goes to my supervisor Prof. Dr. Thomas Rath for his suggestions, helpful criticism, supervision, keen interest, unwavering support and friendship making it possible to complete my research. I am really thankful for your faith in me and giving me the opportunity to carry out my studies under your supervision. I am also very thankful to Prof. Dr. Hartmut Stützel for his advice, support and readiness to help in my research. I am also very grateful to the doctoral committee and wish to thank Prof. Dr. Traud Winkelmann and Prof. Dr. Uwe Schmidt for their engagement.

I am also grateful to the cooperation between WeGa (Wertschöpfung im Gartenbau), Leibniz University of Hannover and Brandkamp GmbH in giving me the opportunity to carry out my research. I am thankful for the financial support and the availability of resources and facilities in making the research work possible. My heartfelt and profound gratitude goes to Dr. Christian Max and Dr. Stefanie Grade for their wonderful ideas, encouragement, valuable support and guidance. I am also grateful to all my former PhD colleagues (Julio, Holger, Thorsten, Sebastian, Ronoh, Frederik, Indera, Anne, Gökhan, Klaus, Serge, Sandra and Johannes) for their helpful criticism, encouragement and support. I am also thankful for the immense support on technical issues from the workshop team (Werner (retired), Andreas, Norbert and Niko).

Also, my immense gratitude goes to my church family (Hannover International Bible Church and International Baptist Church Celle) for their prayers, concern and support during my stay and study in Germany. I thank God for you all. You made my life here in Germany a happy one and I thank God for bringing me to fellowship with you all. My special thanks and gratitude go to Debbie for her time and patience in reading and correcting my articles and thesis.

This research would not have been successful without the unflinching support and encouragement from my wonderful, loving and caring wife Rita and our lovely children Jeanelle and Joella. The growth of our children kept on reminding me of how long I have been doing my PhD in Germany.

My special thanks go to Frank Schaarschmidt (Institute for Biostatistics, University of Hannover) for his advice, patience and assistance in statistically analyzing my data. I am also really grateful for the financial support from the office of the Graduate School and the needed help in dealing with my residential status by the International Office of the Leibniz University of Hannover. I am especially thankful to Dr. Meike Huntebrinker and Dr. Solenne Schwanemann for their assistance and readiness to help. I am also really grateful to Dr. Adelheid Kühne (Institute of Sociology, University of Hannover) for your patience, advice and help in dealing with my situation with the residence permit.

Special thanks go to all my family and friends (Prosper, Alirah, Samuel, Johnny, Charles, Michael, Mildred, Pastor Aseidu) for their encouragement support and prayers. It would truly be a long list to mention everybody I am indebted to. I thank you all for your faith in me and support.

Declaration / Erklärung zur Dissertation

Hiermit erkläre ich, dass ich meine Dissertation mit dem Titel „**Computer Vision Reading on Stickers and Direct Part Marking on Complex Backgrounds**“ selbständig verfasst und die benutzten Hilfsmittel und Quellen sowie gegebenenfalls die zu Hilfsleistungen herangezogenen Institutionen vollständig angegeben habe. Die Dissertation wurde nicht schon als Masterarbeit, Diplomarbeit oder ähnliche Prüfungsarbeit verwendet.

Hannover, 2020

Felix Amenyo Eyahanyo, M. Sc.